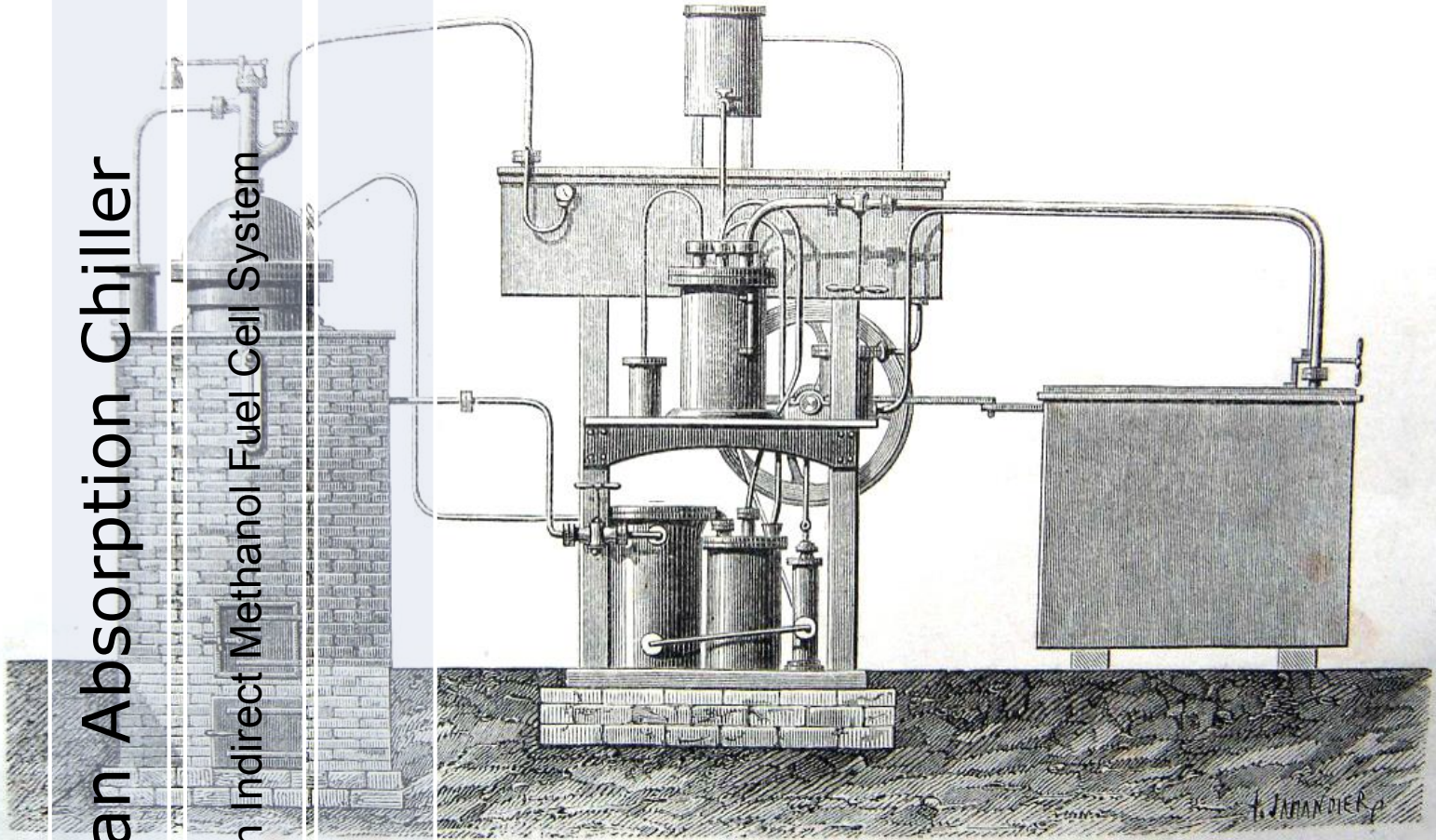


Development of an Absorption Chiller

- Utilizing Waste Heat from an Indirect Methanol Fuel Cell System

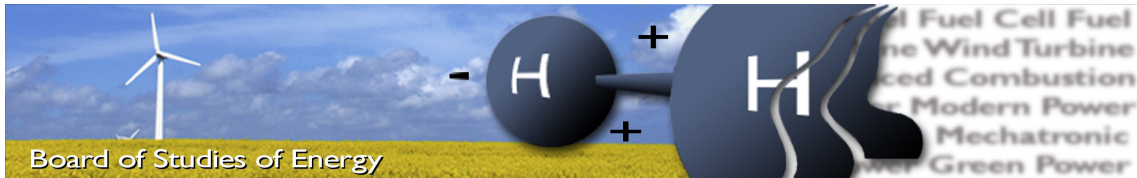
2013



Absorption cooling apparatus invented by Ferdinand Carré.
Published on L'Eau by Gaston Tissandier, Paris 1873

Anders Holten & Lars Houbak-Jensen
Master Thesis, Energy Technology
Aalborg University





Title: Development of an Absorption Chiller Utilizing Waste Heat from an Indirect Methanol Fuel Cell System

Semester: 10th

Semester theme: Master Thesis

Project period: 01.02.2013 to 04.06.2013

ECTS: 30

Supervisor: Mads Pagh Nielsen & Carsten Bojesen

Project group: TEPE4-1004

Lars Houbak-Jensen

Anders Holten

Abstract:

An absorption chiller utilizing waste heat from an indirect methanol fuel cell was developed. It was found that a single-effect water/lithium bromide chiller was most suitable for the purpose. The most inexpensive chiller design was found by optimizing the chiller configuration using a black-box model in EES. The system has an estimated performance of 0.86. The physical design of the components was found by minimizing the material cost using individual component models. An air-cooled chiller concept was developed and it was deemed possible to fabricate the chiller for less than the maximum capital expense of 3700 €.

Copies: 5

Pages, total: 142

Appendix: 42

Supplements: CD

By signing this document, each member of the group confirms that all participated in the project work and thereby all members are collectively liable for the content of the report.



Resume

This report describes the development of an absorption chiller which utilizes waste heat from an indirect methanol fuel cell (IMFC) system. The concept is to replace a current configuration which provides combined power and cooling to off-grid base transceiver stations in India. It was found that the maximum investment cost is 3700€ and the minimum COP is 0.86 in order to keep the return of investment below 1.5 years. A water/ lithium bromide absorption chiller is capable of utilizing the waste heat from the IMFC with a performance high enough to make the concept competitive with the current configuration.

A simple black-box model was developed based on energy and mass balance in order to predict the performance of an absorption chiller dependent on configuration and operation. The design of the chiller was found by minimizing the investment cost of the four main components. It was seen that a single-effect chiller is considerably cheaper than a double-effect configuration. The states of the system were estimated using the black-box model with an optimized configuration. The states in the black-box model were used to dimension the individual heat and mass exchangers.

Individual component models were developed based on energy and mass balance, finite element and empirical correlations found in literature were used for the energy and mass transfer coefficients. The models for the generator and absorber showed reasonable tendencies and consistency in energy balance. A mesh independence study was performed for the absorber model and it was found that the number of cells only had a weak influence on the final results.

The absorber and generator were dimensioned using EES' Direct Search method to minimize the material cost. The evaporator and condenser were designed based on the optimum design of the absorber. It was found that the material cost of the air-cooled heat exchangers is decreasing as the length of the tubes is increased. The limiting factor for the length of the tubes was the maximum allowable velocity of the vapor in the tubes. As the tubes were expanded and the number of tubes decreased, the vapor velocity increased. It is important to consider the velocities in the heat exchangers when dealing with flow in vacuum due to the higher volume flow (lower density). The cheapest configuration tended to be right on the upper bound for the outlet velocity.

The absorber was by far the largest component which is in good agreement with the required overall heat transfer coefficients predicted in the black-box model. The evaporator is the only component which is placed inside the cooling load area. This component was found to have a volume of 26.7 l, which is in the same order as an evaporator used in a traditional air-conditioning system. The outdoor unit will however be larger, than for compression cycles. In the case of an off-grid BTS system space outside the shelter is not a limiting factor.

The cost of the four main components were estimated to 1675€ using cost functions in the black-box model. By determining the use of materials and cost functions for the materials in each component the total material cost was estimated to 557.8€. These costs does not cover any manifolding, tubing, pumps or valves. However with a maximum cost set to be 3700€ the concept is deemed feasible.



Preface

This report is written by TEPE4-1004 on the 10th semester of Thermal Energy and Process Engineering under the Board of Study of Energy. The project report is directed at people at an equivalent level of expertise and knowledge, as that of 10th semester students in Energy Engineering.

We would like to thank Serenergy for the excellent cooperation and for the provided specifications of the fuel cell systems and the requirements for the given case.

Reading guide

The references in the report are made according to the Harvard method, and will in the text appear as [Surname(s), Year]. In the last chapter of the report the bibliography is found, which includes full description of all sources used through the report. Figures, tables and equations are sequentially numbered according to the chapter. I.e. the first figure in chapter 2, will be numbered 2.1, the next figure as 2.2, and so on. A nomenclature with all symbols is available on the following pages. Furthermore, the reader will find attached to the end of the report appendices and a CD-ROM. The appendices contains relevant theory and a description of the developed black-box models.

The CD-ROM contains a PDF version of the report, as well as all the models as individual EES files and as an executable file containing all models. The file can run without EES being installed, the "UserLib" folder has to be in the same folder as the "EES Models.exe" file. The model work by running the executable file and then clicking the "See Models!" tab and choosing the desired model. The equations can be seen by clicking "Windows" and "Equations". The model is executed by pushing "F2" and the indexed results are presented in a matrix.

Nomenclature

Symbol	Description	Units
A	Area	$[m^2]$
cp	Specific heat	$\left[\frac{J}{kg-K}\right]$
D	Diameter	$[m]$
D_{ab}	Mass diffusivity coefficient	$\left[\frac{m^2}{s}\right]$
g	Gravitational acceleration	$\left[\frac{m}{s^2}\right]$
h	Convective heat transfer coefficient	$\left[\frac{W}{m^2-K}\right]$
H	Height	$[m]$
i	Enthalpy	$\left[\frac{J}{kg}\right]$
k	Thermal conductivity	$\left[\frac{W}{m-K}\right]$
κ_m	Mass transfer coefficient	$\left[\frac{m}{s}\right]$
L	Length	$[m]$
\dot{m}	Mass flow	$\left[\frac{kg}{s}\right]$
\dot{m}_a	Absorbed mass flow	$\left[\frac{kg}{s}\right]$
\dot{m}_e	Evaporated mass flow	$\left[\frac{kg}{s}\right]$
MW_{LB}	Molar weight	$\left[\frac{mol}{kg}\right]$
N	Number of control volumes	$[-]$
N_s	Number of passes in generator	$[-]$
Nu	Nusselt number	$[-]$
Pr	Prandtl number	$[-]$
Q	Energy	$[W]$
r	Radius	$[m]$
Re	Reynolds number	$[-]$
s	Longitudinal distance	$[m]$
S_L	Longitudinal tube spacing	$[m]$
S_T	Transverse tube spacing	$[m]$
Sc	Schmidt number	$[-]$
Sh	Sherwood number	$[-]$
T	Temperature	$[K]$
th	Thickness	$[m]$

continues on next page

– continued from previous page

Symbol	Description	Units
U	Overall heat transfer coefficient	$\left[\frac{w}{m^2-K} \right]$
u	Velocity in y-direction	$\left[\frac{m}{s} \right]$
\bar{u}	Mean velocity	$\left[\frac{m}{s} \right]$
v	Velocity in y-direction	$\left[\frac{m}{s} \right]$
W	Width	$[m]$
w	Mass fraction of LiBr	$\left[\frac{kg_{LiBr}}{kg} \right]$
w_m	Molar concentration of LiBr	$\left[\frac{mol}{l} \right]$
x	Quality of vapor	$[-]$

Greek Letters

Symbol	Description	Units
α	Thermal diffusivity	$\left[\frac{m^2}{s} \right]$
Γ	Mass flow per unit length	$\left[\frac{kg}{m-s} \right]$
δ	Film thickness	$[m]$
η	Efficiency	$[-]$
μ	Dynamic viscosity	$\left[\frac{kg}{sm} \right]$
ν	Kinematic viscosity	$\left[\frac{m^2}{s} \right]$
ρ	Density	$\left[\frac{kg}{m^3} \right]$
σ	Surface tension	$\left[\frac{N}{m} \right]$

Subscripts

Symbol	Description
a	Absorber
c	Condenser
g	Generator

continues on next page

Symbol	Description
e	Evaporator
eq	Equivalent
fin	Fin
HEX	Solution heat exchanger
hf	Hot fluid
hi	High
if	Interface
l	Liquid
lo	Low
load	Load
R	Refrigerant
s	Solution
ss	Strong solution
sur	Surface
t	Tube
v	Vapor
w	Wall
ws	Weak solution
∞	Surroundings



Table of Contents

Chapter 1	Introduction	1
Chapter 2	Problem Statement	5
2.1	Methodology	5
Chapter 3	System Description	7
3.1	HTEPM Fuel Cell	7
3.2	Case for System Application	8
3.3	Absorption Chiller	11
3.4	Working Fluids in Absorption Chillers	12
Chapter 4	System Modeling	15
4.1	Equations	16
4.2	Engineering Equation Solver	20
4.3	Optimization Theory	21
4.4	Cost Function	22
4.5	Optimization Problem	25
4.6	Results	26
Chapter 5	Component Modeling	29
5.1	Absorber	30
5.2	Generator	41
5.3	Evaporator	47
5.4	Condenser	48
Chapter 6	Design and Optimization of Components	51
6.1	Cost Function	51
6.2	Absorber	53
6.3	Generator	54
Chapter 7	Results	55
7.1	Verification of Results	55
7.2	Absorber	57
7.3	Generator	63
7.4	Evaporator	68

7.5	Condenser	69
Chapter 8	Discussion	71
8.1	System Design	71
8.2	Validity of Component Models	72
8.3	Components Size and Performance	73
Chapter 9	Conclusion	77
Chapter 10	Future Work	79
	Bibliography	83
Appendix A	Double-Effect Chiller Model	87
Appendix B	Study of Entrance Region	93
Appendix C	EES models	95

Introduction

The purpose of this project was to develop an absorption chiller which can utilize the waste heat from an indirect methanol fuel cell (IM-FC) system. The project was carried out in cooperation with Serenergy A/S. Serenergy provides IM-FC system solutions used for various small scale purposes. The IM-FC systems produced by Serenergy are aimed at applications such as back-up power for telecommunications, generators for off-grid power generation or combined heat and power plants (micro CHP). More specifically one of the applications being as a replacement for off-grid diesel generators in Base Transceiver Stations (BTS), which also deliver power to low efficiency compression cycles used for cooling. The conventional compression heat pumps are used for cooling of power electronics, space cooling etc. The main hypothesis was to replace the compression chiller with an absorption based chiller and in that way reduce the overall fuel consumption.

Indirect Methanol Fuel Cell Application

When considering using the waste heat from an IM-FC system it is important to investigate the application of the system. The waste heat could be used directly in a heat exchanger if heating should be necessary, on the other hand by utilizing the waste heat in an absorption chiller both heating and cooling will be available. In an off-grid system a combination of an IM-FC system and an absorption heat pump can be used for tri-generation of power, heat and cooling.

Usually heating is considered a low value product compared to electricity, cooling however usually requires the use of electricity, which therefore can be considered even more valuable. Therefore utilizing the low value waste heat to produce cooling through an absorption chiller could prove feasible.



Figure 1.1. H3 5000 Methanol Power System [Serenergy A/S, 2011]

Serenergy's H3 5000 Methanol Power System is seen from Figure 1.1. This system has an electrical efficiency of about 50-57%. Serenergy's IM-FC systems uses HTPEM fuel cell technology which means the operating temperature is high (up to 150 - 180°C [Serenergy A/S, 2013b]). The liquid cooled fuel cell systems deliver cooling refrigerant at about 150°C [Serenergy A/S, 2011]. This temperature level is sufficient for driving an absorption heat pump [Herold et al., 1996].

Absorption Heat Pumps

Absorption heat pumps allow for the utilization of waste heat to provide cooling. When comparing absorption heat pumps with traditional compression heat pumps, the compressor unit is replaced by an absorption cycle, while the rest of the refrigeration cycle is similar as illustrated in Figure 1.2.

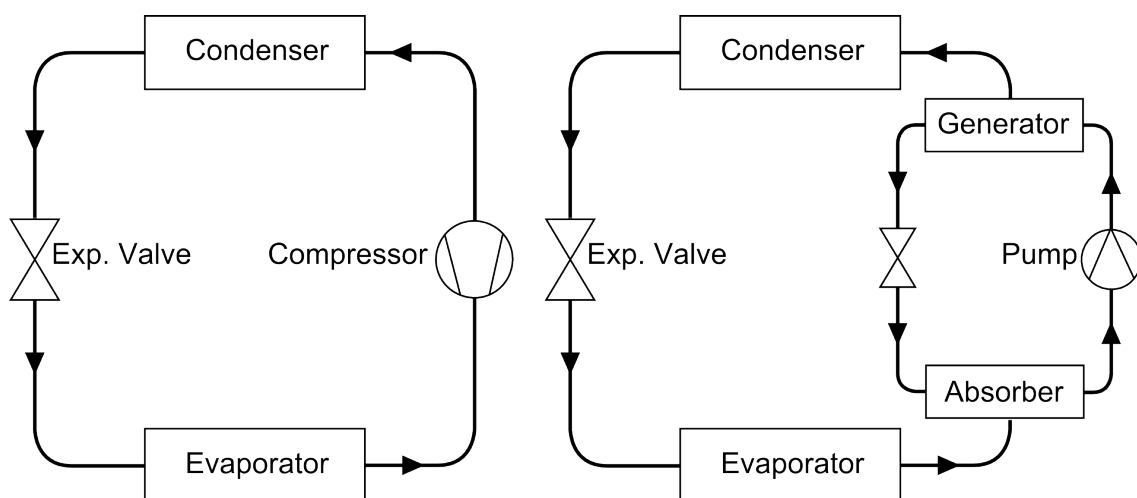


Figure 1.2. The compression cycle is shown to the left while the illustration to the right shows the cycle of an absorption heat pump.

The absorbent cycle consists of an absorber, centrifugal pump, generator and an expansion valve. The absorption heat pump is driven by heat which is supplied to the generator. This means that the only electricity required by the absorption cycle is to power the circulation pump. The power consumed by the pump is only a fraction compared to the power consumed by a compressor driven heat pump.

Utilization of Waste Heat from a Fuel Cell in an Absorption Chiller

A simple schematic of the utilization of waste heat from a fuel cell in an absorption heat pump is shown in Figure 1.3. This concept provides a flexible tri-generation solution.

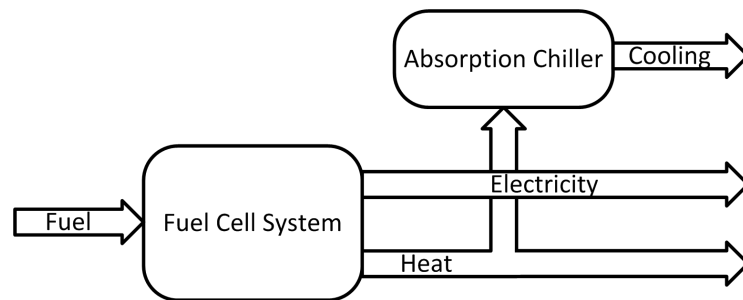


Figure 1.3. A schematic for using a fuel cell to provide tri-generation by utilizing the waste heat to drive an absorption chiller

The type of absorption chiller and the configuration of the components depends on the specific application. The challenge was to develop an absorption chiller which meets the requirements of the specific application and insures a reasonable Return of Investment (ROI) compared to existing solutions.

Problem Statement

The objective of this project is to design an absorption heat pump capable of utilizing the waste heat from an IM-FC system to provide cooling.

How should an absorption chiller be designed for utilization of waste heat from Serenergy's Indirect Methanol Fuel Cell system, with the objective to minimize the Return of Investment compared to other combined power and refrigeration solutions?

2.1 Methodology

The HTPEM fuel cell system from Serenergy will be analyzed in order to determine physical properties and the flexibility of the system. As mentioned earlier one of the applications of the fuel cell systems is to power Base Transceiver Stations. Serenergy has provided a case example where a fuel cell is used in combination with a absorption chiller to supply Base Transceiver Stations in India. A brief economical study will be presented in order to determine the maximum investment cost and the required performance of the chiller in order to obtain a feasible Return of Investment (ROI).

The absorption chiller cycle will be analyzed and the two most common working fluids compared in order to choose the most suitable for the given application.

Black-box models will be developed in order to determine the performance of the chillers based on configuration and operational conditions. Optimization will be performed on the models in order to minimize the investment cost with the given system requirements. The optimal solution will be used as a template for further development of the individual components.

Component models will be developed for the individual heat and mass exchangers and used to find the physical design of each component. Finally a sensitivity analysis will be carried out in order to determine the validity of the models.

System Description

In this chapter the fuel cell system from Serenergy will be described, mainly focusing on the produced waste heat. To be able to design and compare the absorption concept with the traditional technology a case will be described. Following that, a system description will be given, containing an explanation of the operation of the absorption cycle and a decision on the working fluid will be made.

3.1 HTPEM Fuel Cell

The H3 5000 methanol system from Serenergy consists of an HTPEM fuel cell stack and a reformer and uses a mixture consisting of 60% methanol and 40% deionized water as fuel. The H3 5000 is liquid-cooled which is favorable in order to be able to utilize the heat from the fuel cell system. This fuel cell system can be scaled in the range 1 to 6 kW_e. A conceptual schematic of the H3 5000 system is shown in Figure 3.1.

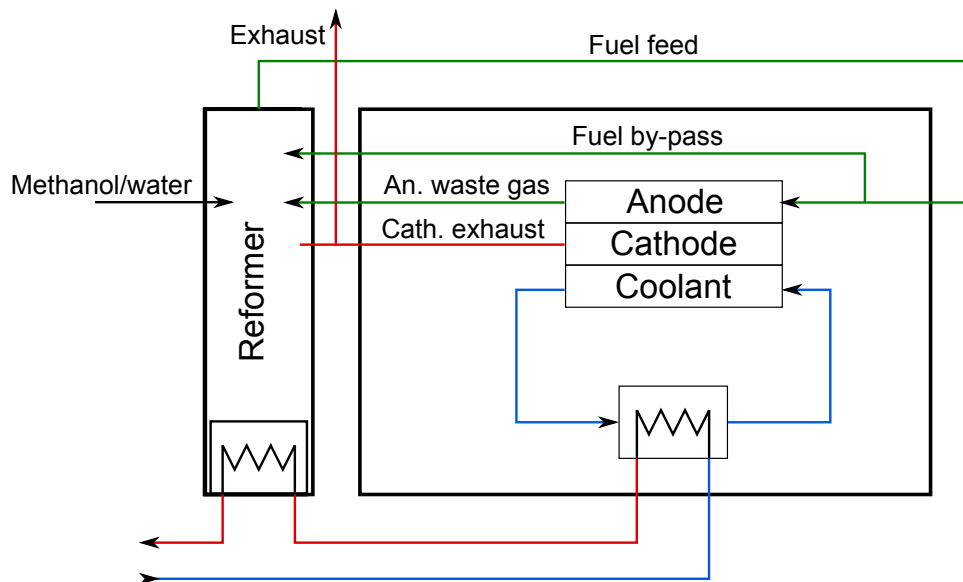


Figure 3.1. Conceptual schematic of the Serenergy H3 5000.

From Figure 3.1 it is shown that the cooling cycle is used to cool both the fuel cell stack and the reformer. However not all the heat will exit through the coolant, the exhaust

gas will still contain some waste heat that cannot be used. From a 3 kW fuel cell system approximately 2.5 kW of heat will be available in the coolant [Serenergy A/S, 2013a].

The schematic in Figure 3.1 on the previous page also shows that there is a fuel by-pass, that leads some of the fuel directly back to the reformer where it is used in a burner. This by-pass function is normally used during startup of the system to heat up the reformer faster. After startup the by-pass is shut off and only anode waste gas is used to retain the temperature in the reformer. The by-pass does however make it possible to increase the heat output from the fuel cell system by sending more fuel in the burner. This possibility means that, if required the heat to electricity ratio can be regulated.

3.2 Case for System Application

To consider the feasibility of such a system with an HTPEM FC and an absorption chiller a case has been selected for further studies. Serenergy are negotiating with an Indian company about delivering off-grid power systems to Base Transceiver Station (BTS) systems for the Indian railways. Currently the power is delivered by diesel generators, which also powers compression heat pumps for cooling. On Figure 3.2 an energy flow chart of the current setup can be seen.

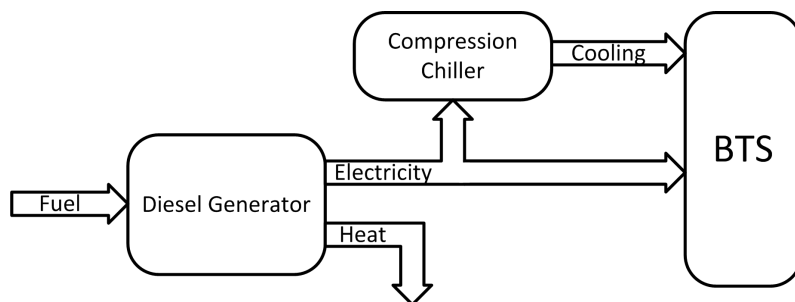


Figure 3.2. An energy flow chart of the current setup.

For a case like the one seen on Figure 3.2 it is evident that no heating is required, only power and cooling for the electronic systems in the BTS. To consider how to design a new solution for this case the system requirements have been listed in Table 3.1.

BTS Power Consumption	2880	W
Cooling requirement	3000	W
Annual operating time	2920	h

Table 3.1. System requirements for the BTS case.

It should be noted that the power and cooling requirements set in Table 3.1 are for peak load situations. In addition to the system demands, the investment and operational

costs will have to be determined to get an economical perspective. In Table 3.2 an economical comparison of three different configurations have been made; the three cases being the current diesel generator setup, a fuel cell combined with a traditional A/C and finally a fuel cell combined with an absorption chiller. For this evaluation it is assumed that the current system has to be replaced by a new, either by the same configuration or a new. The comparison is made based on fuel and maintenance expenses as well as investment costs and expected life service of each technology.

	Diesel Generator	FC with A/C	FC with Abs.	
Fuel cost	0.72	0.5	0.5	€
Fuel consumption	3	4	2.5	l/h
Annual fuel cost	6307	5840	3650	€
Cost diesel/fuel cell	4260	12500	7500	€
Cost comp./abs. chiller	2500	2500	3700	€
Maintenance	1057	200	200	€/PA
Expected service life	5	3	3	Years
Capital expenditures	6760	15000	11500	€
Operational expenses	7364	6040	3850	€/PA
Total cost ownership	8716	11040	7683	€/PA
Operational expense savings	-	1324	3514	€/PA
Return of investment	-	6.23	1.35	Years

Table 3.2. Comparison of technology expenses [Serenergy A/S, 2013a].

The results in Table 3.2 shows the operational expenses (OPEX) savings relative to the diesel generator configuration, the same goes for the return on investment (ROI). It is seen that the investment cost of the fuel cell is more expensive than of diesel generator. The compression chiller used in the two first case is the same with the same price. Since there are no previously examples of absorption chillers used for this purpose there are no available price. It has therefore been assumed that it will be possible to manufacture an absorption chiller for 3700€ or less.

The OPEX for the two cases using fuel cells is lower and will therefore return the extra investment cost over a certain period. This period however should certainly not extend to more than the expected lifetime which have been set to 3 years for the fuel cells. It should be noted that the expected lifetime of an absorption chiller is approximately 20 years for common designs [Herold et al., 1996]. The results in Table 3.2 shows that the ROI of the fuel cell with compression cycle is more than 6 years, which means this case is by far not feasible. Combined with an absorption chiller however the ROI is decreased to 1.35 years for the case shown in Table 3.2. This reduction is due to lower OPEX as well as the required electrical capacity is 3 kW compared to 5 kW for the two other cases, thereby a lower CAPEX.

In the previous Section 3.1 on page 7 it was mentioned that extra heat output from the fuel cell could be generated by burning extra fuel in the reformer burner. However, while doing this the fuel consumption will increase and this will have to be taken into account when the ROI is calculated. First the extra fuel consumption required to provide 1 kW of extra heat output for 1 hour will have to be calculated. For these calculations the reformer efficiency is not taken into account. The lower heating value of methanol (LHV_{Methanol}) is used to directly get the extra fuel required, as shown in Equation 3.1.

$$\dot{V}_{\text{Fuel}} = \frac{3600 \left[\frac{\text{kJ}}{\text{h}} \right]}{LHV_{\text{Methanol}}} , \text{ where } LHV_{\text{Methanol}} = 15780 \left[\frac{\text{kJ}}{\text{l}} \right] \quad (3.1)$$

The results from Equation 3.1 showed that an extra 0.228 l of methanol is required per hour to supply an extra heating output of 1 kW. Since the fuel is only 60% methanol the amount of fuel required is the amount of methanol divided by 0.6, giving 0.377 l per hour of extra fuel. It was decided that the ROI should not exceed 1.5 years to ensure the new configuration being a good investment. It was calculated that the continuous fuel consumption can increase by 0.38 l/h before the ROI exceeds 1.5 years, which corresponds to an extra heat input of 1.007 kW. Based on this calculation the required COP can be found as well. By knowing that the required cooling capacity is 3 kW while the heat output from the fuel cell is 2.5 kW and the maximum extra heat input is about 1 kW, the required COP is calculated from Equation 3.2.

$$COP_{\text{Min}} = \frac{\text{Cooling capacity}}{\text{Max heat input}} = \frac{3}{3.5} = 0.857 \quad (3.2)$$

The minimum COP found in Equation 3.2 will be used as an requirement in the further design and optimization process. To summarize this brief economical study, the chiller solution has to meet the following two requirements to keep the ROI below 1.5 years:

1. The capital expense cannot be higher than 3700 €
2. The COP cannot be less than 0.857

An energy flow chart of the new concept is shown on Figure 3.3 on the next page.

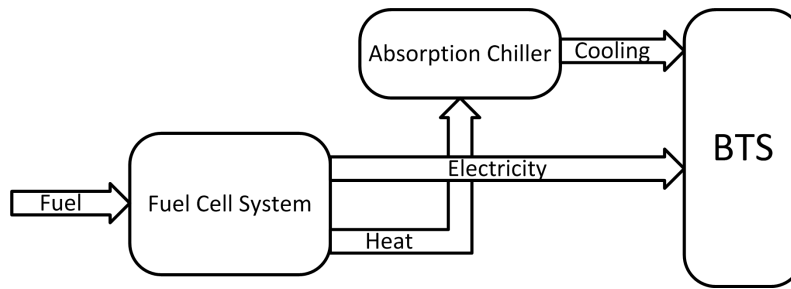


Figure 3.3. Energy flow chart of the fuel cell and absorption chiller concept.

Now that the case has been described and the system requirements have been determined the next step will be to look into the operation and components that makes up an absorption chiller.

3.3 Absorption Chiller

This section will describe the different components in the absorption chiller, covering the working principle of the cycle. From Figure 3.4 it is seen that the absorption chiller consists of two cycles, a refrigerant cycle and an absorbent cycle.

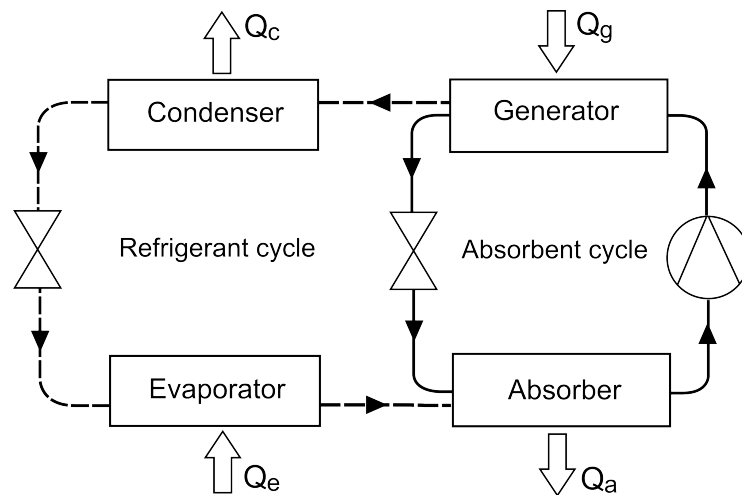


Figure 3.4. Simple schematic showing the key components in an absorption chiller.

The refrigerant cycle consist of a condenser and an evaporator and are similar to that of a traditional compression cycle. The absorption cycle works after the principle of boiling points elevation. In the absorber the concentration of absorbent in the solution decreases by the absorption of refrigerant vapor, which increases the saturation temperature. The increased saturation temperature will in the low pressure result in condensation of refrigerant. The condensation of refrigerant in the absorbent solution releases heat, which implies that the absorber requires cooling. Approximately half of the heat output is rejected from the absorber.

In the generator refrigerant is evaporated of the absorbent at a higher pressure which decreases the saturation temperature. The generator requires heat in order to evaporate the refrigerant from the solution. In this report the absorption cycle is driven by the coolant from the IM-FC system.

The difference between the solution temperatures out of the generator and out of the absorber is called the boiling point elevation. Elevating the boiling point with different concentrations is the principle that enables the absorption chiller to move heat from a lower temperature (evaporator) to a higher temperature (condenser). The types of heat exchangers used for the different applications are shown in Table 3.3.

Component	Type	Purpose
Evaporator	Air-cooled	Cooling load
Condenser	Air-cooled	Heat rejection
Absorber	Air-cooled	Heat rejection
Generator	Liquid-liquid	Heat driven

Table 3.3. Types of heat exchangers used in the absorption chiller.

Now that the components and operation have been described it is important to consider the different working fluids available for absorption chillers.

3.4 Working Fluids in Absorption Chillers

There are mainly two different working fluids used in absorption cycles, water/lithium bromide and ammonia/water. Which working fluid is used is crucial for the design of the chiller and it is important to consider the pros and cons for each working fluid. Some working fluids limitations may conflict with the desired application.

The listing of pros and cons for ammonia/water and water/lithium bromide chillers are based on [Herold et al., 1996] and [Subramaniam, 2008].

Ammonia/Water

Pros

- A high affinity between ammonia and water.
- Ammonia has a low freezing point of -77.7°C at 101.3 kPa which means the chiller is capable of cooling down to sub-zero temperatures.
- Given the high latent heat of ammonia ($1247.3 \frac{\text{kJ}}{\text{kg}}$ at 500 kPa) less refrigerant is needed to cover the cooling/heating load.

Cons

- The efficiency of an ammonia/water chiller is fairly low ($COP \approx 0.5$).
- The relative volatility between water and ammonia is low, resulting in a moderately amount of water vaporizing along with the ammonia in the generator. This means a mixture of ammonia and water enters the condenser and following the evaporator.
- Ammonia is both toxic and flammable, resulting in higher safety regulations.
- An ammonia/water mixture is corrosive, setting requirements for the materials used.

Water/Lithium Bromide

Pros

- The efficiency of a water/lithium bromide chiller is usually higher than that of an ammonia/water chiller ($0.7 < COP < 1.2$).
- High affinity between water and lithium bromide.
- Lithium bromide being a salt, means a large difference in volatility compared to water.
- The high latent heat of water, $2484 \frac{kJ}{kg}$ at 1 kPa, means a small amount of refrigerant is necessary to cover a given load of cooling or heating.
- A water/lithium bromide solution is neither toxic nor poisonous.

Cons

- Because of water freezing at 0°C the chiller cannot operate below this temperature.
- At high concentrations the lithium bromide can crystallize. Therefore it is necessary to limit the concentration and temperatures to avoid this phenomena.
- Water/lithium bromide has a lower mass diffusivity compared to ammonia/water. This means the rates of absorption and diffusion is lower affecting the performance of the chiller.

For this application water/lithium bromide is found most applicable. The latent heat of the water is higher as well as the system efficiency is usually higher meaning the system can be made more compact. Since the chiller is used to cool electronic equipment cooling temperatures below 0°C will not be necessary.

Since the working fluid will be water/lithium bromide it is important to look into the phenomena of crystallization. This can be investigated by using a Dühring plot(also called PTx-plot) as the one seen on Figure 3.5 on the following page.

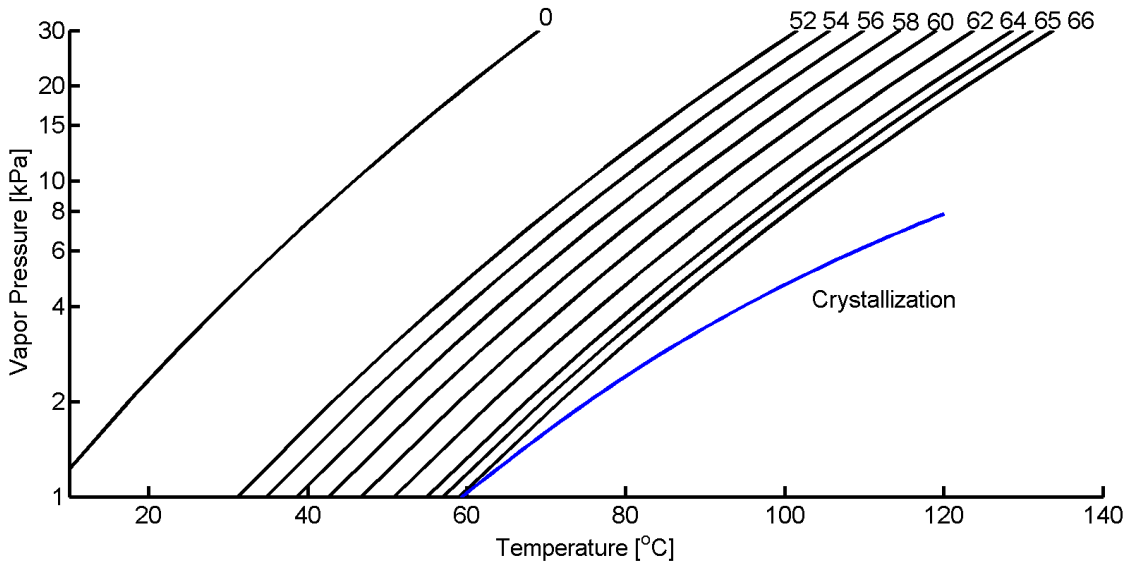


Figure 3.5. Dühring plot for water/lithium bromide solutions. The plot is based on [Arora, 2011]

On the Dühring plot shown in Figure 3.5 crystallization occurs in the area to the right of the crystallization line. The maximum allowed mass fraction before crystallization occurs varies depending on the pressure as well as the solution temperature. The highest mass fraction that does not cause crystallization is 0.65 lithium bromide. The concentration can vary within each component and to avoid the risk of crystallization the upper limit of the mass fraction is set to 0.64. This is assumed to be sufficient, however this is a matter that should be taken into further consideration in future studies.

Now that the case has been described with all requirements and the working fluid has been decided upon the modeling will be gone through.

System Modeling

The purpose of this chapter is to describe the developed models capable of predicting the steady state performance of different water/lithium bromide absorption chiller configurations. The operational conditions are listed in Table 4.1.

Variable	Value	Unit
Hot fluid inlet temperature	150	[°C]
Hot fluid ΔT	10	[°C]
Cooling capacity	3000	[W]
Surrounding temperature	35	[°C]
Load temperature	27	[°C]

Table 4.1. The conditions are given as input to the model.

These inputs will be used in the system models to determine states, mass fractions of lithium bromide and dimensions of the chillers.

The water/lithium bromide absorption cycle is designed different depending on the application. The simplest configuration is the single-effect absorption cycle, which can be seen on Figure 4.1 on the next page. The single-effect absorption cycle is typically used in waste heat applications because it is not able to take advantage of the higher temperatures available in high quality heat sources, such as burners or electric heaters. Furthermore it has a lower performance compared to more advanced technologies, which means that in most cases it is only a feasible solution if the heat input is a by-product.

A slightly more complex configuration is the double-effect absorption cycle which also is seen on Figure 4.2 on the following page. This cycle is capable of utilizing heat sources with higher temperature levels which improves the performance of the cycle. In some cases the more complex double-effect cycle can be built even more compact than the single-effect. Note that the condenser/generator 2 is one component (illustrated as two because of the difference in pressure levels).

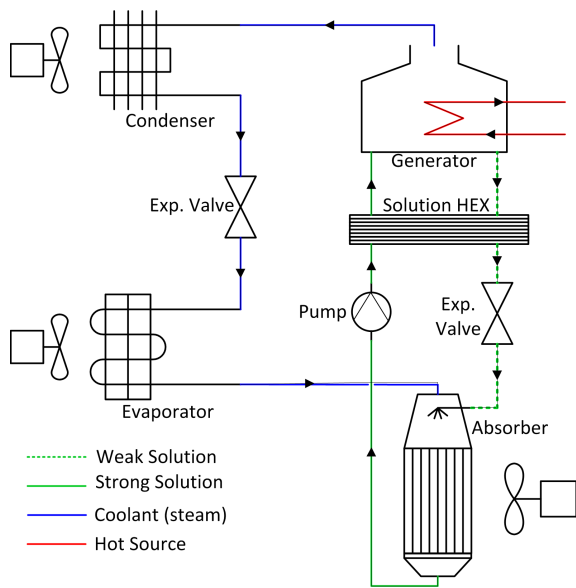


Figure 4.1. Schematic of a single-effect water/lithium bromide absorption cycle.

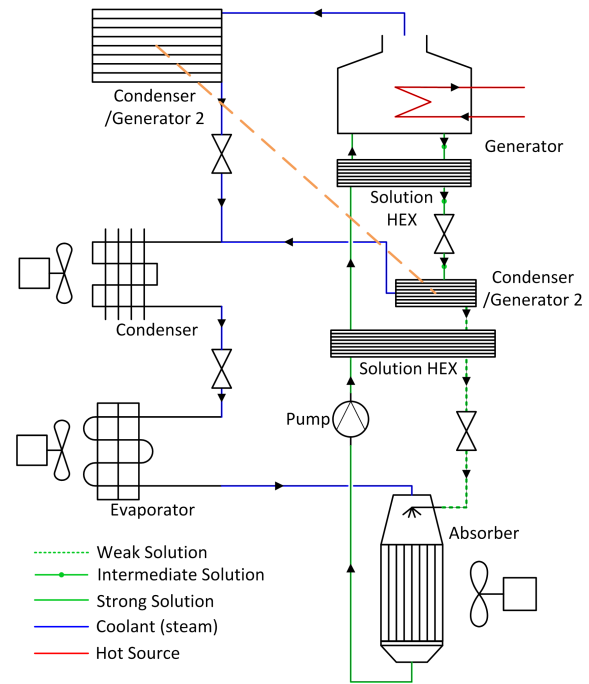


Figure 4.2. Schematic for double-effect water/lithium bromide absorption cycle.

In order to compare the two concepts it is necessary to create mathematical models which are able to predict the performance of the cycles for the given conditions. The cycles are simulated in steady state and the models are based on conservation of energy and mass.

4.1 Equations

This section describes the equations used to model the single-effect water/lithium bromide chiller. Making a black-box model, means that only the inlet and outlet conditions of each component are considered. The purpose of the model is determine the performance of the chiller based on configuration and operational conditions. The model will be used to determine the states of the system. The numbering used in the model is seen from Figure 4.3 on the next page.

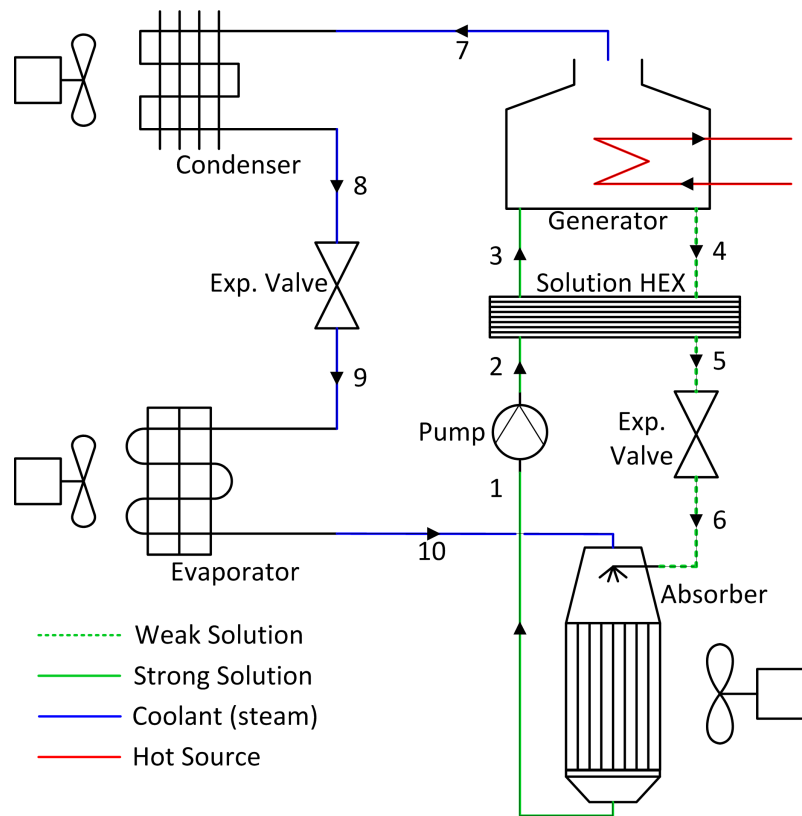


Figure 4.3. Schematic of a single-effect absorption chiller.

It was necessary to make some general assumptions for the system in order to develop the black-box model. These assumptions are listed below:

1. The chiller is assumed to be operated in steady state.
2. Heat losses are not considered.
3. Pressure losses are not considered.
4. Constant heat transfer coefficients.
5. Solution heat exchanger and generator is counter-flow.
6. All air-cooled heat exchangers are cross flow.

Some additional assumptions are made for each component, which can be seen from Table 4.2 on the following page. It is assumed that the solution outlet is saturated liquid from both absorber and generator. In addition to that it is assumed the water leaving the generator and evaporator is saturated vapor and the water exiting the condenser is saturated liquid. Finally the two valves are assumed to be isenthalpic, which means that there are no heat losses.

Point	Equation	Assumption
1	$x_1 = 0$	saturated liquid
4	$x_4 = 0$	saturated liquid
6	$h_6 = h_5$	isenthalpic valve
7	$w_7 = 0, x_7 = 1$	saturated water vapor
8	$w_8 = 0, x_8 = 0$	saturated liquid water
9	$h_9 = h_8$	isenthalpic valve
10	$w_{10} = 0, x_{10} = 1$	saturated water vapor

Table 4.2. Assumptions for the single-effect model.

The assumptions in Table 4.2 are used in the equations for conservation of energy and mass in the model.

Conservation of Mass

In order to determine the mass flow rates in the system some notations are made. In this report the mass fraction $w[\frac{kgLiBr}{kgLiBr+kgWater}]$ is referring to the amount of lithium bromide to the total mass of the solution. The script ws is referring to the weak solution (weak in refrigerant, which in this case is water), and ss represents the strong solution. The refrigerant flow is represented by R .

The mass flow rates in the system are determined from conservation of total mass in Equation 4.1

$$\dot{m}_{ss} = \dot{m}_{ws} + \dot{m}_R \quad (4.1)$$

and conservation of mass of water in Equation 4.2.

$$\dot{m}_R = \dot{m}_{ss} \cdot (1 - w_{ss}) - \dot{m}_{ws} \cdot (1 - w_{ws}) \quad (4.2)$$

Conservation of Energy

The conservation of energy is formulated based on the equations seen from Table 4.3 on the facing page. The calculations of the logarithmic mean temperature difference (ΔT_{LMTD}) are shown for each of the components. The absorber, condenser and evaporator are air-cooled, which means that the temperature on the air side is constant.

Component	Equation	LMTD
Absorber	$Q_a = UA_a \Delta T_{LMTD,a}$ $Q_a = \dot{m}_R \cdot h_{10} + \dot{m}_{ws} \cdot h_6 - \dot{m}_{ss} \cdot h_1$	$\Delta T_{a1} = T_6 - T_\infty$ $\Delta T_{a2} = T_1 - T_\infty$ $\Delta T_{LMTD,a} = \frac{\Delta T_{a1} - \Delta T_{a2}}{\ln(\Delta T_{a1} / \Delta T_{a2})}$
Condenser	$Q_c = UA_c \Delta T_{LMTD,c}$ $Q_c = \dot{m} \cdot (h_7 - h_8)$	$\Delta T_{c1} = T_7 - T_\infty$ $\Delta T_{c2} = T_8 - T_\infty$ $\Delta T_{LMTD,c} = \frac{\Delta T_{c1} - \Delta T_{c2}}{\ln(\Delta T_{c1} / \Delta T_{c2})}$
Evaporator	$Q_e = UA_e \Delta T_{LMTD,e}$ $Q_e = \dot{m}_R (h_{10} - h_9)$	$\Delta T_{e1} = T_{load} - T_9$ $\Delta T_{e2} = T_{load} - T_{10}$ $\Delta T_{LMTD,e} = \frac{\Delta T_{e1} - \Delta T_{e2}}{\ln(\Delta T_{e1} / \Delta T_{e2})}$
Generator	$Q_g = UA_g \Delta T_{LMTD,g}$ $Q_g = \dot{m}_g \cdot cp \cdot (T_{11} - T_{12})$ $Q_g = h_4 \cdot \dot{m}_{ws} + h_7 \cdot \dot{m}_R - h_3 \cdot \dot{m}_{ss}$	$\Delta T_{g1} = T_{12} - T_3$ $\Delta T_{g2} = T_{11} - T_4$ $\Delta T_{LMTD,g} = \frac{\Delta T_{g1} - \Delta T_{g2}}{\ln(\Delta T_{g1} / \Delta T_{g2})}$
HEX	$Q_{HEX} = UA_{HEX} \Delta T_{LMTD,HEX}$ $Q_{HEX} = \dot{m}_{ss} \cdot (h_3 - h_2)$ $Q_{HEX} = \dot{m}_{ws} \cdot (h_4 - h_5)$	$\Delta T_{HEX1} = T_4 - T_3$ $\Delta T_{HEX2} = T_5 - T_2$ $\Delta T_{LMTD,HEX} = \frac{\Delta T_{HEX1} - \Delta T_{HEX2}}{\ln(\Delta T_{HEX1} / \Delta T_{HEX2})}$

Table 4.3. Equations for conservation of energy in the single-effect water/lithium bromide chiller.

The definition of the cooling COP is seen from Equation 4.3. This formulation is different from compression air-conditioners because the input is measured in heat input instead of work done by the compressor.

$$COP_c = \frac{Q_e}{Q_d} \quad (4.3)$$

In order to conclude the equation set a relation between temperatures and enthalpies is required. The enthalpy of water and lithium bromide can be found respectively as a function of temperature and pressure: $h_{\text{component}} = f(T, P)$ and the mixture enthalpy of the water/lithium bromide solution can be found by adding the two enthalpies multiplied with the mass fraction of each component: $h_{w/\text{libr}} = h_{\text{water}} \cdot (1 - w_{\text{LiBr}}) + h_{\text{LiBr}} \cdot w_{\text{LiBr}}$.

The model for the double-effect water/lithium bromide chiller is based on the same general assumptions as the single-effect. The detailed description of the model can be found in Appendix A on page 87.

Both models consist of a set of coupled non-linear equations and require relations between enthalpies and temperatures to conclude the equation set. An obvious choice to solve these equation sets is Engineering Equation Solver (EES), which is a program that provides both fluid properties for water/lithium bromide mixtures and includes a numerical solver.

4.2 Engineering Equation Solver

EES is a mathematical program consisting of a numerical solver and several built-in functions, such as thermodynamic properties for many fluids and solids. There are no preformulated physical equations in EES, the necessary equations and relations will have to be defined.

Numerical Solver

The solver in EES uses a modified Newton-Raphson method capable of solving non-linear algebraic equations. The solver requires a Jacobian Matrix that is numerically evaluated for every iteration. Being a Newton-Raphson solver an initial guess is necessary and the residual Jacobian Matrix is thereafter solved based on the initial guess. Following this a better guess vector is obtained and so the iterations will continue until the residual limits have been met. The residual limits are initially defined and can be changed in the Stop Criteria menu. Having a precision of 96 bit which translates to approximately 20 decimals. There is also implemented a sparse matrix to reduce the computational time [Klein, 2013].

Thermodynamic Properties

When modeling in EES there are correlations for thermodynamic properties of a large amount of liquids and gases. Particularly for this purpose there are thermodynamic properties available for water/lithium bromide solutions at different mass fractions. These correlations are available by using look-up and call functions. Hereby properties such as temperature, mass fraction, enthalpy and pressure can be found. An example of how the temperature can be found, is shown in Equation 4.4.

$$\text{CALL LiBrCalcTfromPX}(P;x:T) \quad (4.4)$$

In the call function the pressure (P) and mass fraction (x, fraction of LiBr) is given and the temperature of the solution is returned. The correlations used to find the thermodynamic properties of water/lithium bromide solutions covers a full range of composition and a temperature range of 273 to 500 K. The correlations have been compared with experimental data and the accuracy have been determined in [Pátek and Klomfar, 2006]. The corresponding accuracies for each of the properties can be seen in Table 4.4 on the next page.

Property	Accuracy
Density	$\pm 0.5\%$
Pressure	$\pm 2.1\%$
Isobaric heat capacity	$\pm 2.0\%$
Enthalpy	$\pm 10 \text{ kJ kg}^{-1}$
Entropy	$\pm 0.03 \text{ kJ kg}^{-1} \text{ K}^{-1}$

Table 4.4. Accuracies for each of the thermodynamic properties for water/lithium bromide solutions in EES [Pátek and Klomfar, 2006].

4.3 Optimization Theory

Mathematical optimization, also called mathematical programming, is a mathematical method for determining the best available values of a given objective function from a specified domain. The solution domain (also called the feasible region) is defined by the constraints. The class of optimization depends on the formulation of the objective function and its constraints. The six general classes of mathematical programming is seen from Table 4.5.

	Real numbers	Real numbers + Integers	Integers
Linear	LP	MILP	ILP
Non-linear	NLP	MINLP	INLP

Table 4.5. Classes of optimization.

The optimization in this report will be Non Linear programming (NLP) because of the nature of the model equations and constraints. The chiller model consist of a set of equality constraints which design is restricted by a set of equality constraints. The general non-linear optimization problem formulation is seen below:

$$\begin{aligned}
 \text{Objective: } & \min_{x \in X} f(x) \\
 \text{where: } & f: R^n \rightarrow R \\
 & x \in R^n \\
 \text{subject to: } & h_i(x) = 0, i \in I = 1, \dots, p \\
 & g_j(x) \leq 0, j \in J = 1, \dots, m
 \end{aligned}$$

The objective function $f(x)$ is the function to be minimized by changing the independent variables x . The equality constraints $h_i(x)$ consists of the model equations previously described in Section 4.1 on page 16. In order to avoid an unphysical solution a set of inequality constraints $g_j(x)$ are formulated. In order to solve the optimization problem a suitable optimization algorithm is required.

EES has built-in optimization algorithms which makes it possible to find the maximum or minimum value of a variable. The user specifies the variable to be optimized and

the independent variables which are to be manipulated. The choice of algorithm is dependent of the number of independent variables. If only one independent variable is specified (one degree of freedom) EES uses either a recursive quadratic approximation method or Golden section method.

The optimization problem in this report involves more degrees of freedom and EES include two algorithms for multi-dimensional optimization; the Variable Metric method and Direct Search method. The Variable Metric method is usually faster than the Direct Search method, but "*it may be confounded if the optimum is constrain to be on a bound*" [Klein, 2013]. Based on experience the Direct Search method is employed in this report, because it is expected that the optimum in some cases will be confined by design constrains.

Direct Search method (also known as Powell's method) minimizes a function by using a bi-directional search along a set of search vectors. The model equations does not need to be differentiable which is important since the chiller model employ call functions to determine fluid properties. In EES Powell's method uses Brent's method to determine optimum values along each search direction.

Brent's method is good for finding optimum values for continuous but complex functions, because it combines the bisection method, the secant method and inverse quadratic interpolation.

4.4 Cost Function

It is desired by Serenergy to get an inexpensive and simple concept, which still is competitive with the current solutions. The objective in the optimization is to minimize the investment cost of the system and the objective function is the total cost of the mass- and heat exchangers.

Cost functions for the individual heat exchangers were found in [Linnhoff et al., 1994]. It was not possible to find heat exchangers matching exactly the types considered for the absorption chillers. In order to estimate the cost of the absorber and generator the price was found for similar heat exchangers. The tables 4.6 on the facing page and 4.7 on page 24 shows the type of heat exchanger and the cost function chosen for each component.

Component	Considered type of HEX	$C \left[\frac{\pounds}{(W/K)} \right]$	$U \left[\frac{W}{(m^2K)} \right]$
Evaporator	Shell and tube bare pipe HEX, Cold side: Boiling water Hot side: Low pressure gas	1.667	105
Condenser	Shell and tube bare pipe HEX, Cold side: Low pressure gas, Hot side: Condensing steam	1.636	107
Absorber	Shell and tube bare pipe HEX, Cold side: Low pressure gas, Hot side: Condensing steam	1.636	107
Generator	Shell and tube bare pipe HEX, Cold side: Boiling water, Hot side: Low viscosity organic fluid	0.96	677
Solution HEX	Plate HEX, Cold side: Low viscosity organic fluid, Hot side: Low viscosity organic fluid	0.055	2734

Table 4.6. Table showing the cost functions (C) for each of the components in the single -effect chiller. U is the assumed U-value for the heat exchangers [Linnhoff et al., 1994].

The cost functions are used to obtain a cost price for the heat exchanger depending on the UA-value necessary for the given component. The output from the cost functions are given in pound sterling. The cost functions are valid for UA-values in the order of magnitude of $1000 \left[\frac{W}{K} \right]$.

Component	Considered type of HEX	$C \left[\frac{\pounds}{(W/K)} \right]$	$U \left[\frac{W}{(m^2K)} \right]$
Evaporator	Shell and tube bare pipe HEX, Cold side: Boiling water, Hot side: Low pressure gas	1.667	105
Condenser	Shell and tube bare pipe HEX, Cold side: Low pressure gas, Hot side: Condensing steam	1.636	107
Absorber	Shell and tube bare pipe HEX, Cold side: Low pressure gas, Hot side: Condensing steam	1.636	107
Generator	Shell and tube bare pipe HEX, Cold side: Boiling water, Hot side: Low viscosity organic fluid	0.96	677
Condenser/Generator	Shell and tube bare pipe HEX, Cold side: Boiling water, Hot side: Condensing steam	0.454	1432
Solution HEX x 2	Plate HEX, Cold side: Low viscosity organic fluid, Hot side: Low viscosity organic fluid	0.055	2734

Table 4.7. Table showing the cost functions (C) for each of the components in the double-effect chiller. U is the assumed U-value for the heat exchangers[Linnhoff et al., 1994].

The cost functions were found in literature from 1997, resulting in the cost being outdated. To bring the cost functions up to date the Chemical Engineering Plant Cost Index (CEPCI) was used. The index for January 1997 and for January 2013 was found and used in Equation 4.5 [Chemical Engineering, 1997], [Chemical Engineering, 2013].

$$\frac{\text{Index 2013}}{\text{Index 1997}} = \frac{630.2}{385.5} = \frac{\text{Cost 2013}}{\text{Cost 1997}} \quad (4.5)$$

With the updated cost functions it was finally possible to obtain a total cost for the heat exchangers in the absorption chiller. There will be additional costs other than the heat exchangers, such as the pump, piping, control units etc. These components will however be necessary for both the single- and double-effect chiller and are assumed to even out. The heat exchangers are also assumed to account for the largest part of the cost.

4.5 Optimization Problem

In this section the optimization problem is formulated. The objective function is the Capital Expenditure (CAPEX) which is the cost of the of the heat and mass exchangers described in previously section. CAPEX is minimized subject to the black-box model of the chiller, constrained by physical constrains, design constrains and operational conditions. Minimize:

$$\text{CAPEX} = \sum_{i=a,c,e,g} \text{Cost}_i(P_{hi}, P_{lo}, w_{ws}, w_{ss}, Q_g) \quad (4.6)$$

$$\text{Cost}_i = C_i \cdot UA_i \cdot \text{index} \quad i \in a, c, e, g \quad (4.7)$$

Subject to:

$$\sum_{i=a,c,e,g,hex} h_{in,i} \cdot \dot{m}_{in,i} - h_{out,i} \cdot \dot{m}_{out,i} + W_{in,i} - W_{out,i} + Q_{in,i} - Q_{out,i} = 0 \quad (4.8)$$

$$\sum_{i=a,c,e,g,hex} \dot{m}_{in,i} - \dot{m}_{out,i} = 0 \quad (4.9)$$

Where:

Physical constrains:	
$P_{lo} \leq P_{hi}$	The low pressure cannot exceed the high pressure
$P_{lo} \leq P(\text{water}; T_c, x = 1)$	The low pressure cannot exceed the vapor pressure at room temperature
$P_{hi} \geq P(\text{water}; T_w, x = 1)$	The high pressure cannot be less than the vapor pressure at ambient temperature
$\dot{m}_{ws} \leq \dot{m}_{ss}$	The mass flow of the weak solution cannot exceed the mass flow rate for the strong solution
Design constrains:	
$COP \geq 0.857$	The COP of the chiller must be higher than 0.857
$Q_e = 3000$	The cooling demand is 3000 W
$\epsilon = 0.64$	The effectiveness of the solution heat exchanger
Operational conditions:	
$T_{g,i} = 150$	The coolant temperature entering the generator
$T_{g,o} = 140$	The coolant temperature leaving the generator
$T_\infty = 35$	Ambient temperature
$T_{load} = 27$	Load target temperature

Table 4.8. Physical and design constrains, as well as operational conditions.

4.6 Results

This section will present the results from the optimization case described previously. The given input to the model was listed as operational conditions and requirements in Table 4.8 on the previous page. From these inputs the built-in optimization algorithm in EES was used to find the results plotted in the Dühring plot in Figure 4.4.

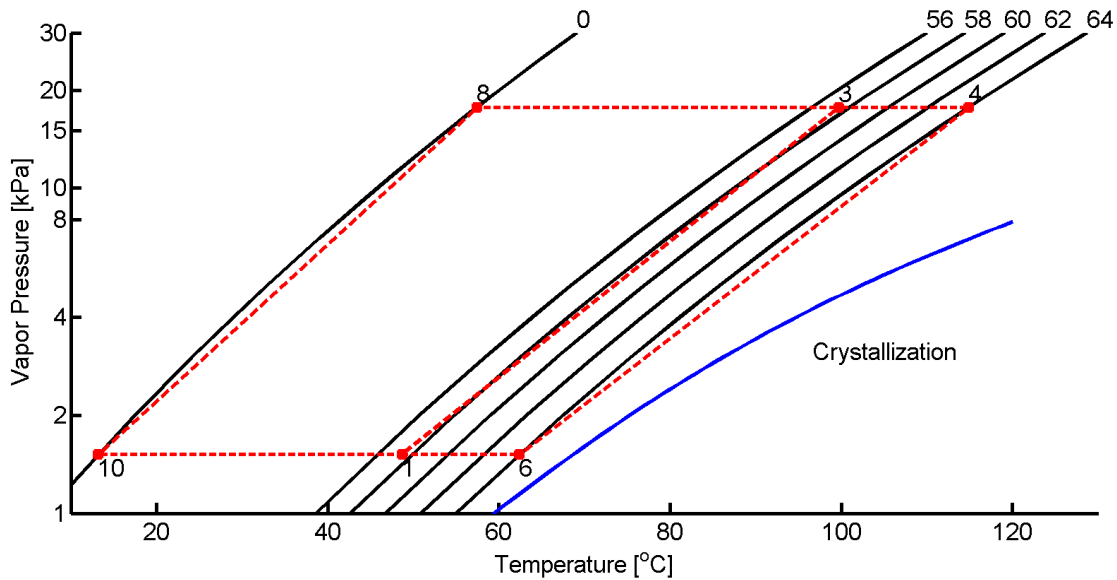


Figure 4.4. Dühring (PTx) plot of the results found by optimizing the black-box model.

The Dühring plot shows the pressure, temperature and mass fraction (%) in each part of the cycle. It can however only be used to present the states in the parts of the cycle where saturated vapor is present. From Figure 4.4 it is seen how the pure water vapor from point 10 is absorbed by the weak solution from point 6 and resulting in a stronger solution in point 1. From point 1 to 3 the pressure is increased in the pump and the temperature raised in the solution heat exchanger. Point 3 represents the generator where water vapor is evaporated to point 8, resulting in a weak solution in point 4. The Dühring plot also verifies that the mass fraction does not exceed 0.65 [kg/kg] lithium bromide, thereby avoiding crystallization.

From the schematic in Figure 4.5 on the next page the exact temperatures, pressures, mass fraction and enthalpies can be found for the different locations in the absorption chiller. The temperatures marked in bold font are inputs given to the model, while the rest are results produced by the model. In the evaporator the temperature is constant while the enthalpy of the water vapor is raised, indicating a phase change taking place. In the absorber the concentration of the solution is lowered because of the water vapor being absorbed. The pressure is raised through the pump and the solution heat exchanger raises the temperature of the strong solution while lowering the temperature of the weak solution. In the generator the temperature of the solution is raised and the mass fraction increased because of the evaporating water. Finally,

in the condenser the temperature is lowered, this because the water vapor from the generator is superheated and is cooled before the phase change takes place. The superheating of the vapor can occur because of the higher boiling point of the solution mixture.

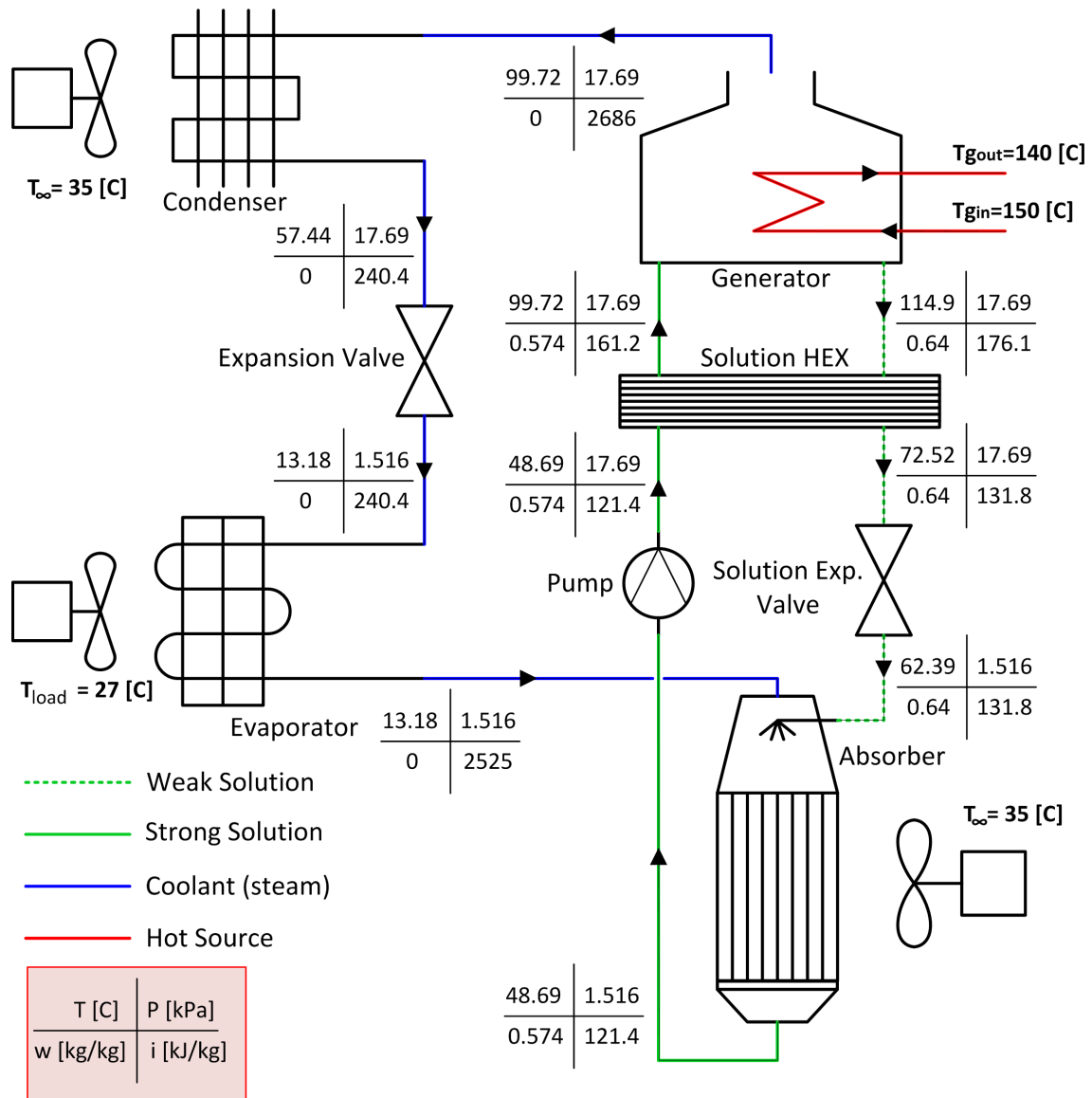


Figure 4.5. Schematic showing the results for the single-effect cycle. The units of the results are marked in the red square in the lower left corner.

Now that the temperatures, pressures and mass fractions have been presented the next step is to look into the heat exchangers required to obtain these results. The UA-value, transferred heat and cost of each heat and mass exchanger are presented in Table 4.9 on the following page.

Component	UA-Value [$\frac{W}{K}$]	Q [W]	Cost [€]
Absorber	168.5	3276	532.2
Condenser	80.44	3211	258.12
Evaporator	217.1	3000	709.92
Generator	92.65	3487	174.48
Solution HEX	26.6	510	-
Total Cost			1674.72

Table 4.9. Results for optimized single-effect chiller configuration.

The results in Table 4.9 shows the required UA-value for each component and it is seen that the evaporator requires the highest UA-value. The transferred heat in the evaporator is also an input given to the model. The energy balance can easily be tested as shown in Equation 4.10.

$$Q_g + Q_e - Q_c - Q_a = 3487 + 3000 - 3211 - 3276 = 0 \quad (4.10)$$

The total cost of all the heat exchangers is found to be 1674.72 €. This however is a rough estimate where the cost of each heat exchanger is purely based on the cost functions previously defined in Table 4.6 on page 23. The calculated UA-value for the solution heat exchanger is so low that it is far from the range the cost functions are valid for, which is why there are no cost presented for it. In addition to the costs being inaccurate estimates there will also be several additional costs, such as the centrifugal pump, electronics/control, fans, valves etc. However, the calculated prize of 1674.72€ is well below the maximum prize of 3700 €.

The optimization in EES had problems giving results for the double-effect model, caused by a lot of constrains in the model. By optimizing on the high pressure only it was seen that the lowest cost was 3575.64 €, which is more than double of the single-effect chiller. Therefore it is assumed that the double-effect chiller will not be a cheaper alternative for this application. The results from the double-effect model can be seen in Appendix A on page 87.

Component Modeling

This chapter will be used to describe the modeling approach used to dimension the components of the chiller. The conceptual illustration of the chiller concept is seen from Figure 5.1.

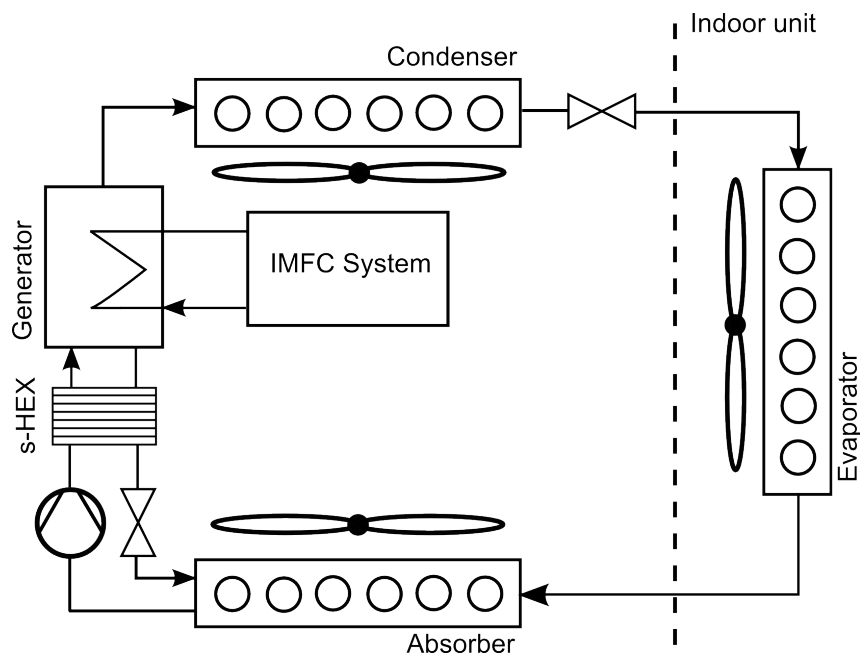


Figure 5.1. Plumbing schematic for chiller concept

The schematic shows the components which comprise the absorption chiller. All heat exchangers except the solution heat exchanger will be of the falling film type. The condenser, evaporator and absorber are air-cooled vertical falling film heat exchangers, while the generator is a liquid-heated horizontal falling film heat exchanger. In this report these four main components will be the scope of the modeling, the rest of the components will not be considered. More effort will be put into modeling the absorber and generator since these components are the most complex. These components are normally designed for a higher capacity and it is therefore necessary to make detailed models to determine the size and geometry. The evaporator and condenser will be modeled with a simpler approach to get an estimate of the physical dimensions. In the models there are some general assumptions:

- All tubing and manifolding are neglected, e.g. in the absorber it is assumed that the flow is divided equally between the parallel vertical tubes. The same goes for the generator, the nozzles used to spread the solution over the tubes are not considered, and the flow is assumed perfectly distributed over the tubes.
- All pressure losses are neglected, both for tubing and components. The pressure losses are important to investigate for an absorption chiller since it is operating with very low pressure differences between evaporator and condenser, but this topic is out of the scope of this report.

5.1 Absorber

In the absorber water vapor from the evaporator is absorbed into the weak aqueous lithium-bromide solution. The latent heat of the absorbed vapor is transferred from the liquid solution to a cooling media. The absorber can be either air- or liquid-cooled. In this particular application it is chosen to use an air-cooled absorber since it is the simplest way to remove the excess heat. The absorber used for this application is a vertical tube falling film absorber and considered as a staggered tube bundle of finned tubes. A simple drawing of the absorber principle can be seen from Figure 5.2.

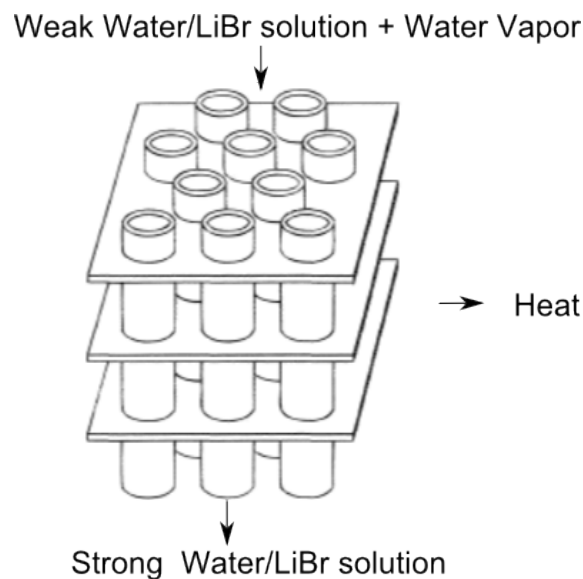


Figure 5.2. Sketch showing the principle of an absorption chiller.

The understanding of the simultaneous heat and mass transfer in a falling film is incomplete, which means that most current design approaches is confined to smooth surfaces and highly dependent on empirical data. This implies that the current design approaches only are valid for certain operational conditions. In order to find a suitable modeling approach for the application a short literature study is performed.

The first paper to present a successful prediction of mixed transport phenomena in horizontal falling film was [Grossman, 1983]. Grossman found an analytical solution

to the energy and diffusion equation for laminar films assuming an adiabatic wall and constant interface properties. The solution was obtained by using a Nusselt's solution velocity profile for the film and applying Fourier's method. The assumptions in the method lead to a 40% under-prediction of the length of absorber required to achieve the desired outlet temperature and concentration level.

The same year [Andberg and Vliet, 1983] presented another approach for solving the energy and diffusion equations for laminar film. The model was numerical and allowed for solutions of non-linear concentration profiles. In addition to that the differential equations were solved numerically using finite difference approach, which allowed film thickness, flow rate and velocity to increase as vapor is absorbed.

In [Yuksel and Schlunder, 1988] a method was developed to predict the mass transfer for non-isothermal absorption in wavy-transition and turbulent films. The model was compared to experimental data and yield agreement in order of 30%. In the model Fick's law formulation allowed a finite dilution of water in the film.

The previous models for falling film absorbers tended to under-predict the mass transfer for low Reynolds numbers. The importance of the mass transfer coefficient on mass transfer in laminar-wavy flow was discovered by [Perez-Blanco, 1988]. They developed a model that predicted the concentrations, heat duty and mass absorbed within 10% of experimental results for low laminar-wavy film.

In [Patnaik et al., 1993] design charts were produced for liquid-cooled vertical tube absorbers using lithium bromide. The design charts are produced from a model which solves the energy and transport equation numerically. In this report a variant of the modeling approach [Patnaik et al., 1993] is applied and rewritten to match the air-cooled concept.

Absorber Model

The absorber consist of a tube bundle of M tubes, but in order to simplify the model the heat and mass transfer is only calculated for one tube, which means that $\dot{m}_{\text{tube}} = \dot{m}_{\text{inlet}}/M_{\text{tubes}}$. This greatly reduces the number of equations to solve and simplifies the model. The assumption will be corrected by introducing the bundle effect when calculating the forced convection outside the tubes. Figure 5.3 on the next page shows the temperature and mass fraction profiles in one element, close to the tube wall.

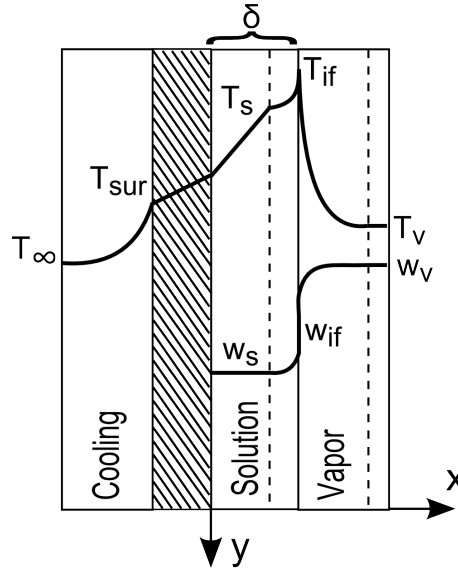


Figure 5.3. Sketch showing the temperature and mass fraction profiles in an element of the absorber. The illustration shows the temperature and mass fraction at surface (sur), solution (s), interface (if) and vapor (v).

The water/lithium bromide solution starts forming a film on the inside of the tube and flows downward under the influence of gravity. The mass flow of the film increases as vapor is absorbed into the liquid film. The absorption process is driven by the difference in lithium bromide mass fraction between the solution w and the solution/vapor interface w_{if} . When vapor is absorbed into the solution it releases latent heat, which has to be removed in order to avoid increase in temperature. The heat transfer from the film is driven by the difference between solution temperature T and surrounding temperature T_{∞} .

The objective is to develop a method for calculating the amount of vapor absorbed into the falling film and the outlet conditions. Based on Figure 5.3 a set of coupled partial differential equations is used to describe the conservation of mass, energy and momentum, these equations can be seen from Equation 5.1, 5.2 and 5.3.

$$u \cdot \frac{\partial w}{\partial x} + v \cdot \frac{\partial w}{\partial y} = D_{ab} \cdot \frac{\partial^2 w(x)}{\partial y^2} \quad (5.1)$$

$$u \cdot \frac{\partial T}{\partial x} + v \cdot \frac{\partial T}{\partial y} = \alpha \cdot \frac{\partial^2 T(x)}{\partial y^2} \quad (5.2)$$

$$u \cdot \frac{\partial u}{\partial x} + v \cdot \frac{\partial u}{\partial y} = g + \nu \frac{\partial^2 u(x)}{\partial y^2} \quad (5.3)$$

There is no analytical solution to this set of partial differential equations, so it is necessary to perform a spatial discretization in order to obtain a numerical solution. Each partial differential equation is formulated as a set of N coupled ordinary differential equations. Each element is assumed to be lumped and the heat and mass transfer in the horizontal direction is assumed to be uniform. The schematic for the discretization can be seen from Figure 5.4.

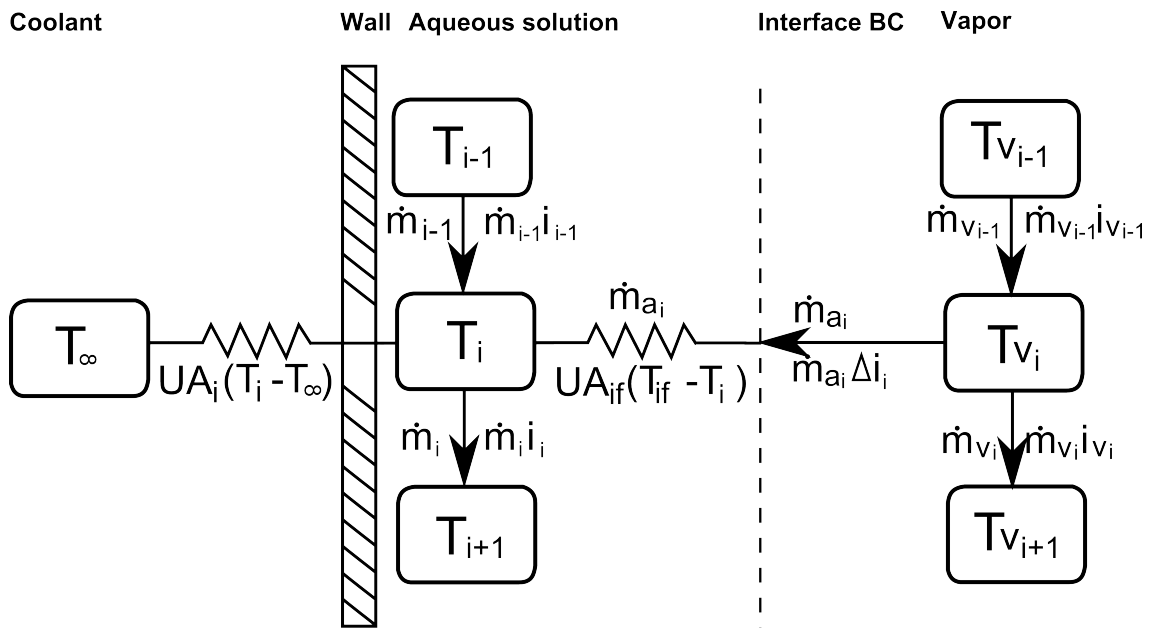


Figure 5.4. Sketch illustrating the spatial discretization of the absorber.

The model is developed based on the following assumptions stated in Table 5.1 on the next page

	Solution
1	The fluid is Newtonian
2	The heat and mass transfer is assumed to be in steady state
3	The heat and mass transfer is assumed to be one-dimensional
4	The falling film is assumed to be wavy-laminar
5	Gravity is the only external force acting on the film
	Vapor
6	The water vapor is saturated and pure
7	The pressure of the water vapor is homogenous
	Interface
8	There is no mass transfer resistance on the vapor/solution interface
9	The heat transfer from the vapor to the falling film is only due to condensation of vapor
10	The vapor drag on the falling film is neglected
11	The mass absorbed is relatively small compared to the film flow

Table 5.1. Assumptions in the absorber model.

The coupled equations describing the conservation of mass, momentum and energy in each of the N elements is written in a general form where $i = 1 : N$.

Conservation of mass

The equations for conservation of mass of lithium bromide and for total mass in the falling film are derived using forward difference and are shown on general form in Equation 5.4 and 5.5 respectively.

$$\dot{m}_{s,i-1} - \dot{m}_i + \dot{m}_{a,i} = 0 \quad (5.4)$$

$$(1 - w_{s,i}) \cdot \dot{m}_i = (1 - w_{s,i-1}) \cdot \dot{m}_{i-1} + (1 - w_v) \cdot \dot{m}_{a,i} \quad (5.5)$$

The mass of the vapor absorbed into the falling film ($m_{a,i}$) is dependent on the mass fraction gradient in the vapor-liquid interface and the mass transfer coefficient, as shown in Equation 5.6. The vapor-liquid interface consist of saturated water/lithium bromide solution and the mass fraction is found as $w_{if} = f(w, P)$.

$$\dot{m}_{a,i} = \kappa_{m,i} \cdot A_{if,i} \cdot \rho_i \cdot (w_{s,i} - w_{if,i}) \quad (5.6)$$

The mass transfer coefficient is found using Equation 5.7.

$$\kappa_{m,i} = \frac{Sh_{s,i} \cdot D_{ab,i}}{\delta_{s,i}} \quad (5.7)$$

In order to determine the mass transfer coefficient it is required to know the Sherwood number(Sh), the mass diffusivity of water vapor into an aqueous water/lithium bromide solution(D_{AB}) and finally the film thickness.

The Sherwood number is estimated with the asymptotic empirical correlation in Equation 5.8 and 5.9 by [Yih and Chen, 1982], which is based on a mass transfer mechanism associated with eddy dissipation at the surface.

$$Sh_{s,i} = \frac{\kappa_{s,i} \delta_{s,i}}{D_{AB,i}} = 1.099 \cdot 10^{-2} \cdot (4 \cdot Re_{s,i})^{0.955} \cdot Sc_{s,i}^{0.5}, Re_{s,i} \leq 75 \quad (5.8)$$

$$Sh_{s,i} = \frac{\kappa_{s,i} \delta_{s,i}}{D_{AB,i}} = 2.995 \cdot 10^{-2} \cdot (4 \cdot Re_{s,i})^{0.2134} \cdot Sc_{s,i}^{0.5}, 75 \leq Re_{s,i} \leq 400 \quad (5.9)$$

The mass diffusivity of water vapor into an aqueous water/lithium-bromide solution is calculated from Equation 5.10. The input to the correlation is the molar concentration of lithium bromide in $\frac{mol}{l}$.

$$D_{ab,i} = (3.11 \cdot 10^{-5} \cdot w_{m,i}^6 - 0.001407 \cdot w_{m,i}^5 + 0.02385 \cdot w_{m,i}^4 - 0.1836 \cdot w_{m,i}^3 + 0.5984 \cdot w_{m,i}^2 - 0.6082 \cdot w_{m,i} + 1.523) \cdot 10^{-9}, 0 < w_{m,i} < 0.55 \quad (5.10)$$

where:

$$w_{m,i} = w_{s,i} \cdot \frac{\rho_{s,i}}{MW_{LB}} \cdot 10^3 \frac{mol}{kmol} \cdot 10^{-3} \frac{m^3}{l} \quad (5.11)$$

The equation is a curve fit with $R = 0.99$ based on a plot from [Potnis et al., 1993]. However the plot found did only cover concentrations in the range 0.5 to 11.5 mol/l or mass fraction of 0.04 to 0.59 kg/kg. Since the concentration in some of the components may reach 0.64 kg/kg some additional points had to be added to the dataset. The curve fitted correlation is shown in Figure 5.5 on the following page, marking the extrapolated region.

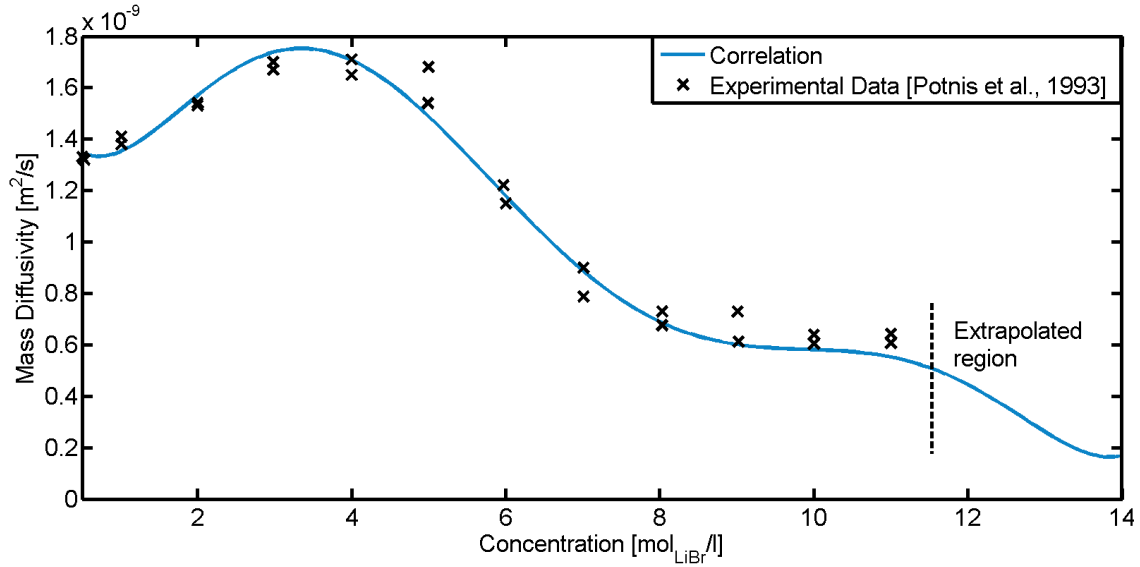


Figure 5.5. Mass diffusivity of a water/lithium bromide solution.

In order to conclude the equations for the mass conservation it is required to know the film thickness and film bulk velocity. The film thickness and the film bulk velocity can be derived from the conservation of momentum.

Conservation of Momentum

Conservation of momentum involves the forces exerted on the liquid film. It is assumed that the only two forces acting on the film is buoyancy and wall shear. The weight of the film is acting downward due to gravity and the wall shear is acting upward. Nusselt's integral solution to laminar film condensation provides the expressions for the film thickness as shown in Equation 5.12.

$$\delta_{s,i} = \left(3 \cdot \frac{\mu_{s,i}}{\rho_{s,i}^2} \cdot \frac{\Gamma_{s,i}}{g} \right)^{1/3} \quad (5.12)$$

where:

$$\Gamma_{s,i} = \frac{\dot{m}_i}{\pi \cdot D_{s,i}} \quad (5.13)$$

And the definitions of the Reynolds number in Equation 5.14 on the facing page and the mean velocity 5.15 on the next page is taken from [Patnaik et al., 1993] in order to use the empirical correlations for heat and mass transfer coefficients.

$$\text{Re}_{s,i} = \frac{\bar{u}_{s,i} \cdot \delta_{s,i} \rho_{s,i}}{\mu_{s,i}} \quad (5.14)$$

where:

$$\bar{u}_{s,i} = \frac{\dot{m}_i}{\rho_{s,i} \cdot \delta_{s,i} \cdot D_t \cdot \pi} \quad (5.15)$$

Conservation of Energy

The partial differential equation describing the conservation of energy is discretized using a forward difference scheme as in Equation 5.16.

$$\dot{m}_{i-1} \cdot i_{s,i-1} - \dot{m}_i \cdot i_{s,i} + \dot{m}_{a,i} \cdot \Delta i_i - U_i \cdot A_{if,i} \cdot (T_i - T_\infty) = 0 \quad (5.16)$$

In order to conclude the equation set the boundary condition at the vapor-liquid interface is formulated as in Equation 5.17. The boundary condition builds on the assumption that heat is only transferred from the vapor to the liquid film by condensation.

$$\Delta i_{s,i} \cdot \dot{m}_{a,i} = \kappa_{s,i} \cdot \frac{A_{if,i}}{\delta_{s,i}} \cdot (T_{if,i} - T_{s,i}) \quad (5.17)$$

In order to solve the energy balance the overall heat transfer coefficient (U) needs to be determined based on the geometry and operational conditions. Heat is transferred from the element to the wall by convection, through the wall by conduction and from the outer wall to the coolant by convection. The overall heat transfer coefficient is calculated in Equation 5.18 from the principle of thermal resistance networks.

$$UA_i = \left(\frac{1}{h_{s,i} \cdot A} + \frac{r_o}{k_{w,i} \cdot A} \cdot \ln\left(\frac{r_o}{r}\right) + \frac{1}{h_\infty \cdot A_{eq}} \right)^{-1} \quad (5.18)$$

First the heat transfer coefficient is found for the convective heat transfer from the film into the wall. The correlation by [Seban, 1978] is valid for the case of fully developed, wavy-laminar flow used, and is seen from Equation 5.19. Because of the relatively long tubes compared to the diameter the entry region will be neglected.

$$\frac{h_{s,i} \delta_{s,i}}{\kappa_{s,i}} = 0.029 \cdot (4 \cdot \text{Re}_{s,i})^{0.53} \cdot \text{Pr}_{s,i}^{0.344} \quad (5.19)$$

The conductivity of the tube wall (considered stainless steel) is determined using EES built-in property functions.

Finally the outer heat transfer coefficient needs to be calculated. In the model it is assumed that it is reasonable to assume that the heat transfer is similar in all the tubes and it only is necessary to consider a single tube. That assumption is justified by taking into account the bundle effect when calculating the outer convective heat transfer. The convective heat transfer is highly dependent on the bundle configuration, since it affects the flow pattern and level of turbulence. The tubes in the absorber are oriented in a staggered grid in two lines as seen on Figure 5.6. The flow enters the absorber normal to the page.

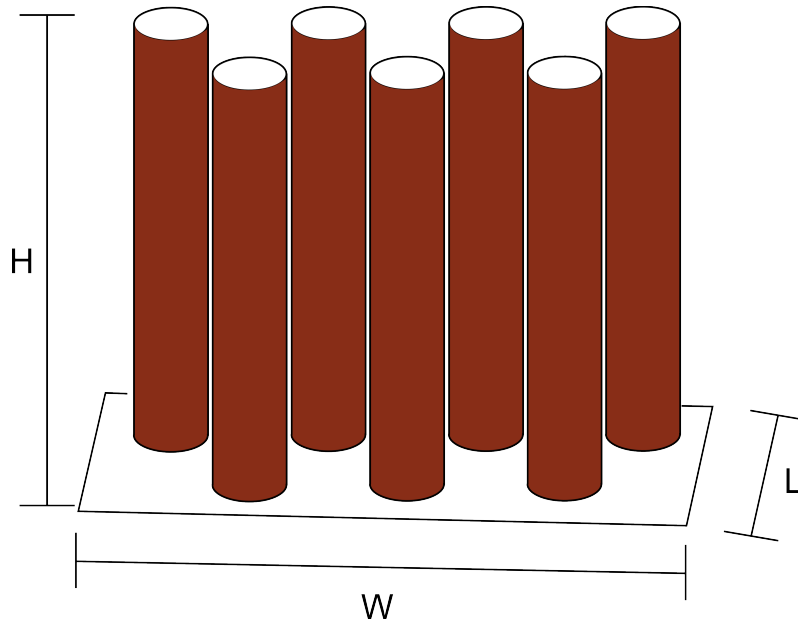


Figure 5.6. Illustration of the staggered grid orientation of the tubes in the absorber.

The illustration in Figure 5.6 does not show the fins on the absorber tubes. The fins chosen for the absorber are rectangular plates placed horizontally with a spacing of 2 mm between each fin, the fins are 0.12 mm thick. The choice of fins are based on a similar design found in [Castro et al., 2007]. The fin area is modeled as circular rectangular fins as shown in Figure 5.7 on the next page.

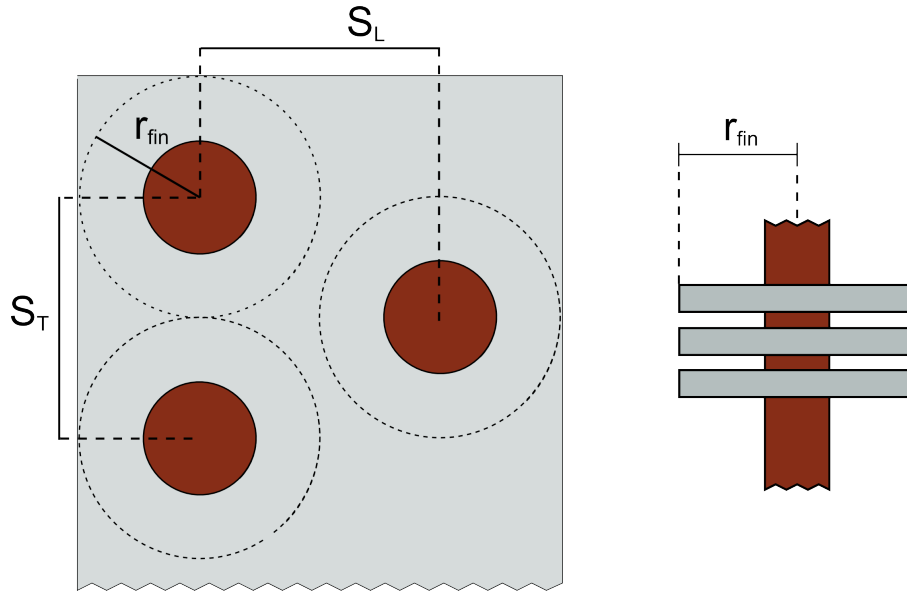


Figure 5.7. Schematic for the staggered bundle.

Figure 5.7 also shows the spacing between the tubes in the flow and normal to the flow direction. The arrangement of the tube bundle is characterized by the transverse pitch S_T and longitudinal pitch S_L . In 1987 Zukauskas developed empirical correlations for the Nusselt number for cross flow over tubes for $0.7 < Pr < 500$ and $1000 < Re < 2 \cdot 10^5$. The correlation used in this model is shown in Equation 5.20 and is valid for staggered grids.

$$Nu_{\infty,i} = 0.35 \left(\frac{S_T}{S_L} \right)^{0.2} \cdot Re_{\infty}^{0.6} \cdot Pr_{\infty}^{0.36} \cdot \left(\frac{Pr_{\infty}}{Pr_{sur,i}} \right)^{0.25} \quad (5.20)$$

where:

$$Re_{\infty} = \frac{\rho_{\infty} \cdot V_{\infty} \cdot D_o}{\mu_{\infty}} \quad (5.21)$$

The surface Prandtl number Pr_{sur} is determined based on the surface properties on the outer tube wall.

The correlation showed in Equation 5.20 is valid for tube banks with 16 or more rows. If the tube bank consists of fewer rows a correction factor will have to be multiplied to the Nusselt number correlation. The correction factors can be seen in Table 5.2 on the next page.

No. Rows	1	2	3	4	5	7	10	13
In-line	0.7	0.8	0.86	0.9	0.93	0.96	0.98	0.99
Staggered	0.64	0.76	0.84	0.89	0.93	0.96	0.98	0.99

Table 5.2. The correction factors for number of rows in staggered and in-line tube banks [Cengel, 2002].

The heat transfer in the absorber is enhanced by the fins added to the tubes. The fins add extra surface to the outside of the tubes and effective heat transfer area is calculated from Equation 5.22 where A is the surface area of one element.

$$A_{eq} = A_{unfinned} + \eta_{fin} \cdot A_{finned} \cdot N_{fins} \quad (5.22)$$

The fin efficiency η_{fin} is calculated based on Equation 5.23 which is valid for circular fins with a rectangular profile [Cengel, 2006]. Equation 5.23 is an analytical solution of the conduction throughout the fin, found by applying Fourier's Law.

$$\eta_{fin} = C_2 \cdot \frac{K_1(m \cdot r_1) \cdot I_1(m \cdot r_{2c}) - I_1(m \cdot r_1) \cdot K_1(m \cdot r_{2c})}{I_0(m \cdot r_1) \cdot K_1(m \cdot r_{2c}) - K_0(m \cdot r_1) \cdot I_1(m \cdot r_{2c})} \quad (5.23)$$

where:

$$m = \sqrt{\frac{2 \cdot h}{k \cdot t}} \quad r_{2c} = r_2 + \frac{t}{2}$$

$$C_2 = \frac{2 \cdot r_1}{r_{2c}^2 - r_1^2}$$

I_0 , I_1 , K_1 and K_0 are Bessel functions which can be found in EES as $Bessel_I(x)$ and $Bessel_K(x)$. The physical dimensions used in the calculation of the fin efficiency are displayed in Figure 5.8.

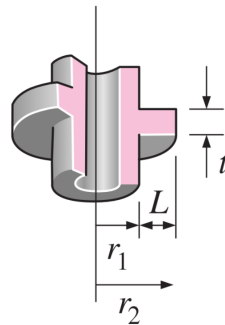


Figure 5.8. Physical dimensions used in the calculations of fin efficiency [Cengel, 2006].

The explained calculation of fin efficiency is built-in as an internal algorithm in EES called `eta_fin_annular_rect(t; r1; r2; h∞; k)`.

5.2 Generator

In the generator (also called desorber) water is evaporated from the strong aqueous lithium-bromide solution reducing the water content. The falling film generator consists of a bundle of horizontal tubes and is basically the same as a shell-and-tube heat exchanger. The heat source of the evaporation is introduced on the tube side, where the shell side liquid is introduced through spray nozzles in the top forming a thin film falling from tube to tube. A simple schematic of a horizontal falling film generator can be seen from Figure 5.9.

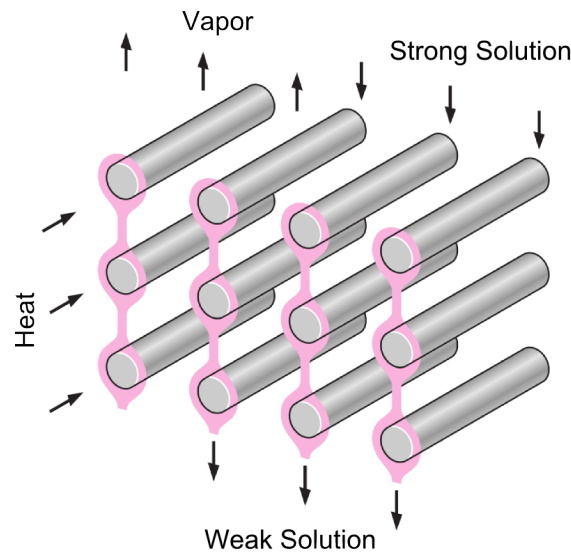


Figure 5.9. The conceptual drawing of a horizontal falling film generator, based on [Cengel, 2006].

The simultaneous heat and mass transfer in an evaporating falling film is complex and the description incomplete, which means that current design approaches are highly dependent on application and operational conditions. In order to find a suitable modeling approach for the generator a brief literature study is performed.

The first to simplify the complex phenomena of liquid falling film and develop a predictive model was [Nusselt, 1916]. The model described the film condensation on a vertical wall assuming laminar, fully developed flow. The model did not account for impingement, developing region or convection. The equations for the heat conduction through the film was solved by numerical integration. Nusselt's solution for condensing falling film has later been rewritten to predict evaporating film heat transfer as well.

Nusselt's solution was reformulated by [Bromley, 1950] in order to predict falling film evaporation on horizontal tubes including both conductive and radiant heat transfer. The most significant assumption for the model was that; the latent heat is so large that the heat required to heat the film is negligible. The assumptions in the model were corrected by evaluating a suitable constant factor determined from experiments.

Until the seventies the knowledge on film heat transfer coefficients were limited and most models was based on Nusselt's film theory and its modifications. In [Chun and Seban, 1972] the film heat transfer coefficient is determined experimentally and the results were presented as empirical correlations. The heat transfer was investigated for both laminar and turbulent flow, but did only consider the fully developed region.

It was necessary to examine the limitations of the conduction based models for horizontal tube falling film heat evaporation. In [Chyu and Bergles, 1987] a model was proposed which considered three different heat transfer regions: Jet impingement region, thermal developing region and fully developed region. The model used the empirical correlations of [Chun and Seban, 1972] to predict heat transfer in the fully developed region. The study showed that the heat transfer coefficient is less dependent on feed height for low Reynolds number and the fully developed region is the major contribution to the average heat transfer coefficient for low Reynolds numbers. An aqueous liquid bromide is more viscous ($\approx x10$) compared to pure water and the Reynolds numbers for the generator is expected to be in the lower range of the experiments conducted in [Chyu and Bergles, 1987]. For that reason it is found reasonable to use the empirical correlation in [Chun and Seban, 1972] to predict the average film heat transfer coefficient in the model.

Generator Model

The objective of the model is to estimate the amount of water evaporated and thereby the outlet concentration of the weak liquid solution. The generator will be designed as a bank of parallel tubes with a number of passes each. The principle is the same as a falling film heat exchanger with the addition of a vapor outlet as shown on Figure 5.10.

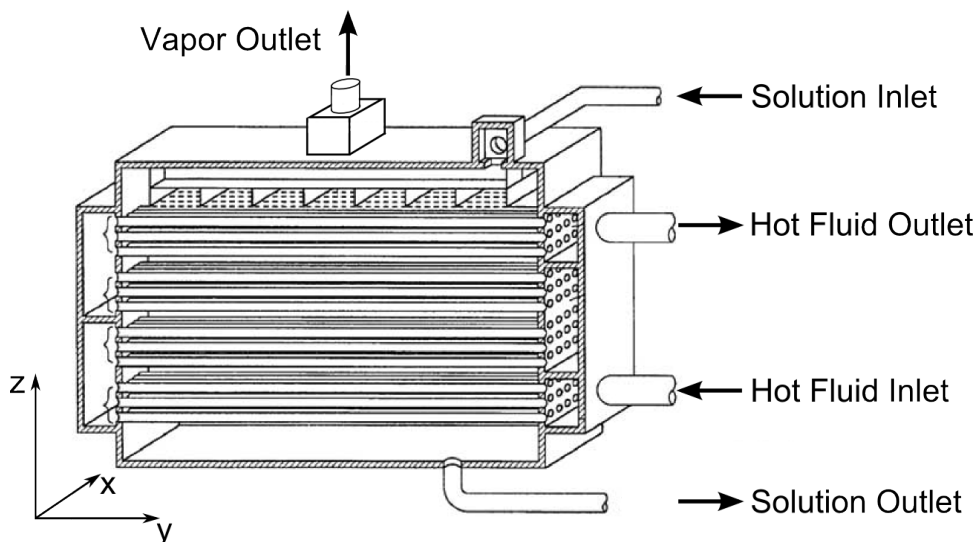


Figure 5.10. Illustration showing the principle of the generator design. Based on illustration from [Wang and Chua, 2009].

The partial differential equations describing the conservation of mass, energy and momentum can be seen from Equation 5.24, 5.25 and 5.26.

$$u \cdot \frac{\partial w}{\partial x} + v \cdot \frac{\partial w}{\partial y} = 0 \quad (5.24)$$

$$u \cdot \frac{\partial T}{\partial x} + v \cdot \frac{\partial T}{\partial y} = \alpha \cdot \frac{\partial^2 T(x)}{\partial y^2} \quad (5.25)$$

$$u \cdot \frac{\partial u}{\partial x} + v \cdot \frac{\partial u}{\partial y} = g + \nu \frac{\partial^2 u}{\partial y^2} \quad (5.26)$$

The mathematical model is developed based on the following assumptions:

	Falling Film
1	The fluid is Newtonian
2	The heat and mass transfer is assumed to be in steady state
3	The heat and mass transfer is assumed to be one-dimensional and uniform across a tube
4	Gravity is the only external force acting on the film
	Vapor
6	The water vapor is saturated and pure
7	The pressure of the water vapor is homogenous
	Interface
8	The heat transfer and mass transfer from the falling film to vapor is only due to evaporation of water
9	The vapor drag on the falling film is neglected
10	The mass evaporated is relatively small compared to the film flow

Table 5.3. Assumptions for the generator model.

There is no analytical solution to this set of partial differential equations, so it is necessary to perform a spatial discretization in order to obtain a numerical solution. When performing the discretization of the generator the flow of the heat source is considered as a row of parallel tubes with several passes, with inlet in the bottom. The modeling will only be performed for one of the parallel tubes and then summed up for the number of tubes. For the discretization of one tube each pass is considered as one

cell. The falling film enters in the top and will be modeled as one cell for each tube pass the film is covering. Figure 5.11 shows the concept of discretization used in the modeling.

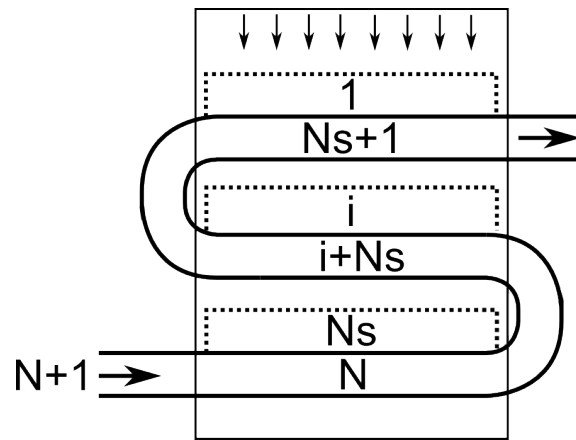


Figure 5.11. Illustration of the discretization and numbering used in the generator model.

The generator is divided into N cells with $N_s = \frac{N}{2}$, thereby $1 : N_s$ being the number of cells of the falling film, while $N_s + 1 : N$ are the cells of the heat source flow. N_s is also the number of passes of each tube in the generator.

While Figure 5.11 shows the numbering used in the discretization, Figure 5.12 illustrates the interaction between the cells. Again it is seen that the flow of the heat sources is upwards, while the falling film flow is downwards. Figure 5.12 shows the heat transfer between the heat source and the film, as well as the heat and mass transfer from the film to the vapor.

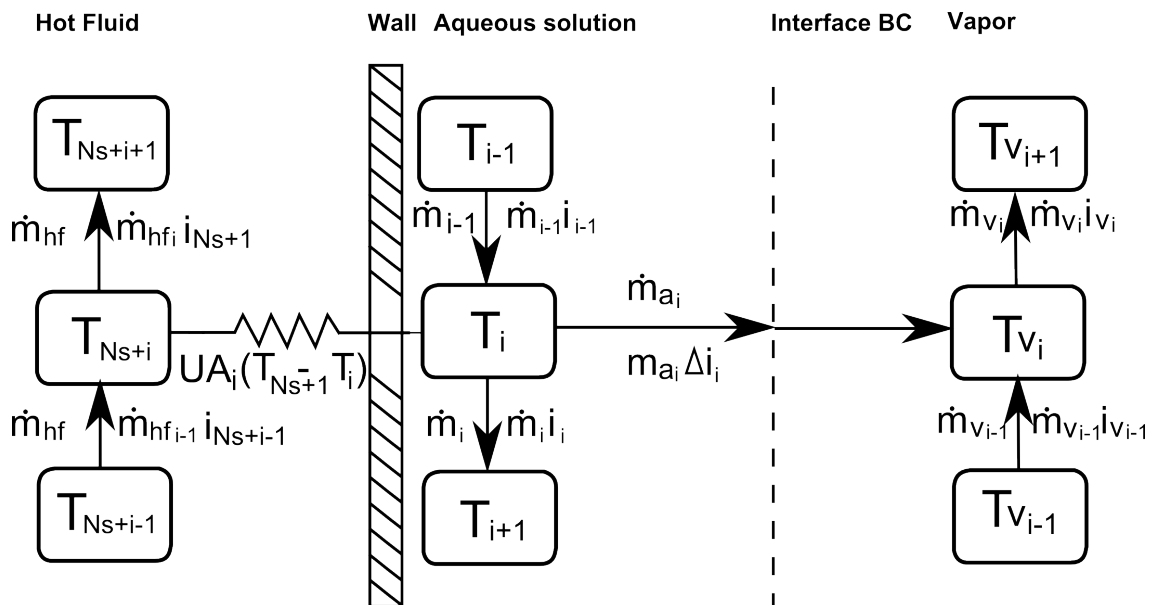


Figure 5.12. Sketch illustrating the spatial discretization of the generator.

Conservation of Mass

The equations for conservation of mass is derived using forward difference and is shown in 5.27, 5.28 and 5.29, respectively with index $i=1:N$.

$$\dot{m}_{\text{hf},i} = \dot{m}_{\text{hf},i+1} \quad (5.27)$$

$$\dot{m}_i = \dot{m}_{i-1} - \dot{m}_{e,i} \quad (5.28)$$

$$w_i \cdot \dot{m}_i = w_{i-1} \cdot \dot{m}_{i-1} \quad (5.29)$$

Equation 5.27 shows that there is no change in the mass flow in the flow of the heat source. This flow is inside the tubes and the flow will be constant all the way through each tube. The mass flow of the film, however is changing due to the boiling and thereby evaporation of parts of the flow. From Equation 5.29 it is also seen that the change in concentration in the film is also due to the evaporation. Only the water in the solution evaporates and thereby the change in concentration.

Conservation of Momentum

The Reynolds number of the falling film can be determined based on the mass flow per unit length and the viscosity of the solution, as shown in Equation 5.30.

$$\text{Re}_i = \frac{4 \cdot \Gamma_i}{\mu_i} \quad (5.30)$$

Where the mass flow per unit length is found by Equation 5.31.

$$\Gamma_i = \frac{\dot{m}_i}{2 \cdot L_t} \quad (5.31)$$

Conservation of Energy

The energy balance for the generator is described using Equation 5.32. Again the partial differential equation has been discretized using a forward difference scheme.

$$\dot{m}_i \cdot c_{p,i} \cdot T_i + \dot{m}_{e,i} \cdot \Delta i_i = \dot{m}_{i-1} \cdot c_{p,i-1} \cdot T_{i-1} + U_i \cdot A \cdot (T_{i+N_s} - T_i) \quad (5.32)$$

In order to be able to solve the energy balance the heat flux (UA) will have to be calculated. The total heat transfer consists of convection inside the tube, conduction through the wall of the tubes and convection of the film outside the tubes. Each of the heat transfer coefficients will have to be found in order to find the total heat transfer, as shown in Equation 5.33.

$$U_i = \left(\left(\frac{1}{h_{s,i}} \right) + \left(\frac{1}{h_{hf,i}} \right) + \left(\frac{r_o}{k_{w,i}} \right) \cdot \ln \left(\frac{r_o}{r_i} \right) \right)^{-1} \quad (5.33)$$

To calculate the convection inside the tubes (h_g) it is necessary to find the Reynolds number to determine if the flow is in the laminar and turbulent regime. To calculate the Reynolds number the density and viscosity is required, however the flow inside the tubes consists of triethylene glycol from the fuel cell system and the properties of triethylene glycol are not available in EES. These properties were therefore found in [Sun and Teja, 2003]. The density and conductivity was found for a mixture with 75% triethylene glycol, while the viscosity was found for pure triethylene glycol. The density was found to be $1016 \left[\frac{kg}{m^3} \right]$ at 425.35 K, the conductivity $0.198 \left[\frac{W}{mK} \right]$ at 422.5 K and the viscosity $0.00139 \left[\frac{Pa}{s} \right]$ at 428.10 K. Since the temperature of the flow in the tubes does only varies approximately $10^\circ C$ from 150 to $140^\circ C$ the properties were found as constant values.

$$Re_{hf,i} = \frac{\rho_{hf,i} \cdot D_t \cdot u_{hf,i}}{\mu_{hf,i}} \quad (5.34)$$

where:

$$u_{hf,i} = \frac{\dot{m}_{i+N_s}}{\rho_{hf,i} \cdot \pi \cdot \left(\frac{D_t}{2} \right)^2} \quad (5.35)$$

Due to the high viscosity of triethylene glycol the flow is surely in the laminar region, and the Nusselt number can be considered constant. The heat flux is assumed to be constant due to the temperature of the film changing as well, and the Nusselt number is found in Equation 5.36 [Cengel, 2002].

$$Nu_{hf,i} = \frac{48}{11} \approx 4.36 \quad (5.36)$$

When the Nusselt number is found the convective heat transfer coefficient is found from Equation 5.37.

$$Nu_{hf,i} = \frac{h_{hf,i} \cdot D_t}{k_{hf,i}} \quad (5.37)$$

The convective heat transfer coefficient of the film boiling h_s will have to be calculated. The film will have a varying thickness depending on the angle around the tube and the velocity will be affected as well. To determine the size of the convection coefficient it was deemed necessary to use an empirical correlation. [Chun and Seban, 1972] suggests correlations covering the laminar, wavy laminar and turbulent region. The correlation assumes developed flow for the entire flow on each tube.

Laminar:

$$\frac{h_{s,i}}{k_s} \left(\frac{v_s^2}{g} \right)^{\frac{1}{3}} = 1.10 \cdot \text{Re}_{s,i}^{-\frac{1}{3}}, \quad \frac{\Gamma_s}{\mu_s} \leq 0.61 \left(\frac{\mu_s^4 \cdot g}{\rho_s \cdot \sigma_s^3} \right)^{-\frac{1}{11}} \quad (5.38)$$

Wavy laminar:

$$\frac{h_{s,i}}{k_s} \left(\frac{v_s^2}{g} \right)^{\frac{1}{3}} = 0.822 \cdot \text{Re}_{s,i}^{-0.22}, \quad 0.61 \left(\frac{\mu_s^4 \cdot g}{\rho_s \cdot \sigma_s^3} \right)^{-\frac{1}{11}} < \frac{\Gamma_s}{\mu_s} \leq 1450 \cdot \text{Pr}_s^{-1.06} \quad (5.39)$$

Turbulent:

$$\frac{h_{s,i}}{k_s} \left(\frac{v_s^2}{g} \right)^{\frac{1}{3}} = 3.8 \cdot 10^{-3} \cdot \text{Pr}_s^{0.65} \text{Re}_{s,i}^{0.4}, \quad \frac{\Gamma_s}{\mu_s} > 1450 \cdot \text{Pr}_s^{-1.06} \quad (5.40)$$

The surface tension of the water/lithium bromide solution, σ , was assumed to be 0.085 $\left[\frac{N}{m} \right]$ and constant, based on results from [Yao et al., 1991].

By using the correlation corresponding to the actual flow regime the film boiling convection heat transfer coefficient can be determined.

Now that the inner and outer convection has been determined the remaining coefficient is the conduction through the tube wall (k_w). The tube is considered to be stainless steel, and the conduction coefficient can easily be found using EES property functions.

5.3 Evaporator

In the evaporator refrigerant is evaporated absorbing heat from the surroundings. The evaporator is assumed to be an air-cooled falling film heat exchanger as the absorber. Saturated liquid is entering the evaporator from the top and forming a falling film on the inside of the tubes. Heat is transferred through the tube wall to the liquid which evaporates. The geometry is similar to the one for the absorber described in Section 5.1 on page 30. Less effort is put into the modeling of the evaporator compared to the absorber and it will only be used to give an estimate of the size of the evaporator. There are made some simplification and assumptions in order to predict the performance of the evaporator:

- The geometry of the evaporator is similar to the one described for the absorber.
- The vapor leaving the absorber is saturated.
- An average overall heat transfer coefficient is applied.

The overall heat transfer coefficient is determined after the same principle as in the absorber which can be seen in Equation 5.41.

$$U = \left(\left(\frac{1}{h_s} \right) + \left(\frac{1}{h_{hf}} \right) + \left(\frac{r_o}{k_w} \right) \cdot \ln \left(\frac{r_o}{r_i} \right) \right)^{-1} \quad (5.41)$$

The only difference is the calculation of the film heat transfer coefficient h_s . The film coefficient for boiling of water inside vertical tubes is seen in Equation 5.42 [Shilling, 2008].

$$h_s = \frac{k_l}{D} \cdot (1.3 + 180 \cdot D) \cdot Pr_l^{0.9} \cdot Re_l^{0.23} \cdot Re_v \cdot \left(\frac{\rho_l}{\rho_v} \right)^{0.25} \cdot \frac{\rho_v}{\rho_l} \quad (5.42)$$

Where:

$$Re_l = \frac{V_l \cdot D \cdot \rho_l}{\mu_l} \quad (5.43)$$

$$Re_v = \frac{V_v \cdot D \cdot \rho_v}{\mu_v} \quad (5.44)$$

$$V_l = \frac{\dot{m} \cdot (1 - x)}{r^2 \cdot \pi \cdot \rho_l} \quad (5.45)$$

$$V_v = \frac{\dot{m} \cdot (x)}{r^2 \cdot \pi \cdot \rho_v} \quad (5.46)$$

A mean film heat transfer coefficient is calculated in order to be able to determine the size of the evaporator.

The film heat transfer coefficient is dependent on the on the vapor fraction x and the mean coefficient is found as an average for all values between x_{in} and x_{out} .

5.4 Condenser

In the condenser heat is rejected to the surroundings, condensing the refrigerant at the high pressure. The condenser is air-cooled and the geometry will be considered the same as the absorber and evaporator. The superheated vapor from the generator enters the condenser and as heat is transferred from the vapor through the wall and by forced convection on the outside of the tubes.

In the modeling of the condenser there will be made some assumptions:

- The geometry of the condenser will be the same as the absorber.
- A heat transfer coefficient for condensation will be used for the entire condenser, also the area with superheating to saturated vapor.
- The liquid leaving the condenser will be saturated.

The overall heat transfer is found the same way as for the evaporator and the absorber by formula 5.41 on the preceding page.

The convective heat transfer coefficient for the condensation inside the vertical tubes is found using the correlation shown in Equation 5.47 [Geankoplis, 1993].

$$Nu_R = \frac{h_R \cdot L_t}{k_l} = 1.13 \left(\frac{\rho_l(\rho_l - \rho_v)g \cdot \Delta i \cdot L_t^3}{\mu_l \cdot k_l \cdot \Delta T} \right)^{\frac{1}{4}} \quad (5.47)$$

This correlation is valid for laminar flow condensing down a vertical surface. The heat transfer coefficient for the condensation is orders higher than the one for the desuperheating section, but the heat transfer required for the desuperheating is much lower than for the phase change.

Design and Optimization of Components

The purpose of this section is to determine the physical design of the components. The models for the generator and absorber will be used to determine the required design in order to obtain the desired outlet conditions. The inlet conditions and the desired outlet conditions are determined by the results from the black-box model in Section 4.1 on page 16. When designing a chiller there can be various objectives, which could be either to minimize the size or minimize the investment cost. In this section the component design is found by minimizing the material cost. First a cost function is developed based on the material cost for the component and later the optimization problem is defined.

6.1 Cost Function

The generator consists of stainless steel tubes in a shell of stainless steel plates and the absorber consist of stainless steel tubes with aluminum fins. The cost of stainless steel plates is found to be 30 €/m² [Metals Depot, 2013] and the cost of aluminum fins is found to be 3€/m² [Rapid Fab., 2013]. The tubes on the other hand are available in standard sizes, which can be seen from Table 6.1 based on the outer diameter.

D [in]	D [mm]	Cost [€/m ²]
0.5	12.7	6.3
0.625	15.9	8.1
0.75	19.1	7.1
1	25.4	9.1
1.5	38.1	15.9
2	50.8	18.2
3	76.2	36.3

Table 6.1. Cost of tubes of different diameters [Metals Depot, 2013]. The wall thickness of all the tubes is 1.651 mm.

The cost of the steel tubes is a discrete dataset which means that the class of optimization is Mixed Integer Non Linear programming (MINLP). Since EES cannot

handle MINLP the cost function needs to be reduced to Non Linear programming (NLP). The discrete cost function is fitted to a third order polynomial in order to produce a continuous cost function. The cost function for the stainless steel tube is seen in Figure 6.1.

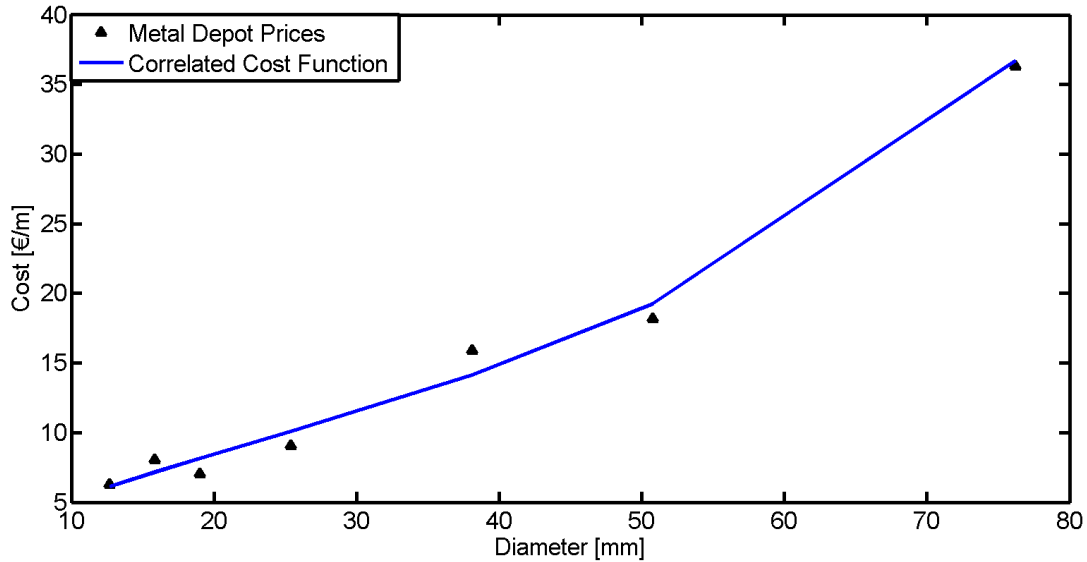


Figure 6.1. Cost of tubes of standard diameters ranging from 1/2" to 3".

Since it is inconvenient to have tubes of a non standard diameter it is necessary to compare the two adjacent points in the discrete dataset if a non integer solution is found. The cost function for the stainless steel plate, aluminum fins and stainless steel tube is seen from Equation 6.1, 6.2 and 6.3

$$\text{cost}_{\text{plate}} = 30[\text{€/m}^2] \quad (6.1)$$

$$\text{cost}_{\text{fin}} = 3[\text{€/m}^2] \quad (6.2)$$

$$\text{cost}_{\text{tube}}(D) = 8 \cdot 10^{-5} \cdot D^3 - 0.0058 \cdot D^2 + 0.442 \cdot D + 1.2957[\text{€/m}], \quad R^2 = 0.9894 \quad (6.3)$$

6.2 Absorber

In this section the optimization problem for the absorber is formulated. The objective is to minimize the material cost (MC) of the tubes and fins used to construct the absorber. MC is minimized subject to the absorber model, constrained by physical constrains, design constrains and operational conditions.

Minimize:

$$MC(D, m, H) = H \cdot m \cdot \text{cost}_{\text{tube}}(D) + L \cdot W \cdot H \cdot n_{\text{fin}} \cdot \text{cost}_{\text{fin}} \quad (6.4)$$

$$\text{cost}_{\text{fin}} = 3 \text{ [€/m}^2\text{]} \quad (6.5)$$

$$\text{cost}_{\text{tube}}(D) = 8 \cdot 10^{-5} \cdot D^3 - 0.0058 \cdot D^2 + 0.442 \cdot D + 1.2957 \text{ [€/m]} \quad (6.6)$$

Subject to:

$$\sum_{i=1:N} h_{in,i} \cdot \dot{m}_{in,i} - h_{out,i} \cdot \dot{m}_{out,i} + \Delta \dot{m}_{a,i} \cdot \Delta h_{v,i} - UA_i \cdot \Delta T_i = 0 \quad (6.7)$$

$$\sum_{i=1:N} \dot{m}_{in,i} - \dot{m}_{out,i} + \Delta \dot{m}_a = 0 \quad (6.8)$$

where:

Fixed parameters:	
$n_{\text{fin}} = 500$	The fin density on each tube is 500 fins/m
$th_{\text{fin}} = 0.12 \cdot 10^{-3}$	The fin thickness is $0.12 \cdot 10^{-3}$
Design constrains:	
$H \leq 1.2$	The total height of absorber cannot exceed 1.2m
$L_{fin} \leq D$	The fin length cannot be less than the diameter of the tube
$0.01 \leq D \leq 0.08$	The diameter of each tube has to be between 10 and 80 mm
$1 \leq m \leq 200$	The number of tubes has to be between 1 and 200
$0.001 \leq L_{\text{fin}} \leq 0.1$	The length of the fins has to be between 1 mm and 100 mm
Operational conditions:	
$P_{lo} = 1.1516$	The pressure in the absorber is 1.1516 kPa
$\dot{m}_{in} = 0.01027$	The total inlet mass flow is 0.01027 kg/s
$w_{in} = 0.574$	Inlet mass fraction is 0.574 $\text{kg}_{\text{LiBr}}/\text{kg}_s$
$w_{out} = 0.64$	Outlet mass fraction is desired to be 0.64 $\text{kg}_{\text{LiBr}}/\text{kg}_s$
$T_{in} = 62.4$	The inlet temperature of the solution is 62.4°C
$T_{\infty} = 25$	The ambient temperature is 25°C
$g = 9.81$	The gravitation is 9.82 m/s^2
$V_{\text{fan}} = 2.5$	The fan speed is 2.5 m/s

The optimization was performed using EES' Direct Search with a relative convergence tolerance of 10^{-4}

6.3 Generator

In this section the optimization problem for the generator is formulated. The objective function is the material cost (MC) of the tubes used to construct the generator and the steel plates used as outer shell. MC is minimized subject to the generator model, constrained by fixed design parameters, design constrains and operational conditions. Since the number of passes equals number of cells it was not possible to optimize this variable. A short study of the effect of number of passes on total cost showed that more passes proved more feasible, after 12 passes the effect on the cost was negligible. A similar study showed that a tube diameter of 12.7 mm resulted in the lowest cost of the system.

Minimize:

$$MC(n, m, L) = L \cdot m \cdot n \cdot \text{cost}_{\text{tube}} + 2 \cdot (H \cdot W + H \cdot L + L \cdot W) \cdot \text{cost}_{\text{plate}} \quad (6.9)$$

$$\text{cost}_{\text{tube}} = 8.42 \text{ [€/m]} \quad (6.10)$$

$$\text{cost}_{\text{plate}} = 30 \text{ [€/m}^2\text{]} \quad (6.11)$$

Subject to:

$$\sum_{i=1:N} h_{\text{in},i} \cdot \dot{m}_{\text{in},i} - h_{\text{out},i} \cdot \dot{m}_{\text{out},i} - \Delta \dot{m}_{g,i} \cdot \Delta h_{v,i} + UA_i \cdot \Delta T_i = 0 \quad (6.12)$$

$$\sum_{i=1:N} \dot{m}_{\text{in},i} - \dot{m}_{\text{out},i} - \Delta \dot{m}_e = 0 \quad (6.13)$$

where:

Fixed parameters:	
$D = 12.7$	The diameter of the tubes used is a standard 12.7 mm (1/2")
$s_t = 1.651$	The wall thickness of the tubes used is 1.651 mm
Design constrains:	
$1 \leq n \leq 100$	The number of passes for each tube cannot exceed 100
$1 \leq m \leq 100$	The number of tubes cannot exceed 100
Operational conditions:	
$Q = 3487$	The heat input is 3487 W
$P_{hi} = 17.69$	The pressure in the generator is 17.69 kPa
$T_{\text{in}} = 99.7$	The solution inlet temperature is 99.7°C
$W_{\text{in}} = 0.574$	The inlet solution mass fraction is 0.574 kg/kg
$W_{\text{out}} = 0.64$	The desired outlet solution mass fraction is 0.64 kg/kg
$T_{\text{hf,in}} = 150$	The hot fluid inlet temperature is 150°C
$T_{\text{hf,out}} = 150$	The hot fluid desired outlet temperature is 140°C

The optimization was performed using EES' Direct Search with a relative convergence tolerance of 10^{-4}

Results

In this chapter the results from the optimized component models will be described. The results will be described for each component and used to check if the tendencies are correct.

7.1 Verification of Results

Before using the model to generate results it was deemed necessary to look into the correctness of the model. This was done by performing a mesh independence study, to make sure the number of cells for each tube in the absorber does not affect the results obtained, and verifying the energy conservation in each cell.

Mesh Independence Study

The mesh independence study was done by varying the number of cells and comparing the outlet mass fraction of LiBr in the solution. The number of cells was varied in the range 5 to 35 cells, and the results are shown in Table 7.1.

No. Cells	w_{outlet}	Relative Error [%]	Absolute Error [kg/kg]
35	0.574400	0	0
30	0.574433	$3.30 \cdot 10^{-05}$	$5.75 \cdot 10^{-05}$
25	0.574480	$8.00 \cdot 10^{-05}$	$1.39 \cdot 10^{-04}$
20	0.574550	$1.50 \cdot 10^{-04}$	$2.61 \cdot 10^{-04}$
15	0.574667	$2.67 \cdot 10^{-04}$	$4.65 \cdot 10^{-04}$
10	0.574901	$5.01 \cdot 10^{-04}$	$8.72 \cdot 10^{-04}$
5	0.575616	$1.22 \cdot 10^{-03}$	$2.12 \cdot 10^{-03}$

Table 7.1. Mesh independence study for the absorber.

The results from the mesh independence study shows that the number of cells has little effect on the results. Having five cells for the whole length of the absorber only gives an error of 0.2% compared with having 35 cells. Because of small calculation time in general the number of cells was set to 10 for further simulations.

In the generator the number of cells equals the number of passes of each tube. Therefore no mesh independence study has been carried out for the generator.

Energy Conservation

To verify that the conservation of energy is valid for the absorber and generator model, the residuals for the energy balances have been listed in Table 7.2 for each cell.

Cell No.	Absorber	Generator
1	$6.22 \cdot 10^{-15}$	$-7.52 \cdot 10^{-14}$
2	$2.67 \cdot 10^{-14}$	$6.14 \cdot 10^{-14}$
3	$2.81 \cdot 10^{-14}$	$1.55 \cdot 10^{-13}$
4	$2.32 \cdot 10^{-14}$	$9.92 \cdot 10^{-14}$
5	$1.07 \cdot 10^{-14}$	$-1.51 \cdot 10^{-13}$
6	$-7.99 \cdot 10^{-15}$	$-5.86 \cdot 10^{-13}$
7	$1.47 \cdot 10^{-15}$	$-1.15 \cdot 10^{-12}$
8	$7.27 \cdot 10^{-16}$	$-1.76 \cdot 10^{-12}$
9	$5.40 \cdot 10^{-16}$	$-2.33 \cdot 10^{-12}$
10	$4.48 \cdot 10^{-16}$	$-2.73 \cdot 10^{-12}$
11	-	$-2.82 \cdot 10^{-12}$
12	-	$1.25 \cdot 10^{-11}$

Table 7.2. Residuals for energy conservation for each cell in absorber and generator.

The residuals have been found using the energy balance for each component (Equation 5.16 on page 37 and 5.32 on page 45).

Propagation of Uncertainty

The uncertainty of some key variables are investigated for the absorber and condenser. For the absorber correlations for the mass diffusivity D_{ab} , the film heat transfer coefficient h_s and Sherwood number Sh are found in literature. The influence of the uncertainty of these parameters on the outlet mass fraction is seen from Table 7.3 on the next page.

Variables (Var)	D_{ab}	h_s	Sh
Relative uncertainty of Var	$\pm 10\%$	$\pm 10\%$	$\pm 10\%$
$\frac{\partial w_{out}}{\partial Var}$	-0.01731	-0.00598	-0.03462
Absolut error of w_{out}	± 0.001731	± 0.0006	± 0.00346
Relative uncertainty of w_{out}	0.30136%	0.104%	0.603%
Percentage of uncertainty	19.54%	2.33%	78.13%

Table 7.3. Uncertainty propagation of absorber outlet mass fraction ($w=0.5744$) based on relative uncertainty of three variables

The relative error of the investigated variables was assumed to be 10%. It is seen that the highest relative uncertainty of the outlet mass fraction is 0.6% for the Sherwood number. Furthermore, it is seen that the outlet mass fraction is weakly affected by the uncertainty of the mass diffusivity. This means that the extrapolation of the mass diffusivity data does not have a significant impact on the total mass transfer in the absorber.

The uncertainty of the film heat transfer coefficient for the generator has also been investigated. The influence of the heat transfer coefficient on the generator outlet mass fraction w_{out} can be seen in Table 7.4.

Relative uncertainty of h_s	$\pm 10\%$
$\frac{\partial w_{out}}{\partial h_s}$	-0.01731
Absolut error of w_{out}	± 0.001731
Relative uncertainty of w_{out}	0.30136%

Table 7.4. Uncertainty propagation of generator outlet mass fraction ($w=0.64$) based on relative uncertainty of the film heat transfer coefficient.

It is seen that a relative change in the film heat transfer coefficient of 10% affects the uncertainty of the outlet mass fraction with 0.3 %.

7.2 Absorber

Absorber Design

This section will be used to describe the results from the absorber component model. The results will be discussed and used to check if the tendencies of the model are correct. The results of the absorber design optimization are seen from Table 7.5 on the next page.

	Initial design	Final design
Type	4-row staggered	
D	16.77 mm	15.9 mm
L_a	1.2 m	1.285 m
m_a	41.21 tubes	41 tubes
L_{fin}	16.77 mm	15.9 mm
Material cost	161.9 €	162.1 €

Table 7.5. Optimized absorber design.

Since it is unphysical to have half tubes and it is desired to use standard sized tubes it is necessary to find a realizable adjacent solution. The combination of 41 and 42 tubes and a tube diameter of 15.875 and 19.05 mm was compared and the final design is seen in Table 7.5. The results for this configuration will be used in this section. An illustration of the final design is seen in Figure 7.1.

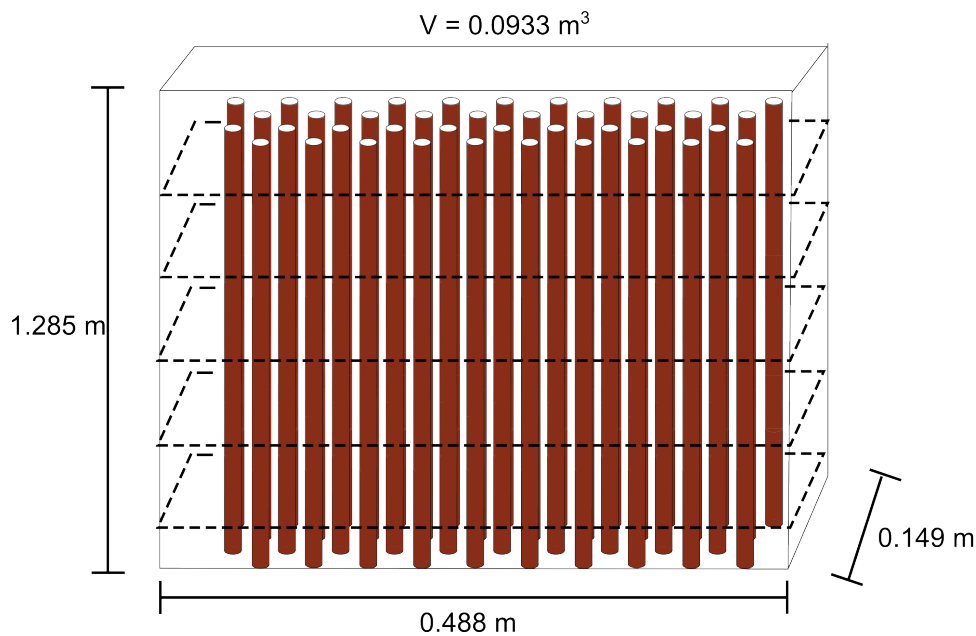


Figure 7.1. Visualization of the absorber design, with dimensions (the fin density is higher than illustrated).

Model Results

The absorber is divided into 10 cells and the results are presented for each cell. The results are also plotted for cell 0 which represents the inlet conditions where an inlet condition is present.

In the absorber the water vapor is absorbed into the solution, resulting in a lower mass fraction of lithium bromide in the solution. This is verified by looking at the mass fraction in the each cell in Figure 7.2 on the facing page.

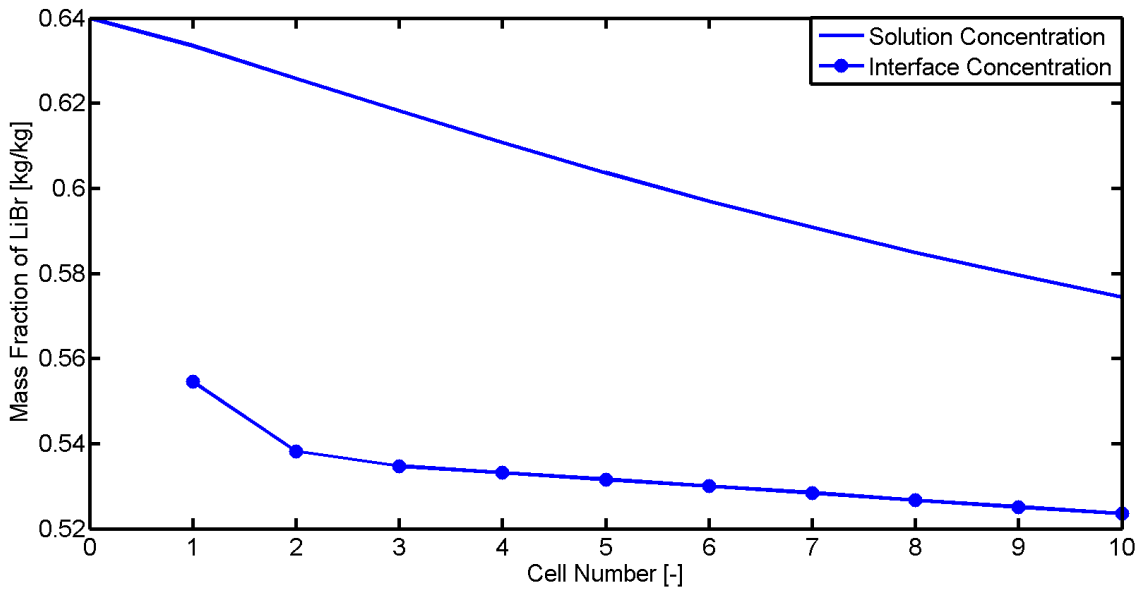


Figure 7.2. Mass fraction of the solution and at the interface.

Figure 7.2 shows that the weak solution enters at a mass fraction of 0.64 lithium bromide and the mass fraction is lowered to 0.574. The interface mass fraction is also plotted in Figure 7.2, which is the mass fraction at the interface between the vapor and the solution. The mass flux of absorbed vapor is depending on the difference in mass fraction between the interface and the solution. Since the interface is where the vapor is absorbed the mass fraction of lithium bromide will be lower here than for the cell center.

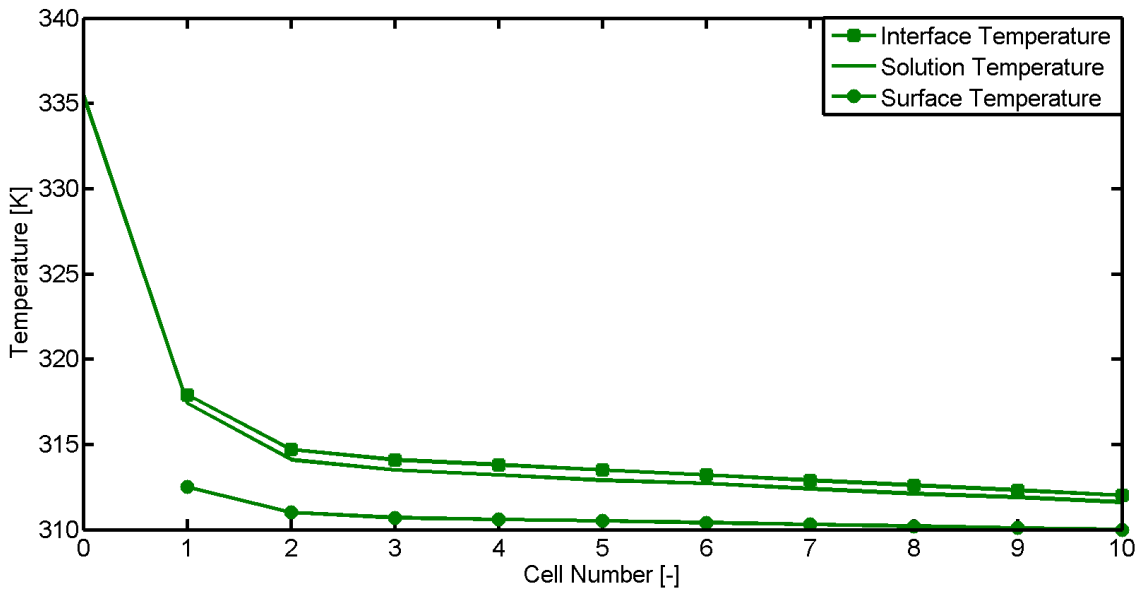


Figure 7.3. Temperature at the interface, in the solution and at the surface of the tube.

The absorber is cooled by forced convection meaning that the solution temperature should be lowered, which is also seen from Figure 7.3 on the previous page. At the interface the temperature is higher due to the heat generated from the condensation of the vapor. The heat is then lead through the solution by conduction, through the tube wall by conduction and finally by forced convection to the surrounding air. The temperature level at the surface is the lowest of the three.

The solution mass flow should increase due to the absorbed vapor mass flow, and this tendency is confirmed by Figure 7.4. The tendency of the absorbed mass can be explained by looking at the difference in mass fraction shown on Figure 7.2 on the previous page. Initaly the difference is increasing, thereafter decreasing giving the absorbed mass a peak in the third cell of the absorber. The relation between the difference in mass fraction and the absorbed mass was also described in Equation 5.6 on page 34.

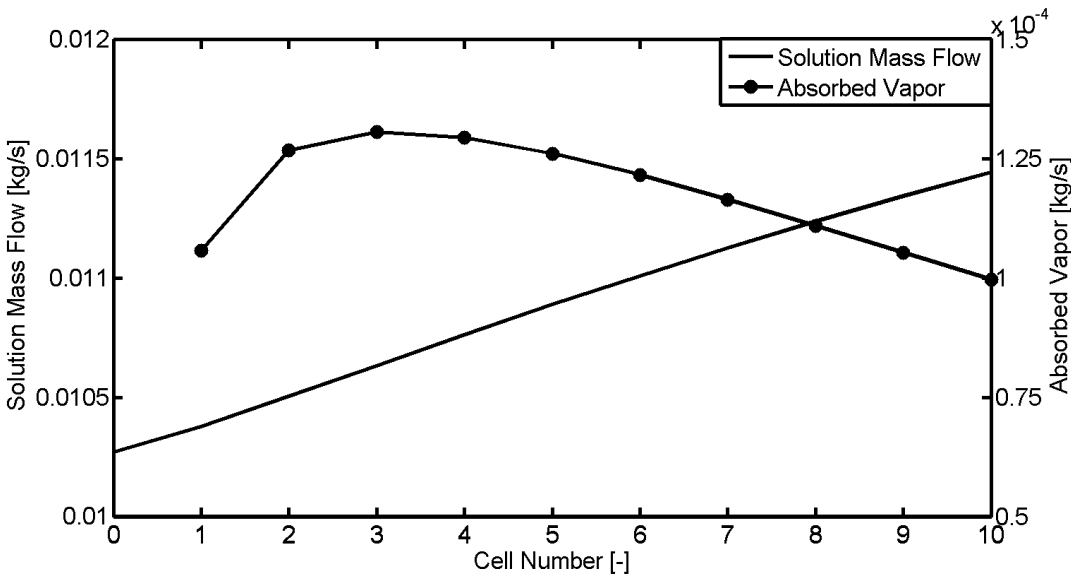


Figure 7.4. Mass flow of solution and absorbed vapor.

It is important to consider the velocity of the vapor in the tubes. In the design criteria a limit of 20 m/s was defined and the velocity in the bottom of the absorber was set to 0 (boundary condition). From Figure 7.5 on the next page it is seen that the vapor velocity in the bottom is zero and in the top just under 20 m/s.

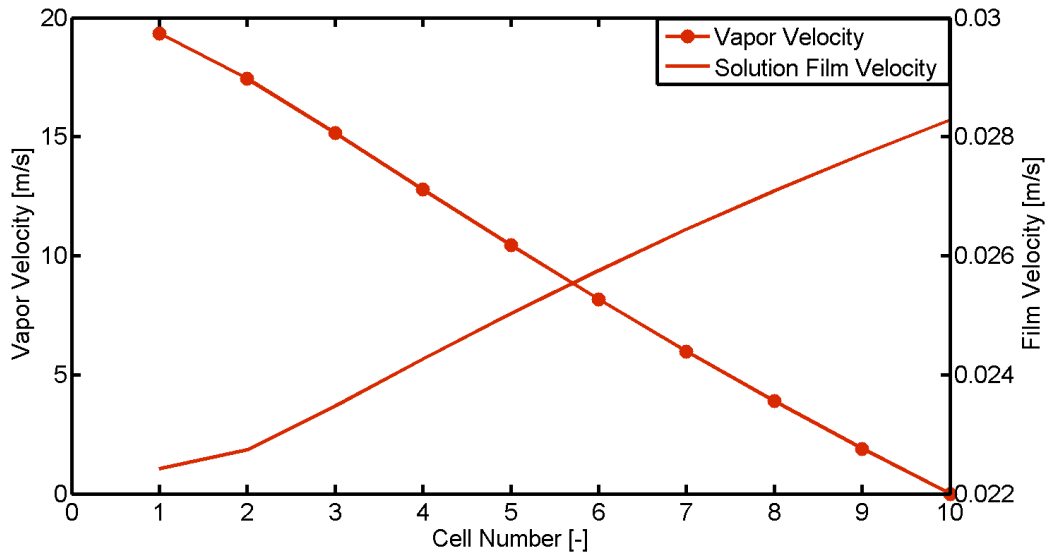


Figure 7.5. Velocity of the vapor and solution film in the tube.

The film velocity is also shown in Figure 7.5, showing that the film velocity is increasing in the absorber. The increase in velocity can be explained by looking at the increase in mass flow shown in Figure 7.4 on the preceding page and the decrease in film thickness from Figure 7.7 on the following page.

The mass flux is defined as $\frac{\Delta \dot{m}}{A}$ and can be used in comparison with results from other models, despite differences in geometries. The same goes for the heat flux $\frac{Q_a}{A}$. Both the mass and heat flux are shown in Figure 7.6.

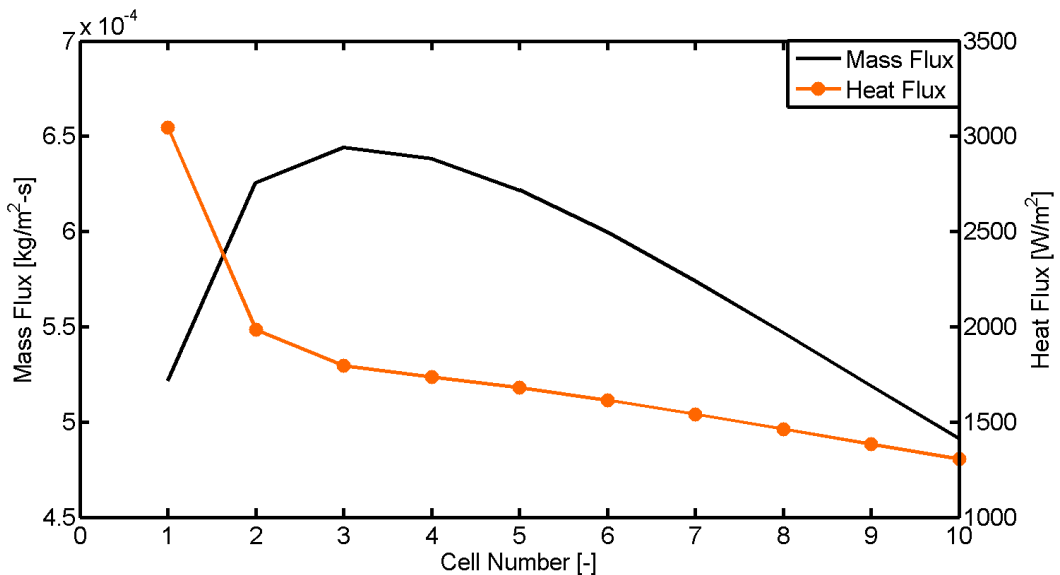


Figure 7.6. Mass and heat flux for the absorber.

The drop in heat flux is due to the lower solution temperature and thereby temperature difference relative to the surroundings. The mass flux has the same tendency as the absorbed mass on Figure 7.4 on page 60 which has already been explained.

In [Medrano et al., 2003] a model is developed for a liquid-cooled water/lithium bromide absorber and is used to predict the mass flux at different operational conditions. In the paper a mass flux of $10^{-3} \frac{kg}{m^2s}$ is calculated for an absorber operating at pressure of 1.3kPa with an inlet mass fraction of 0.62 and inlet temperature of 35°C and. The predicted mass flux in [Medrano et al., 2003] is approximately double compared to the one presented in this paper. However, the configurations are not the same and the comparison shows that the mass fluxes are within the same order of magnitude.

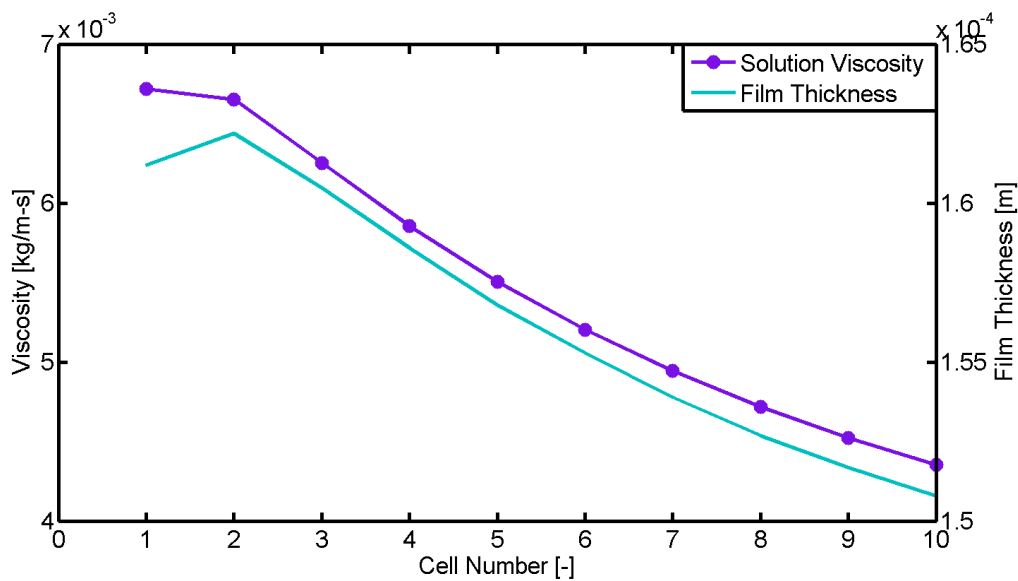


Figure 7.7. Viscosity of the solution and film thickness in the absorber.

Figure 7.7 shows the film thickness and the solution viscosity throughout the absorber. The film thickness decreases down the absorber, which is due to the lower viscosity of the solution. The viscosity is lowered because of the change in the mass fraction of lithium bromide in the solution, the more water the lower viscosity.

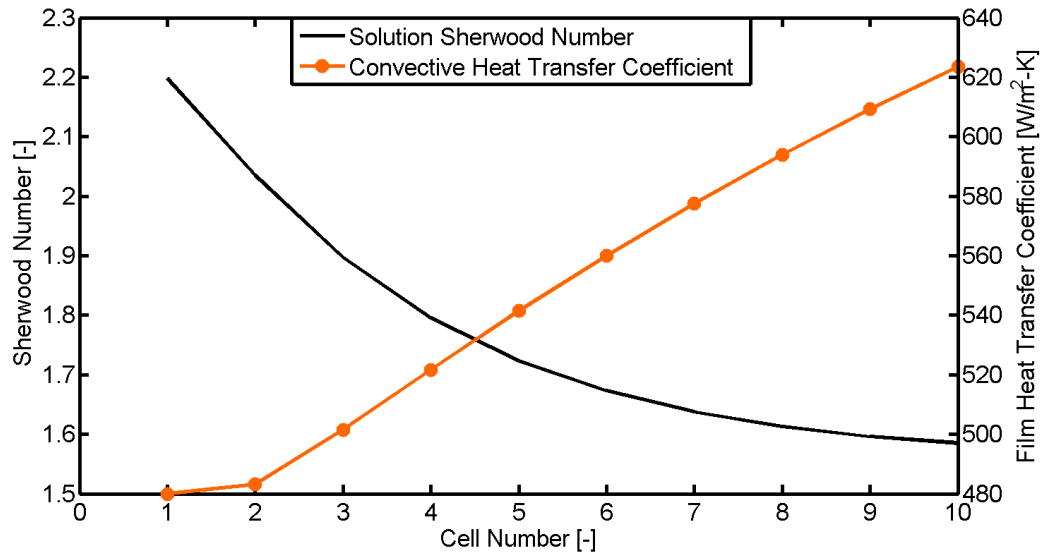


Figure 7.8. Sherwood number and the convective heat transfer coefficient for the film.

Finally the Sherwood number and heat transfer coefficient have been plotted in Figure 7.8. These two variables are found by empirical correlations. The film heat transfer coefficient increases due to an increase in velocity and thereby Reynolds number. The Sherwood number however is mostly affected by the Schmidt number which again is decreased because of the decreasing viscosity.

7.3 Generator

Generator Design

The results from the component model of the generator will be presented in this section. The result of the generator design optimization is seen from Table 7.6.

D_t	12.7 mm
L_g	0.699 m
m_g	11 tubes
n_g	12 passes
Material cost	314.3 €

Table 7.6. Optimized generator design.

The generator design has been visualized in Figure 7.9 on the following page.

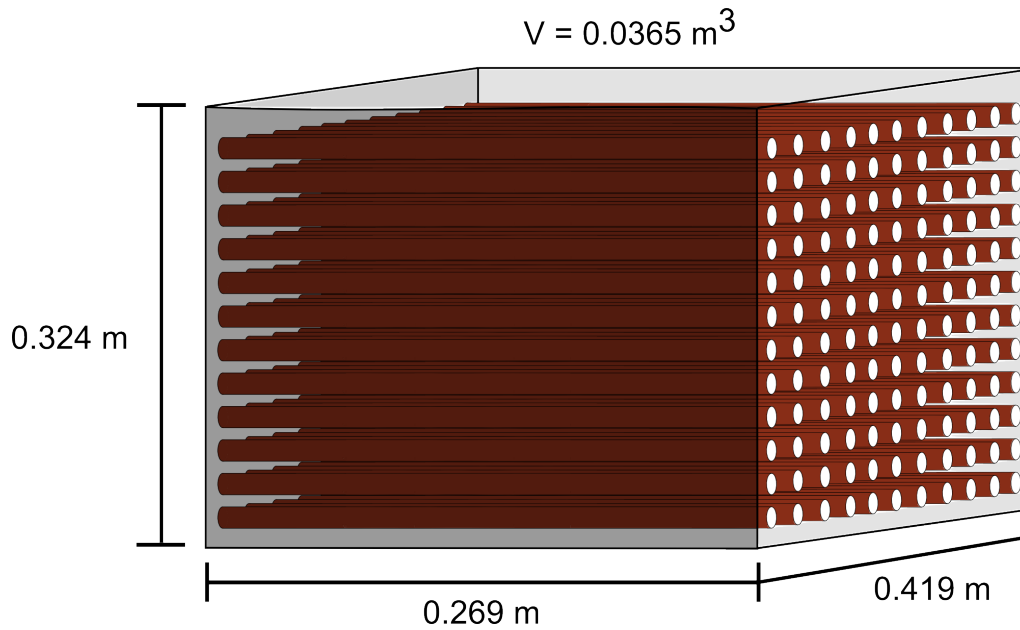


Figure 7.9. Illustration showing the design and dimensions of the generator.

Model Results

The generator consists of 12 passes and thereby 12 cells as well. As for the absorber cell 0 represents inlet conditions.

The empirical correlation used in the generator model is for laminar film flow, and the transition Reynolds number is defined as $2.43 \left(\frac{\mu^4 \cdot g}{\rho \cdot \sigma^3} \right)$. The Reynolds number and transition Reynolds number are both plotted in Figure 7.10.

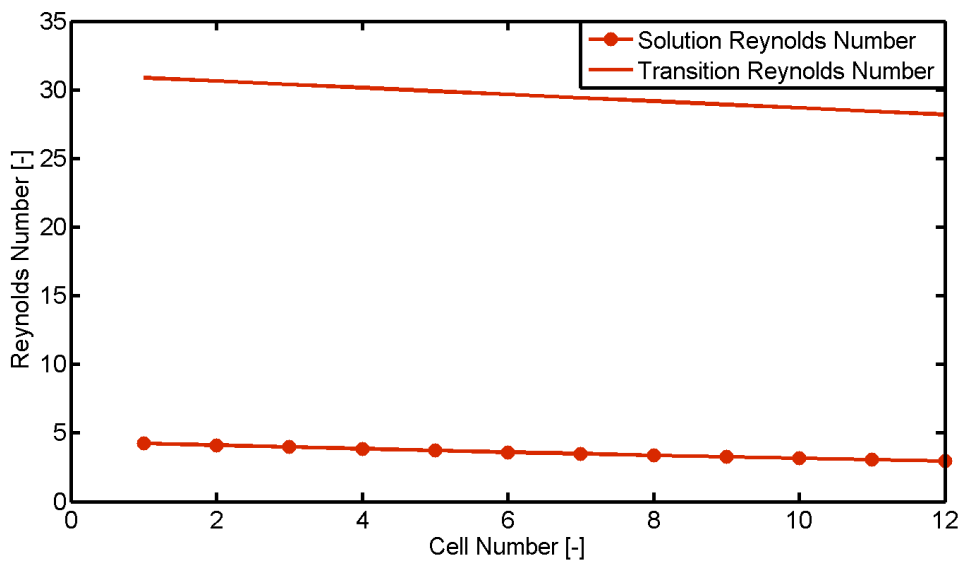


Figure 7.10. Reynolds number and transition number from laminar to wavy laminar flow regime.

From Figure 7.10 on the facing page it is seen that the solution flow is clearly in the laminar flow in all cells of the generator. This means the correlation is valid and the rest of the results can be considered.

The mass fraction of the solution is increased in the generator due to the evaporation of water vapor. The solution enters with a mass fraction of 0.574 and is then increased to 0.64, as seen on Figure 7.11.

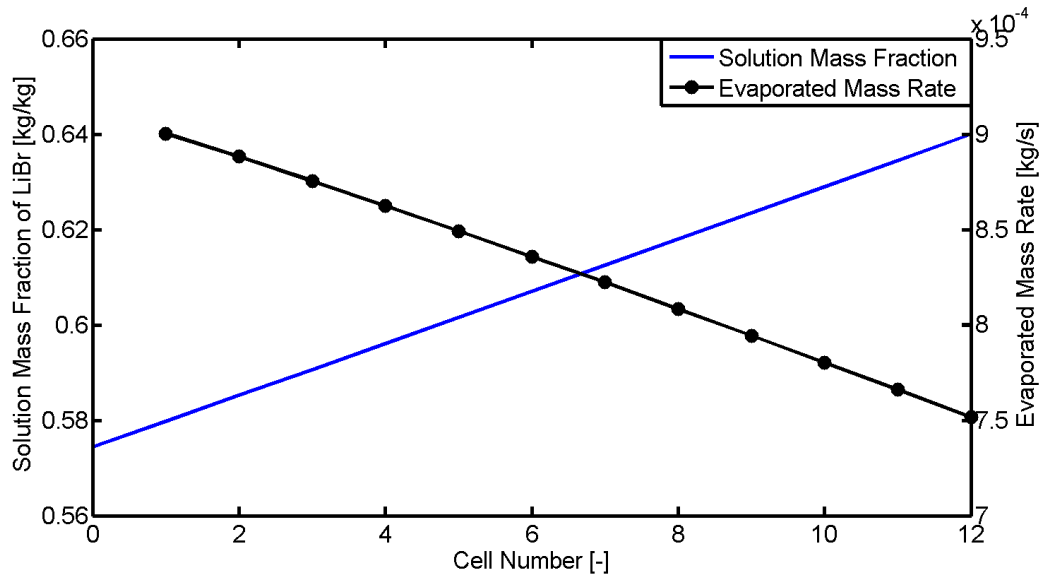


Figure 7.11. Solution mass fraction and amount of evaporated water in each cell.

While the mass fraction increases the amount of evaporated water decreases for each cell. This decrease in evaporation is due to the higher boiling point for a solution with a higher lithium bromide mass fraction.

The mass flow of the solution and the vapor is plotted in Figure 7.12 on the following page. A decrease in the solution mass flow is seen and is caused by the evaporated mass of water. The vapor mass flow is higher in the top, due to the vapor outlet being in the top, meaning that the water evaporated in the bottom rises and adds to the vapor from the top cells.

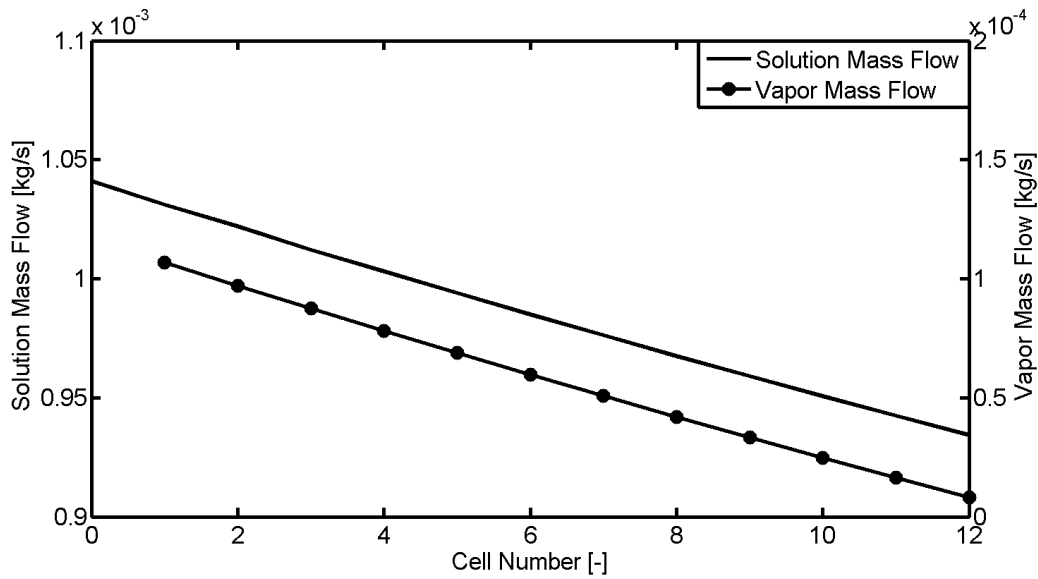


Figure 7.12. Solution mass flow and mass flow of vapor in the generator.

The mass and heat flux in the generator are shown in Figure 7.13. The heat and mass flux are defined as described in the results from the absorber model.

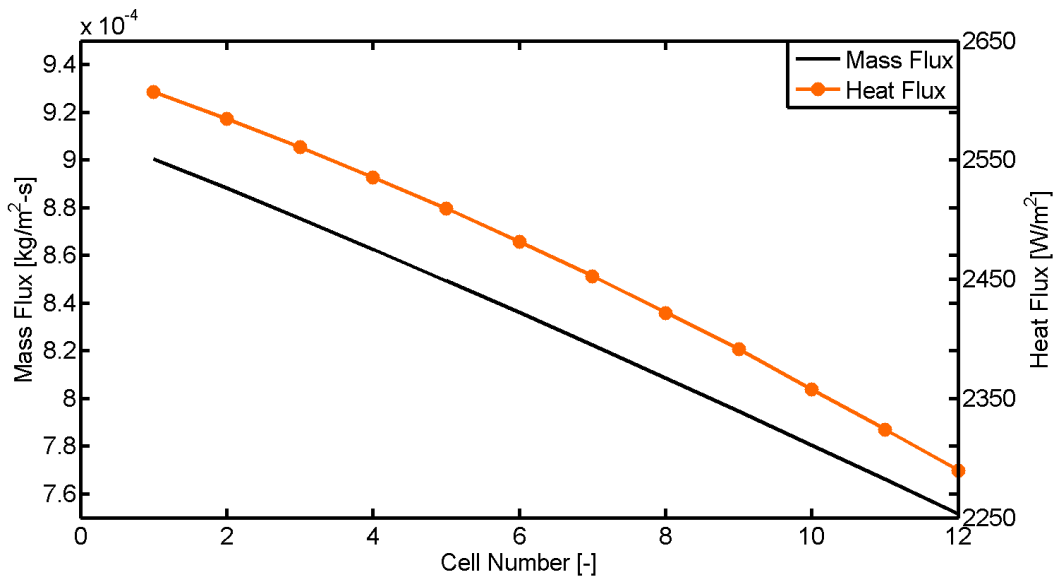


Figure 7.13. Heat and mass flux in the generator.

The heat flux obtained in the model have been compared with results from [Chyu and Bergles, 1987]. The wall is only superheated by about one degree Kelvin as seen from Figure 7.14 on the facing page, and based on this the results are in the same range.

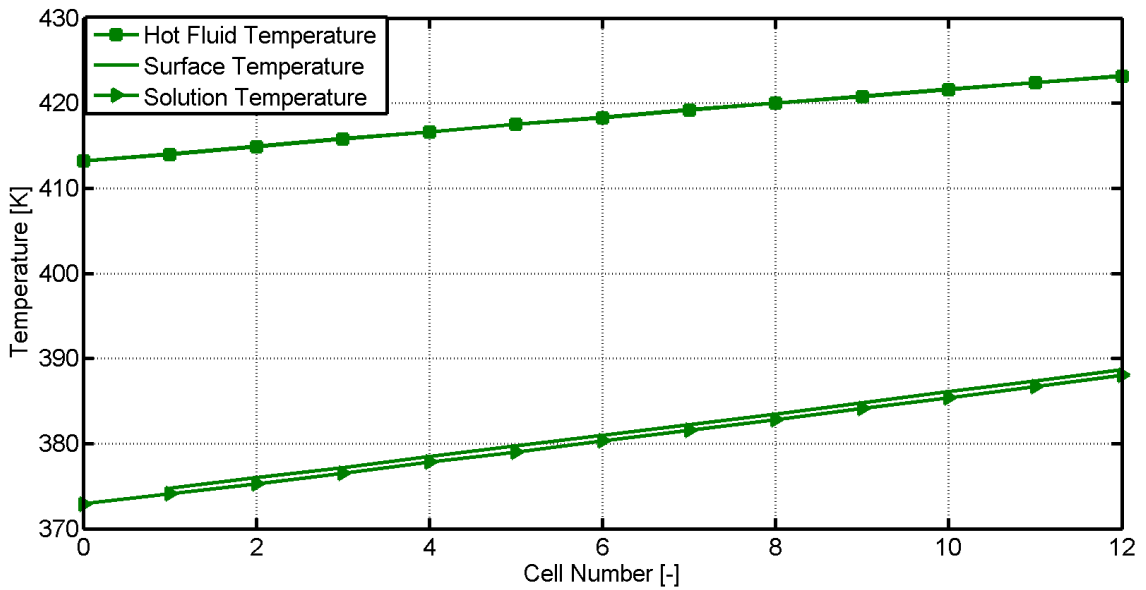


Figure 7.14. Hot fluid, solution and surface temperature.

The results presented in Figure 7.14 shows that the temperature of the solution and the surface of the tube is increased. The flow of the hot fluid shall be seen from right to left, and it is thereby seen that the hot fluid temperature is decreased. This corresponds well with a heat transfer from the hot fluid to the solution.

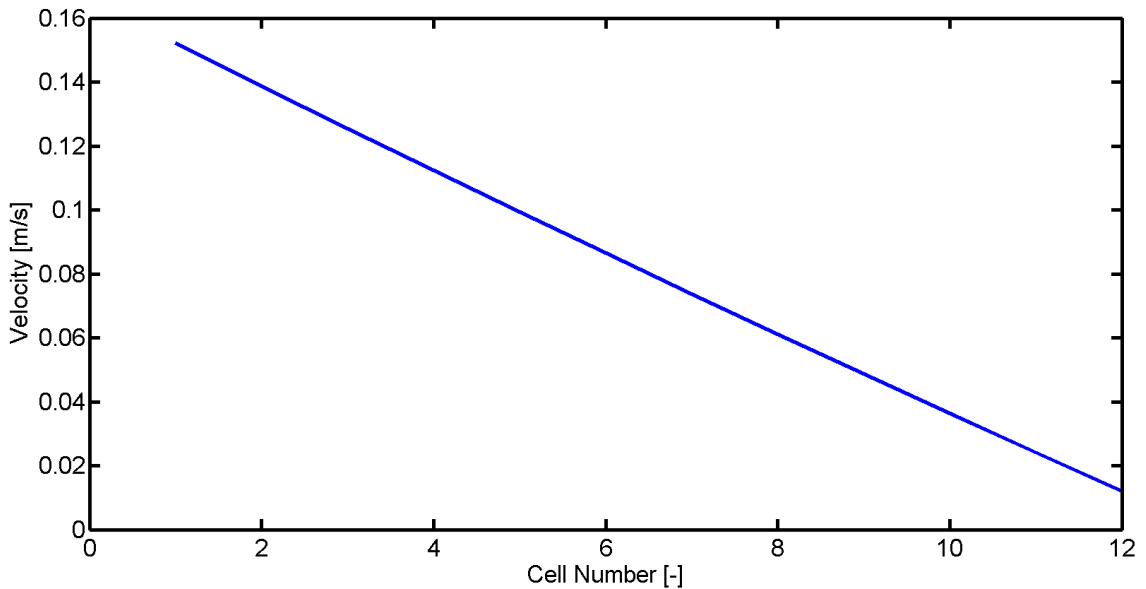


Figure 7.15. Velocity of the vapor through the generator.

The velocity of the vapor is plotted in Figure 7.15 showing that the temperature is highest in the top. This corresponds well with the mass flow of the vapor shown in Figure 7.12 on the preceding page. The geometry and thereby cross sectional area is constant for the generator.

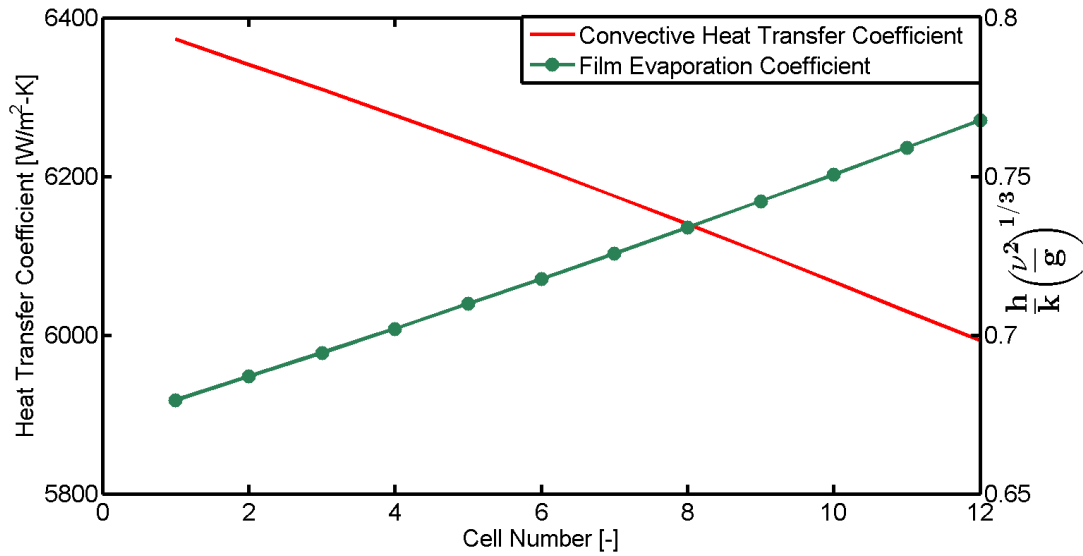


Figure 7.16. Heat transfer and film evaporation coefficients for the generator.

Figure 7.16 shows the convective heat transfer coefficient and the film evaporation coefficient for the generator. The heat transfer coefficient was found by using the correlation proposed by [Chun and Seban, 1972]. The film evaporation coefficient is calculated and plotted to be able to compare the results with other models. By comparison with [Chyu and Bergles, 1987] it is seen that the Reynolds numbers used in this model is lower and thereby not completely comparable. However it is seen that there is an increase in the film evaporation coefficient at lower Reynolds numbers and the found coefficient is assumed to be of the right order.

7.4 Evaporator

The evaporator is designed using the optimum configuration for the absorber, since they have the same geometry. The diameter of the tubes and the fin length is the same as found for the absorber, which can be seen from Table 7.7.

Type	2-row staggered grid
D_t	15.9 mm
L_e	0.6 m
m_e	23 tubes
L_{fin}	15.9 mm
Material cost	58 €

Table 7.7. Evaporator design.

An illustration of the evaporator is shown on Figure 7.17 on the facing page.

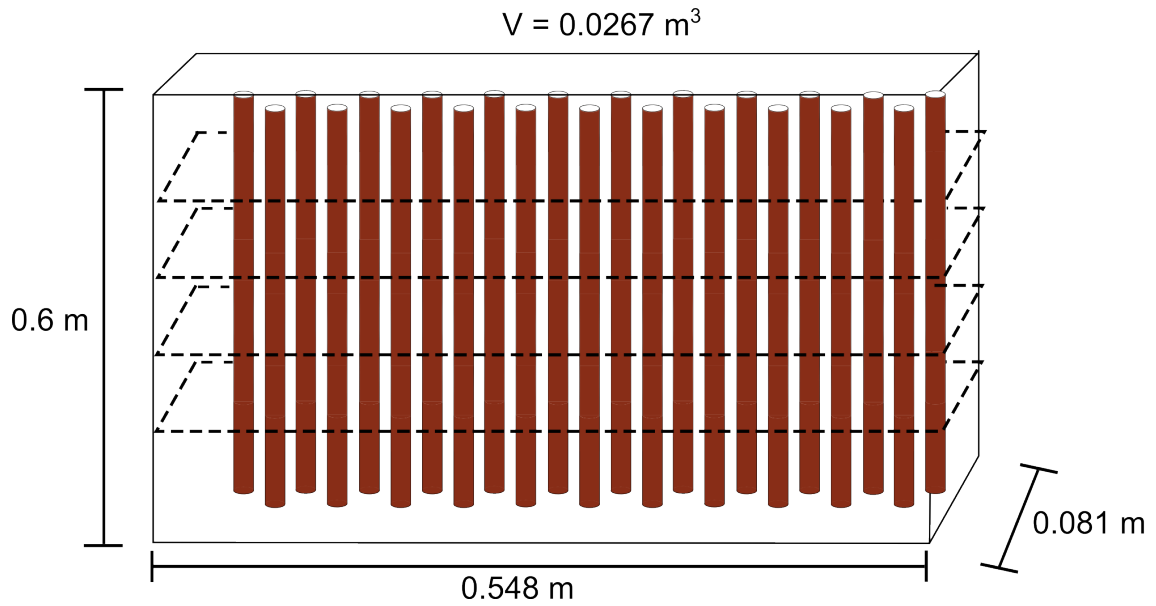


Figure 7.17. Visualization of the evaporator design, with dimensions (the fin density is higher than illustrated).

The only geometry parameters which has been changed compared to the absorber is the height and number of tubes. The overall size of the evaporator is smaller because the average film heat transfer coefficient ($1047[\frac{W}{m^2K}]$) is higher compared to the absorber.

7.5 Condenser

The condenser is also designed using the optimum configuration from the absorber, since they have the same geometry. The condenser design can be seen from Table 7.8.

Type	1-row in-line grid
D_t	15.9 mm
L_c	0.4 m
m_c	10 tubes
L_{fin}	15.9 mm
Material cost	23.4 €

Table 7.8. Condenser design.

The condenser design has been visualized on Figure 7.18 on the following page.

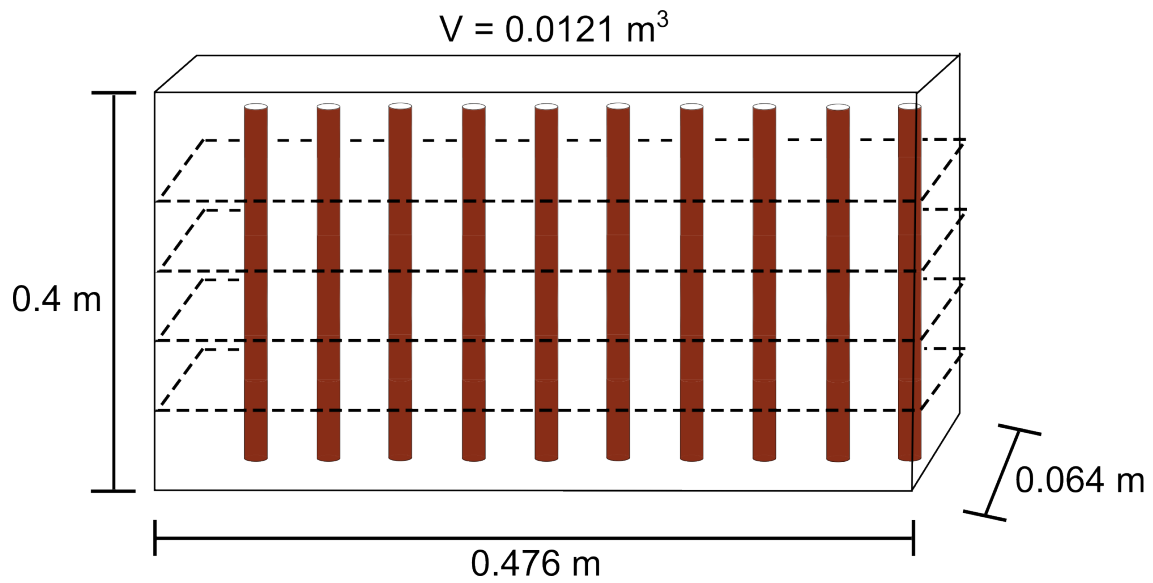


Figure 7.18. Illustration of the final design of the condenser. The dimensions are shown (the fin density is higher than illustrated).

The number of tubes in the condenser is lower compared to the evaporator since the film heat transfer coefficient ($6840[\frac{W}{m^2K}]$) is higher and the temperature difference is higher as well.

Discussion

This chapter will summarize and evaluate the results obtained during this project period. The design, performance and economical aspect will be covered.

8.1 System Design

The absorption chiller was dimensioned using the black-box model. The results from the model were reasonable and the model showed consistency in the energy balance. The optimized absorption chiller configuration had a COP of 0.86 and an estimated cost of 1674 €. The cost of the chiller is a rough estimate and is by no means to be taken as the actual cost. Even though the estimated cost is not precise the cost function suited its purpose and was used as a design parameter.

The sizes of the heat exchangers (UA-values) are not unrealistic and there was only a factor of three between the lowest and largest UA-value of the four main components. The cheapest design has a COP of 0.86 which is exactly on the lower bound of the feasible region. The upper limit of the weak solution mass fraction was defined to be 0.64 which also is the optimum. This upper limit of mass fraction was chosen in order to avoid crystallization of lithium bromide. From the Dühring plot it can be concluded that the chiller has not penetrated the crystallization line. As the optimal solution tends to be at the upper bound of the weak solution mass fraction the possibility to go even higher than 0.64 should be investigated.

A better performance can also be obtained by increasing the size of the solution heat exchanger. It is however, important keep in mind that the occurrence of crystallization is most likely to take place in the weak solution outlet of the solution heat exchanger. Crystallization in the solution heat exchanger is common because of the combination of high lithium bromide content and a low temperature. By increasing the effectiveness of the solution heat exchanger and thereby cool the weak solution further, it is possible to obtain a better performance, but the likelihood of crystallization increases [Herold et al., 1996].

The black-box model does not take into account heat losses, so it is likely that the performance is slightly over-predicted for the simulated case. It is possible to increase the heat into the generator by adjusting the output of the IM fuel cell system. Therefore it is possible to supply sufficient cooling capacity even at extreme cases.

8.2 Validity of Component Models

Absorber

The differential equations describing the heat and mass transfer in the falling film absorber were discretized into finite elements. A mesh independence study showed that the number of elements have a weak influence on the prediction of the performance of the absorber. The reason for that could be that the change in mass fraction and temperature from inlet to outlet is relatively small compared to the total mass and energy transport in the absorber. In the model it was found that the steepest temperature gradient occurred at the inlet of the absorber. The current discretization is insufficient for representing this rapid change in temperature. The temperature of the solution affects the heat transfer from the film to the surrounding, therefore a denser discretization could be considered for future simulations.

In the absorber model three empirical datasets are used: Sherwood number, convective film heat transfer coefficient and mass diffusivity of aqueous water/lithium bromide mixture. The important parameter to investigate is mass diffusivity, because this correlation was extrapolated from the original dataset. It was found that the mass fraction of the solution deviated 0.3% when the uncertainty of the mass diffusivity was assumed to be 10%. This relatively small change in mass fraction is acceptable and does not have a major impact on the design of the absorber. The manual extrapolation of the dataset was done conservatively, which means that the absorber may be over dimensioned.

The flow was assumed to be fully developed and the heat and mass transfer coefficients for the fully developed flow were applied for the entire length of the absorber. To verify this assumption a correlation was used to determine the length of the entrance region [Lel and Kneer, 2011]. This correlation is shown in Equation 8.1.

$$L_{\delta} = a \cdot \text{Re}_0^b \cdot \text{Pr}_s \cdot \text{Ka}_s^{0.0606} \cdot \left(\frac{\text{Pr}_s}{\text{Pr}_w} \right)^{-0.29} \cdot \left(\frac{v^2}{g} \right)^{\frac{1}{3}} \quad (8.1)$$

$$\text{for Re} < 8 \begin{cases} a = 0.8367 \\ b = 0.718 \end{cases}, \quad \text{for Re} > 8 \begin{cases} a = 0.022 \\ b = 1.36 \end{cases} \quad (8.2)$$

Re_0 is defined as $\text{Re}_0 = \frac{\dot{V}}{v \cdot B}$, where \dot{V} is the volume flow and B is the unit width of the flow area, in the case of the absorber the circumference of the vertical tube. Pr_w is the Prandtl number of the solution at the temperature of the wall, and the Kapitza number is defined as $\text{Ka}_s = \left(\frac{\sigma^3 \cdot \rho}{g \cdot \mu^4} \right)$. The entrance region was calculated to be approximately 8 mm for the absorber. It is therefore assumed to be an acceptable assumption to use the correlations for fully developed flow for the entire length of the heat and mass exchanger.

Generator

The generator was modeled using an empirical correlation to predict the average film heat transfer coefficient. An uncertainty analysis was performed in order to investigate the influence of the heat transfer coefficient on the overall mass transfer in the generator. It was found that the uncertainty of the outlet mass fraction was 0.3% assuming an uncertainty of 10% for the heat transfer coefficient.

The correlation for the average film heat transfer coefficient is dependent on the Reynolds number and it was found that the flow was laminar in all cases which support the simplification of assuming the flow to be fully developed.

As for the absorber the entrance region was also calculated for the generator. From Equation 8.1 on the facing page the length of the entrance region was found to be 2.3 mm, which is small relative to the perimeter of the tube. It is there for assumed to be an acceptable assumption to use the heat transfer coefficient for the fully developed region for the entire perimeter of the tubes in the generator.

In the model it was assumed that the tubes were fully wetted and the minimum wetting ratio was not considered. Achieving an uniform distribution is difficult and there is a possibility of misdistribution or even local dry zones, which affects the overall heat transfer in the generator. In order for the model to be valid the minimum wetting ratio needs to be investigated.

Evaporator and Condenser

The evaporator and condenser were both modeled using the same principle of geometry as the absorber. Therefore the calculation of the outer convective heat transfer and conduction through the tube is the same. Both models used empirical correlations in order to predict an average film heat transfer coefficient.

In the evaporator model it is assumed to be acceptable to use an average film heat transfer coefficient since the temperature is constant during the evaporation of the refrigerant.

The refrigerant is superheated when entering the condenser and will have to be cooled and then condensed. This means that the UA-value predicted in the black-box model is slightly underestimated due to the assumption of a logarithmic mean temperature difference. Even with the slightly under-predicted UA-value it is assumed to be acceptable to use an average heat transfer coefficient since the heat of condensation is much higher than the energy of desuperheating.

8.3 Components Size and Performance

In this section the size and performance of the four main components are analyzed. The absorber and generator were designed by minimizing the material cost while the

evaporator and condenser were designed based on the optimum absorber design. The tube diameter and fin length of the evaporator and condenser were the same as for the absorber. The only parameters which are changed are the length and number of tubes in order to reach a sufficient heat transfer area. A summarization of the previous design results are presented in Table 8.1. The Face Area is the cross sectional area seen by the fan for the air-cooled heat exchangers and the volume covers the space taken up by tubes, fins and chassis. The volumes do not cover manifolds and fans.

	Absorber	Evaporator	Condenser	Generator	
Type	4-row stag.	2-row stag.	1-row in-line	12 passes	
N_{tube}	41	23	10	11	tubes
D_{tube}	15.9	15.9	15.9	12.7	mm
L_{tube}	1.285	0.6	0.4	0.699	m
L_{fin}	15.9	15.9	15.9	-	mm
Face Area	0.62	0.289	0.172	-	m^2
Volume	92	26.7	12.1	36.5	l
Cost	162.1	58	23.4	314.3	€

Table 8.1. Summarization of component design.

Looking at Table 8.1 it is seen that the largest component is the absorber, while the generator is the most expensive. This is consistent with the fact that the absorber is the component which requires the highest UA-value according to the black-box model. The smallest and cheapest component is the condenser which also is in good agreement with the fact that this is the component which requires the least heat exchanger area. The average film heat transfer coefficient for the condenser is high ($6840 \frac{W}{\text{m}^2 \cdot K}$) compared to the absorber ($550 \frac{W}{\text{m}^2 \cdot K}$) which also explains the difference in sizes. The volumes listed in Table 8.1 are not covering manifolding, fans and chassis required, it is simply the area taken up by heat exchanger tubes and fins.

Comparing the absorber, evaporator and condenser it is seen that they all have approximately 10 tubes per row which is equivalent to a width of approximately 0.50m . Having heat exchangers of equal width is convenient if the components are to be built into a chassis.

The optimum absorber design was found where the length of the tubes were right on the upper edge of the feasible region. The design constrain for the tube length was 1.20m and this was also the optimum solution. The absorber was subsequently expanded slightly because the optimum solution was a non-integer number of tubes. The optimization showed that longer tubes can reduce the material cost of the absorber. Longer tubes mean a taller absorber, which can become a problem when it comes to the forced convection and the number of fans required increase with the height of the absorber. The required steam inlet velocity to the absorber is currently equal to 20m/s which also is on the edge of a design constrain. By decreasing the number of tubes

and increasing the length of the tubes more vapor has to be absorbed in each tube. If the number of tubes are decreased the steam inlet velocity of each tube will increase which can affect the film heat transfer coefficient and the pressure drop.

The generator model was based on assuming a uniform distribution of liquid along the tubes. It is difficult to achieve a complete wetting of the tubes and a suitable spray nozzle must be chosen. Since the water/lithium bromide is more viscous than water (approximately $\times 10$) the falling film in the generator is laminar. In [Chyu and Bergles, 1987] it is found that the jet height has less impact on the film heat transfer coefficient for laminar flow.

All components are meant to be placed outside the cooling load area (BTS shelter) except for the evaporator and therefore it is important to consider the size of the evaporator. The evaporator consist of 23 tubes arranged in a 2-row staggered tube bundle, the volume is 26.7 l and the face area is 0.289m^2 . The designed evaporator does not take up more space than an evaporator used in a traditional compression air-conditioning system.

Conclusion

The general purpose of this project was to develop an absorption chiller capable of utilizing the waste heat from an IM-FC system and thereby deliver cooling capacity. The combination of absorption chiller and IM-FC system is meant as a replacement for a diesel generator and compression chiller supplying power and cooling to a base transceiver station in India.

A case study was performed in order to clarify the economical aspects of the concept, both in comparison with the traditional setup. The maximum Return of Investment was assumed to be 1.5 years and it was found that the maximum investment cost is 3700€ and the minimum COP 0.857.

It was found that a water/lithium bromide chiller will be the best choice of concept, and only this principle was considered in the report. A simple black-box model was developed based on mass and energy balance in order to predict the performance of the chiller based on configuration and operational conditions. The model showed reasonable tendencies and consistency in energy balance. The chiller configuration was optimized based on an estimated cost of each of the components. It was found that a single-effect chiller was considerably cheaper in comparison with a double-effect system. Since it was possible for the single-effect to achieve a COP higher than 0.86 the simpler and cheaper system was chosen.

The configuration with the lowest cost and a minimum COP of 0.86 was found by using EES' Direct Search algorithm. It was seen from a Dühring plot that the chiller cycle is far from the crystallization line and the temperature and pressure levels are reasonable.

Component models were developed for the four main heat and mass exchangers. The evaporator and condenser were modeled using a rough estimation of the overall heat transfer coefficients. More advanced models were developed for the absorber and generator since the mass and heat transfer is more complex in these components. The four heat and mass exchangers were designed based on inlet and outlet conditions determined by the black-box model. The absorber and generator were designed by minimizing the material cost and the evaporator and condenser were designed based on the optimal design of the absorber. The residuals of the energy equations for the absorber and generator were calculated and they both showed consistency in the

energy equation. A mesh independence study was also performed for the absorber and it was found that the mesh only has a weak influence on the final solution.

It was found that the cheapest solution for absorber is to have as few and as long tubes as possible. When designing the absorber it is important to consider the required steam inlet velocity, because it increases as the number of tubes is reduced. The optimal solution was found with a maximum steam velocity just below the design constrain.

The physical size of each component was estimated and it was found that the largest component is the absorber and the condenser is the smallest. These result were in good agreement with the estimated UA-values from the black-box model and the predicted heat transfer coefficients. The evaporator is the only component which is placed inside the cooling load area and has a volume of approximately 26 l which is in the same order of size as evaporators in traditional compression air-conditioners. The absorber and the condenser were designed to have approximately the same width which is favorable if they are to be installed in the same chassis.

The cost functions used in the black-box model showed the total cost of the four main components to be 1674.72€. These cost functions are based on the total cost if the heat exchangers are to be bought from a supplier. By using the component models more specific costs could be determined, however only for the materials used to produce the heat and mass exchangers. The total material cost for the same four components was found to be 557.8€. Assuming the materials can be obtained at the cost used in this report there will be 3142.2€ left for assembling, pump, tubing, valves, chassis and control systems. Even with the rough estimation of the component costs it is deemed realistic to fabricate an air-cooled water/lithium bromide chiller for less than the maximum capital expense of 3700€.

Future Work

This section will be used to describe some of the future perspectives in this concept of tri-generation.

There are vast opportunities for different applications of a system consisting of an IM-FC system and an absorption chiller. By not only using the fuel cell as a range extender for EV's, but at the same time utilize the waste heat to deliver air-conditioning in the cabin the range can be greatly improved. In EV's waste heat from other components could also be utilized by the absorption chiller, such as heat from the batteries, electric motors/generators and power electronics.

In addition to look into other applications of the system, other designs could also be considered. This project has looked into components of traditional design, scaled to fit the purpose. Other design may prove to be better for small capacity systems for a case like the BTS power supply. There may also be more flexible solutions that could be considered. The work in [Determan and Garimella, 2010] describes the development of a prototype microscale absorption heat pump consisting of monolithic plates stacked together. The concept is seen on Figure 10.1. The capacity of the absorption heat pump can be scaled by the number of plates stacked together. The work is based on an ammonia/water cycle with higher pressure levels, and the low pressure levels in a water/lithium bromide cycle may cause high velocities and pressure losses. Ammonia/water cycles usually have a lower COP than water/lithium bromide, but may prove to be more compact.

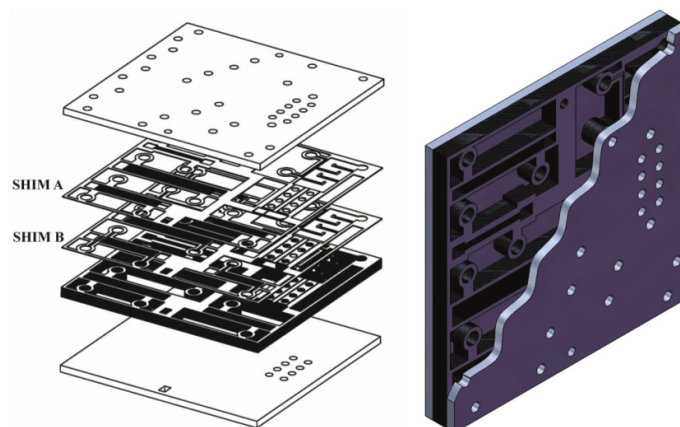


Figure 10.1. Microscale Monolithic Absorption Heat Pump [Determan and Garimella, 2010]

To be able to determine a final design it will be necessary to consider the pressure losses in such a system. Especially for the design of the absorber and the evaporator the pressure losses will have to be taken into account. The large volume of water vapor at low pressures results in high velocities and thereby high pressure losses. At the low pressures in a water/lithium bromide chiller drops in pressure can cause large influence on the temperature due to the slope of the vapor pressure curve of water [Herold et al., 1996].

The design found in this report is optimized for a an extreme case where the power consumption of the BTS is at maximum, there is no free-cooling available and at the same time the temperature level inside (load temperature) is set to 27°C which is a comfort temperature used during service work. By looking more into the actual operation of the BTS a smaller/less expensive chiller may prove sufficient. The chiller developed in this project is dimensioned to be capable of delivering the entire cooling capacity. In reality parts of the cooling could be achieved by free-cooling from the ambient and the combination of these should be investigated.

In this work little effort have been put into calculating the fan and pump power consumption. To be able to determine the work required for the pump the pressure losses will have to be considered. Being air-cooled the chiller will require an substantial amount of forced convection and thereby power consumption in the fans.

It is important to consider the possibility of using alternative configurations and equipment. One possibility is to use recirculation in the heat exchangers, which means extracting some of the excess liquid of the outlet and returning it to the inlet. Recirculation can be used to control the amount of superheating/subcooling and insure complete wetting in the heat exchangers. In the evaporator recirculating liquid can even enhance the heat transfer coefficient, because the heat transfer coefficient is highly dependent on the inlet quality [Shilling, 2008].

It is also possible to avoid recirculation by using another concept for the evaporator. The principle of rising film is often used in industrial chemical plants. The configuration is similar to the falling film except the feed product enters the bottom of the tube. The ascending force which is produced by the boiling causes the vapor and liquid to rise upwards. The production of vapor increases and the liquid is pressed against the tube wall as a thin film. The co-current movement of vapor and rising film against the force of gravity tends to create a high degree of turbulence in the film which benefits the film heat transfer coefficient [GEA Process Engineering Inc., 2013].

The crystallization of the lithium bromide should also be considered. The salt components in the aqueous lithium bromide solution precipitate when the mass fraction of lithium bromide surpasses the limit of solubility. This limit depends on the temperature and pressure [Herold et al., 1996]. Therefore should the flow of the weak solution be considered and particularly after the solution heat exchanger which cools the weak solution.

A study of the corrosive effect of aqueous lithium bromide solutions could also be beneficial for the consideration of lifetime of the system. The lithium bromide solutions are aggressive to copper and carbon steel as well as many other metals. Different alloys or corrosion inhibitors could be considered as measures to limit the corrosion. It should however be noted that in subatmospheric environments with little oxygen present the corrosion rates are relatively low [Herold et al., 1996].

The control of the system is something this report does not cover. The pump and valves will have to be regulated, as well as the monitoring equipment required should also be considered.



Bibliography

- Andberg and Vlient, 1983.** J.W Andberg and G.C. Vlient. *Design guidelines for water-lithium-bromide absorbers*. ASHRAE Transactions, 89(1B), 220–232, 1983.
- Arora, 2011.** Ramesh Chandra Arora. *Refrigeration and Air Conditioning*. ISBN: 978-81-203-3915-6. PHI Learning Private Limited, 2011.
- Bromley, 1950.** LeRoy A. Bromley. *Heat Transfer in Stable Film Boiling*. Chemical Engineering Progress, 46(5), 221–227, 1950.
- Castro, Olivia, Perez-Segarra, and Cadafalch, 2007.** Jesus Castro, Assensi Olivia, Carlos David Perez-Segarra, and Jordi Cadafalch. *Evaluation of a Small Capacity, Hot Water Driven, Air-Cooled H₂O-LiBr Absorption Machine*. HVAC&R Research, 13(1), 59–75, 2007.
- Cengel, 2006.** Yunus A. Cengel. *Heat and Mass Transfer: A Practical Approach*. ISBN: 978-007-125739-8. McGraw Hill, 2006.
- Cengel, 2002.** Yunus A. Cengel. *Heat Transfer: A Practical Approach*. ISBN: 978-007-245893-0. McGraw Hill, 2002.
- Chemical Engineering, 2013.** Chemical Engineering. *Current Trends*. Chemical Engineering, 120, 4, 72, 2013.
- Chemical Engineering, 1997.** Chemical Engineering. *Economic Indicators*. Chemical Engineering, 104, 4, 187, 1997.
- Chun and Seban, 1972.** K. R. Chun and R. A. Seban. *Performance Prediction of Falling-Film Evaporators*. Journal of Heat Transfer, 94(4), 432–436, 1972.
- Chyu and Bergles, 1987.** M.C. Chyu and A.E. Bergles. *An Analytical and Experimental Study of Falling-Film Evaporation on a Horizontal Tube*. Journal of Heat Transfer, 109, 983–990, 1987.
- Determan and Garimella, 2010.** Matthew D. Determan and Srinivas Garimella. *A Microscale Monolithic Absorption Heat Pump*. International Refrigeration and Air Conditioning Conference at Purdue, 2516, 1–7, 2010.
- GEA Process Engineering Inc., 2013.** GEA Process Engineering Inc. *Rising film evaporators, June 1st 2013*, 2013. URL www.niroinc.com.

- Geankoplis, 1993.** Christie J. Geankoplis. *Transport Processes and Unit Operations, 3rd ed.* ISBN: 0-13-045253. Prentice-Hall International, 1993.
- Grossman, 1983.** G. Grossman. *Simultaneous heat and mass transfer in film absorption under laminar flow.* International Journal of Heat and Mass Transfer, 26(3), 357–371, 1983.
- Herold, Radermacher, and Klein, 1996.** Keith E. Herold, Reinhard Radermacher, and Sanford A. Klein. *Absorption Chillers and Heat Pumps.* ISBN: 978-0-8493-9427-5. CRC Press, 1996.
- Hobler, 1966.** T. Hobler. *Mass transfer and absorbers.* Warsaw: Wydawnictwa Naukowo-Techniczne, 1, 94–96, 1966.
- Klein, 2013.** S.A. Klein. *EES - Engineering Equation Solver for Microsoft Windows Operating Systems,* 2013.
- Knudsen, 1973.** J. G. Knudsen. *Mass transfer and absorbers.* Chemical Engineers' Handbook, 5. ed, 10–14, 1973.
- Lel and Kneer, 2011.** Viacheslav V. Lel and Reinhold Kneer. *Heat Transfer Phenomena in Laminar Wavy Falling Films: Thermal Entry Length, Thermal-Capillary Metastable Structures, Thermal-Capillary Breakdown, Heat Transfer - Theoretical Analysis, Experimental Investigations and Industrial Systems, Prof. Aziz Belmiloudi (Ed.).* ISBN: 978-953-307-226-5. InTech, 2011.
- Linnhoff, Townsend, Boland, Hewitt, Thomas, Guy, and Marsland, 1994.** B. Linnhoff, D.W. Townsend, D Boland, G.F Hewitt, B.E.A Thomas, A.R. Guy, and R.H. Marsland. *User Guide on Process Integration for the Efficient use of Energy.* Macmillian Publishing co., 1994.
- Medrano, Bourouis, and Perez-Blanco, 2003.** Marc Medrano, Mahmoud Bourouis, and Horacio Perez-Blanco. *A simple model for falling film absorption on vertical tubes in the presence of non-absorbables.* International Journal of Refrigeration, 26, 108–116, 2003.
- Metals Depot, 2013.** Metals Depot. *Cost of stainless steel tubes, May 27th 2013,* 2013. URL www.metalsdepot.com.
- Nusselt, 1916.** W. Nusselt. *Die oberflächenkondensation des wasserdampfes.* Verein Deutscher Ingenieure (VDI), 60, 541–569, 1916.
- Patnaik, Perez-Blanco, and Ryan, 1993.** P. Patnaik, H. Perez-Blanco, and W.A. Ryan. *A Simple Analytical Model for the Design of Vertical Tube Absorbers.* ASHRAE Transactions, 99(2), 69–80, 1993.
- Perez-Blanco, 1988.** H. Perez-Blanco. *A model of an ammonia-water falling film absorber.* ASHRAE Transactions, 94(1), 467–483, 1988.

- Potnis, Lenz, and Dunlop, 1993.** Shailesh V. Potnis, Terry G. Lenz, and Eric H. Dunlop. *Measurement of water diffusivity in aqueous lithium bromide solution.* Thermophysical properties for industrial process design-, 1, 1–5, 1993.
- Pátek and Klomfar, 2006.** J. Pátek and J. Klomfar. *A computationally effective formulation of the thermodynamic properties of LiBr-H₂O solutions from 273 to 500 K over full composition range.* International Journal of Refrigeration, 29, 566–578, 2006.
- Rapid Fab., 2013.** Rapid Fab. *Cost of aluminum sheets, May 27th 2013,* 2013. URL www.fab.net.au.
- Seban, 1978.** R. A. Seban. *Transport to falling film.* Heat Transfer Conference, Toronto, 6, 417–428, 1978.
- Serenergy A/S, 2011.** Serenergy A/S. *Advantages of HTPEM fuel cells over LTPEM fuel cells,* 2011.
- Serenergy A/S, 2013a.** Serenergy A/S. *Spreadsheet provided by Mads Friis Jensen,* 2013.
- Serenergy A/S, 2013b.** Serenergy A/S. *HT PEM basics, June 3rd 2013,* 2013. URL serenergy.com.
- Shilling, 2008.** Richard L. Shilling. *Perry's Chemical Engineers' Handbook 8th ed., Section 11-14.* ISBN: 0-07-151134-2. The McGraw-Hill Companies, 2008.
- Subramaniam, 2008.** Vishwanath Subramaniam. *Computational Analysis of Binary-fluid Heat and Mass Transfer in Falling Film and Droplets,* 2008.
- Sun and Teja, 2003.** Tongfan Sun and Aryn S. Teja. *Density, Viscosity, and Thermal Conductivity of Aqueous Ethylene, Diethylene, and Triethylene Glycol Mixtures between 290 K and 450 K.* Journal of Chemical and Engineering Data, 48, 198–202, 2003.
- Wang and Chua, 2009.** Xiaolin Wang and Hui T. Chua. *Absorption Cooling: A Review of Lithium Bromide-Water Chiller Technologies.* Recent Patents on Mechanical Engineering, 2, 192–213, 2009.
- Yao, Bjurstrom, and Setterwall, 1991.** Wen Yao, Henrik Bjurstrom, and Fredrik Setterwall. *Surface Tension of Lithium Bromide Solutions with Heat-Transfer Additives.* Journal of Chemical and Engineering Data, 36, 96–98, 1991.
- Yih and Chen, 1982.** S.M. Yih and K.Y. Chen. *Gas absorption into wavy and turbulent falling liquid films in a wetted-wall column.* Chemical Engineering Community, 17, 123–136, 1982.

Yuksel and Schlunder, 1988. M.L. Yuksel and E.U. Schlunder. *Heat and mass transfer in non-isothermal absorption of gases in falling liquid films.* Waerme- und Stoffubertragung, 22(3-4), 209–217, 1988.

Double-Effect Chiller Model

This appendix will describe the black-box model of a double-effect absorption chiller, developed during the project period. An illustration showing the double-effect chiller and the numbering system used is shown in Figure A.1.

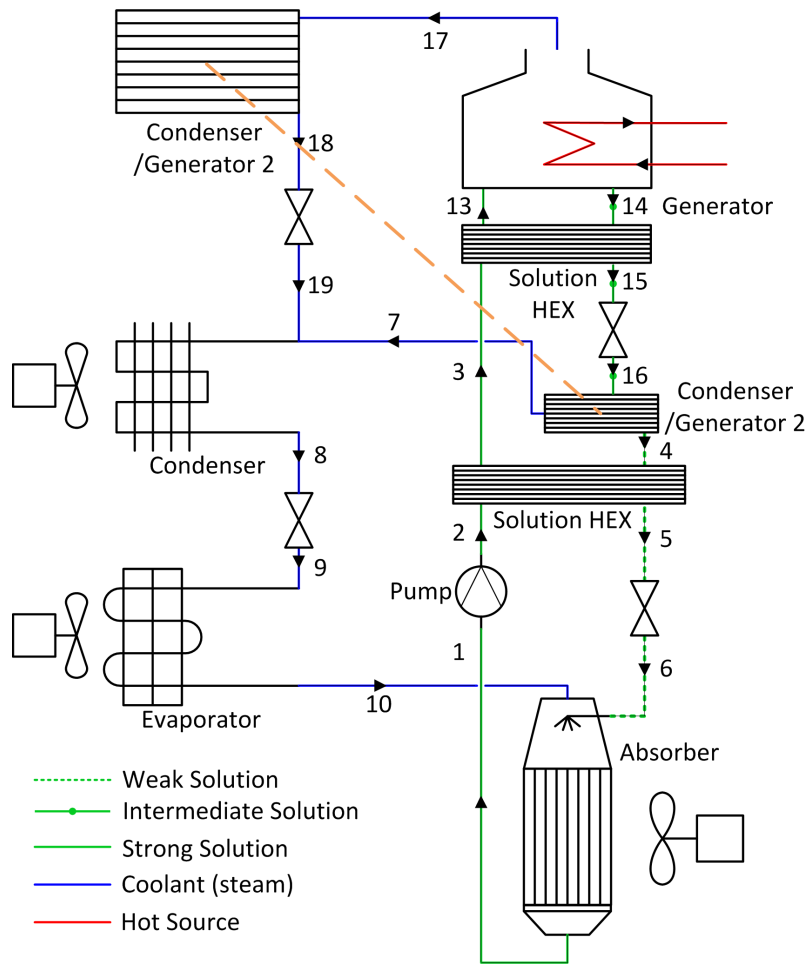


Figure A.1. Illustration of double-effect cycle

The assumptions used when modeling the double-effect chiller are listed in Table A.1 on the following page.

Point	Equation	Assumption
1	$x_1 = 0$	saturated liquid
4	$x_4 = 0$	saturated liquid
6	$h_6 = h_5$	isenthalpic valve
7	$w_7 = 1, x_7$	saturated water vapor
8	$w_8 = 1, x_8 = 1$	saturated liquid water
9	$h_9 = h_8$	isenthalpic valve
10	$w_{10} = 1, x_{10} = 1$	saturated water vapor
11	$x_{11} = 0$	saturated liquid
14	$x_{14} = 0$	saturated liquid
16	$h_{16} = h_{15}$	isenthalpic valve
17	$w_{17} = 1, x_{17} = 1$	saturated water vapor
18	$w_{18} = 1, x = 0$	saturated liquid water
19	$h_{19} = h_{18}$	isenthalpic valve

Table A.1. Assumptions for the states in the double-effect model.

The mass balances for each component shown in the equations below:

Condenser/Generator 2

$$m_{16} = m_7 + m_4 \quad (\text{A.1})$$

$$m_{16} \cdot w_{16} = m_4 \cdot w_4 \quad (\text{A.2})$$

Condenser

$$m_8 = m_{19} + m_7 \quad (\text{A.3})$$

Generator

$$m_{13} = m_{14} + m_{17} \quad (\text{A.4})$$

$$m_{17} = m_{13} \cdot (1 - w_{13}) - m_{14} \cdot (1 - w_{14}) \quad (\text{A.5})$$

The conservation of energy is based on the equations shown in Table A.2 on the next page. The logarithmic mean temperature difference is also shown for each component in the chiller system.

Component	Equation	LMTD
Absorber	$Q_a = UA_a \cdot \Delta T_{LMTD,a}$ $Q_a = m_{10} \cdot h_{10} + m_6 \cdot h_6 - m_1 \cdot h_1$	$\Delta T_{LMTD,a} = \frac{(T_6 - T_\infty) - (T_1 - T_\infty)}{\ln\left(\frac{T_6 - T_\infty}{T_1 - T_\infty}\right)}$
Condenser	$Q_c = UA_c \cdot \Delta T_{LMTD,c}$ $Q_c = m_7 \cdot h_7 + m_{19} \cdot h_{19} - m_8 \cdot h_8$	$\Delta T_{LMTD,c} = \frac{(T_7 - T_\infty) - (T_8 - T_\infty)}{\ln\left(\frac{T_7 - T_\infty}{T_8 - T_\infty}\right)}$
Condenser/ Generator 2	$Q_{cg} = UA_{cg} \cdot \Delta T_{LMTD,cg}$ $Q_{cg} = m_{17} \cdot h_{17} - m_{18} \cdot h_{18}$ $Q_{cg} = m_{17} \cdot h_{17} + m_{16} \cdot h_{16} - m_7 \cdot h_7 - m_4 \cdot h_4 - m_{18} \cdot h_{18}$	$\Delta T_{LMTD,cg} = \frac{(T_{18} - T_4) - (T_{18} - T_{16})}{\ln\left(\frac{T_{18} - T_4}{T_{18} - T_{16}}\right)}$
Generator	$Q_g = UA_g \cdot \Delta T_{LMTD,g}$ $Q_g = m_{21} \cdot cp \cdot (T_{21} - T_{22})$ $Q_g = m_{17} \cdot h_{17} + m_{14} \cdot h_{14} - m_{13} \cdot h_{13}$	$\Delta T_{LMTD,g} = \frac{(T_{21} - T_{14}) - (T_{22} - T_{17})}{\ln\left(\frac{T_{21} - T_{14}}{T_{22} - T_{17}}\right)}$
Evaporator	$Q_e = UA_e \cdot \Delta T_{LMTD,e}$ $Q_e = m_9 \cdot (h_{10} - h_9)$	$\Delta T_{LMTD,e} = \frac{(T_{load} - T_{10}) - (T_c - T_9)}{\ln\left(\frac{T_{load} - T_{10}}{T_{load} - T_9}\right)}$
HEX 1	$Q_{HEX1} = UA_{HEX1} \cdot \Delta T_{LMTD,HEX1}$ $Q_{LMTD} = m_1 \cdot (h_3 - h_2)$ $Q_{HEX1} = m_5 \cdot (h_4 - h_5)$	$\Delta T_{LMTD,HEX1} = \frac{(T_4 - T_3) - (T_5 - T_2)}{\ln\left(\frac{T_4 - T_3}{T_5 - T_2}\right)}$
HEX 2	$Q_{HEX2} = UA_{HEX2} \cdot \Delta T_{LMTD,HEX2}$ $Q_{HEX2} = m_3 \cdot (h_{13} - h_3)$ $Q_{HEX2} = m_{14} \cdot (h_{14} - h_{15})$	$\Delta T_{LMTD,HEX2} = \frac{(T_{14} - T_{13}) - (T_{15} - T_3)}{\ln\left(\frac{T_{14} - T_{13}}{T_{15} - T_3}\right)}$

Table A.2. Equations for conservation of energy in the double-effect water/lithium bromide chiller.

The results obtained from the modeling of the double-effect chiller is shown on the Figure A.2 on the following page. The enthalpy, temperature, pressure and mass fraction of lithium bromide is presented for all locations in the chiller system.

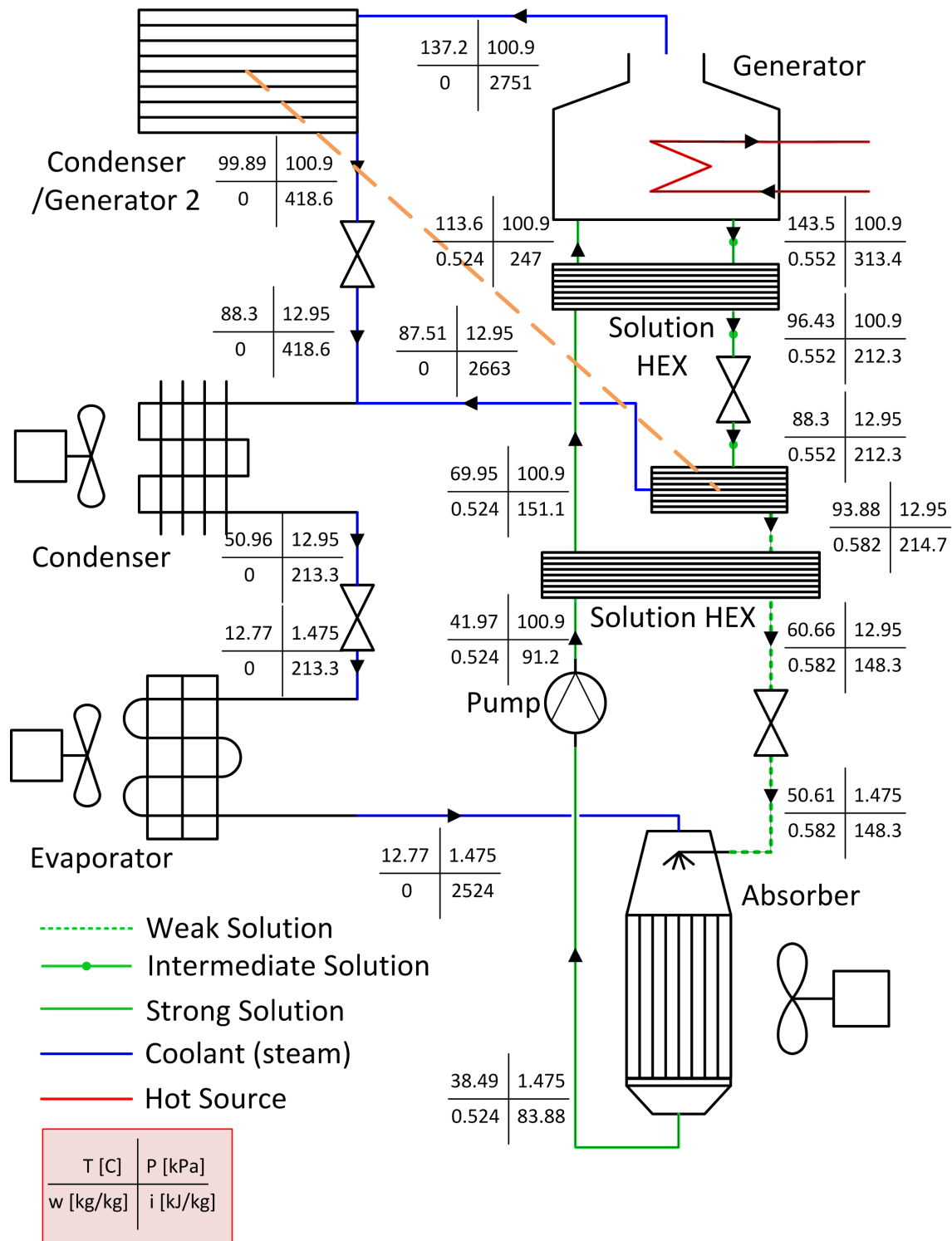


Figure A.2. Results for the optimum double-effect chiller configuration.

The required heat exchangers are based on the UA-value and cost functions presented in Table 4.7 on page 24. The UA-value, heat transfer and cost of each heat and mass exchanger are presented in Table A.3 on the facing page.

Component	UA-Value [$\frac{W}{K}$]	Q [W]	Cost [€]
Absorber	485.2	3925	1518.66
Condenser	54.5	1674	170.70
Condenser/Generator	184.2	1565	159.94
Evaporator	210.8	3000	672.17
Generator	2.504	2504	1054.17
Total Cost			3575.64

Table A.3. Results for optimized double-effect chiller configuration.

The energy conservation for the double-effect model is checked by using equation A.6.

$$Q_g + Q_e + P_{\text{pump}} - Q_c - Q_a = 2504 + 3000 + 95 - 1674 - 3925 = 0 \quad (\text{A.6})$$

B**Study of Entrance Region**

In some cases it is necessary to consider the entrance region of the tube if the entrance region takes up a considerable amount of the total tube length. Both the heat and mass transfer is calculated different for the entrance region.

The estimation of the Sherwood number for the entrance region is based on Higbie's penetration theory. This is valid because it is assumed that the effect of the interfacial waves is neglectable due to the short time exposures in the entry region. Based on that assumption Equation B.1 is used to find the Sherwood number for the entrance region [Hobler, 1966].

$$\text{Sh}_{s,i} = 1.381 \cdot \left(\frac{s_i}{\delta_{s,i}} \cdot \frac{1}{\text{Re}_{s,i}} \cdot \frac{1}{\text{Sc}_{s,i}} \right)^{-1/2} \quad (\text{B.1})$$

where:

$$\text{Re}_{s,i} = \frac{4 \cdot \Gamma_{s,i}}{\mu_{s,i}} \quad (\text{B.2})$$

$$\text{Sc}_{s,i} = \frac{\mu_{s,i}}{\rho_{s,i} \cdot D_{ab,i}} \quad (\text{B.3})$$

The heat transfer coefficient for the thermal entrance region is determined from the correlation in Equation B.4 by [Knudsen, 1973] assuming an intermediate between constant heat flux wall and an isothermal wall.

$$h_{s,i} = \left(1.29 \cdot \left(\frac{(k_{s,i})^2 \cdot \rho_{s,i}^{4/3} \cdot (\text{cp}_{s,i})}{s_i \cdot \mu_{s,i}^{1/3}} \right)^{1/3} \cdot \text{Re}_{s,i}^{1/9} \right) \quad (\text{B.4})$$

EES models

In this appendix the EES code for the models will be presented. The models will be shown in the order:

- Single-effect system model
- Double-effect system model
- Absorber component model
- Generator component model
- Condenser component model
- Evaporator component model

The EES models are also available on the CD in the back of the report, as an executable file. The file can run without EES being installed, the "UserLib" folder has to be in the same folder as the "EES Models.exe" file. The model work by running the executable file and then clicking the "See Models!" tab and choosing the desired model. The equations can be seen by clicking "Windows" and "Equations". The model is executed by pushing "F2" and the indexed results are presented in a matrix.

Single-Effect Model

Equations

Inputs

$$Ph = 17,69$$

High pressure

$$Pl = 1,516$$

Low Pressure

$$w_{ss} = 0,5744$$

Strong solution

$$w_{ws} = 0,64$$

Weak solution

$$T_{inf} = 35$$

Ambient temperature

$$T_l = 27$$

The load temperature

$$cp_{hf} = 2721$$

Heat capacity of the hot fluid

$$Q_e = 3000$$

The cooling demand is 3000 W

$$COP_c = \frac{Q_e}{(Q_g)}$$

Heat transferred in generator from heat source

$$T_{11} - T_{12} = 10$$

Temperature difference of hot fluid is 10 degrees through generator

$$T_{11} = 150$$

The inlet temperature of the hot fluid is 150 C

$$Q_g = 3487$$

The energy input has been found by optimization

Mass Balance

$$\dot{m}_{ss} = \dot{m}_{ws} + \dot{m}_R$$

$$\dot{m}_R = \dot{m}_{ss} \cdot (1 - w_{ss}) - \dot{m}_{ws} \cdot (1 - w_{ws})$$

Pump

$$T_2 = T_1$$

$$\rho = \rho_{LiBrH_2O}(T_1; w_{ss})$$

$$P_p = \dot{m}_{ss} \cdot (Ph - Pl) \cdot 1000 / \rho$$

$$h_2 = h_1 + P_p$$

HEX

$$eps = \frac{T_4 - T_5}{T_4 - T_2}$$

$$h_{5w} = h(\text{water}; T = T_5; p = Ph)$$

$$h_{5lb} = h(LiBr; T = T_5)$$

$$h_5 = h_{5w} \cdot (1 - w_{ss}) + h_{5lb} \cdot w_{ss}$$

$$(h_3 - h_2) \cdot \dot{m}_{ss} = (h_4 - h_5) \cdot \dot{m}_{ws}$$

$$\text{call } LiBrCalcTfromPX(Ph; w_{ss} \\ T_3)$$

$$Q_{hex} = \dot{m}_{ss} \cdot (h_3 - h_2)$$

$$lmt_d_{hex} = \frac{(T_4 - T_3) - (T_5 - T_2)}{\ln\left(\frac{T_4 - T_3}{T_5 - T_2}\right)}$$

$$UA_{hex} = Q_{hex} / lmt_d_{hex}$$

Generator

$$T_4 = T_{LiBrH_2O}(Ph; w_{ws})$$

$$T_7 = T_{LiBrH_2O}(Ph; w_{ss})$$

$$h_{4w} = h(\text{water}; T = T_4; p = Ph)$$

$$h_{4lb} = h(LiBr; T = T_4)$$

$$h_4 = h_{4w} \cdot (1 - w_{ss}) + h_{4lb} \cdot w_{ss}$$

$$h_7 = h(\text{water}; T = T_7; p = Ph)$$

$$dT_{o_d} = T_{12} - T_3$$

$$dT_{i_d} = T_{11} - T_4$$

$$lmt_d_d = \frac{dT_{o_d} - dT_{i_d}}{\ln(dT_{o_d} / dT_{i_d})}$$

$$Q_g = UA_g \cdot lmt_d_d$$

$$Q_g = \dot{m}_g \cdot cp_{hf} \cdot (T_{11} - T_{12})$$

$$Q_g = h_4 \cdot \dot{m}_{ws} + h_7 \cdot \dot{m}_R - h_3 \cdot \dot{m}_{ss}$$

Condenser

$$T_8 = T_{\text{sat}}(\text{water}; P = Ph)$$

$$h_8 = h(\text{water}; T = T_8; x = 0)$$

$$dT_{o_c} = T_7 - T_{inf}$$

$$dT_{i_c} = T_8 - T_{inf}$$

$$lmt d_c = \frac{dT_{o_c} - dT_{i_c}}{\ln(dT_{o_c}/dT_{i_c})}$$

$$Q_c = UA_c \cdot lmt d_c$$

$$Q_c = \dot{m}_R \cdot (h_7 - h_8)$$

Refrigerant Valve

$$h_9 = h_8$$

$$T_9 = T(\text{water}; h = h_9; p = Pl)$$

Evaporator

$$T_{10} = T(\text{water}; p = Pl; x = 1)$$

$$h_{10} = h(\text{water}; T = T_{10}; x = 1)$$

$$lmt d_e = T_l - T_{10}$$

$$Q_e = UA_e \cdot lmt d_e$$

$$Q_e = (h_{10} - h_9) \cdot \dot{m}_R$$

Solution Valve

$$h_6 = h_5$$

$$\text{call } LiBrCalcTfromPX(Pl; w_{ws}, T_6)$$

Absorber

$$dT_{o_a} = T_1 - T_{inf}$$

$$dT_{i_a} = T_6 - T_{inf}$$

$$lmt d_a = \frac{dT_{o_a} - dT_{i_a}}{\ln(dT_{o_a}/dT_{i_a})}$$

$$Q_a = UA_a \cdot lmt d_a$$

$$Q_a = \dot{m}_R \cdot h_{10} + \dot{m}_{ws} \cdot h_6 - \dot{m}_{ss} \cdot h_1$$

$$\text{call } LiBrCalcTfromPX(Pl; w_{ss}, T_1)$$

$$h_1 = h_{LiBrH_2O}(T_1; w_{ss})$$

Cost Functions

$$Index = 630,2/385,5$$

$$Cost_e = C_e \cdot UA_e \cdot Index$$

$$Cost_c = C_c \cdot UA_c \cdot Index$$

$$Cost_a = C_a \cdot UA_a \cdot Index$$

$$Cost_d = C_d \cdot UA_d \cdot Index$$

$$C_e = 1,667$$

$$C_c = 1,636$$

$$C_a = 1,636$$

$$C_d = 0,960$$

$$Cost = (Cost_e + Cost_c + Cost_a + Cost_d) \cdot 8,7$$

Slack variables used for optimization

$$P_{sw} = P(Water; T = T_{inf}; X = 1)$$

$$P_{sc} = P(Water; T = T_l; X = 1)$$

$$Pl + z1 = Ph$$

$$\dot{m}_{ws} \cdot 1000 + z2 = \dot{m}_{ss} \cdot 1000$$

$$Pl + z3 = P_{sc}$$

$$P_{sw} + z4 = Ph$$

Double-Effect Model

Equations

Model of a Double-effect LiBr-H₂O Absorption Heat Pump/Chiller

Inputs

$$Q_e = 3$$

$$T_{inf} = 35$$

$$T_l = 27$$

$$T_{21} = 150$$

$$T_{21} - T_{22} = 10$$

$$cp = 2,721$$

Calculate Pressures

$$Ph = P(\text{Water}; T = T_{18}; X = 0)$$

$$Pm = P(\text{Water}; T = T_8; X = 0)$$

$$Pl = P(\text{Water}; T = T_{10}; X = 1)$$

Absorber

$$LMTD_a = \frac{(T_6 - T_{inf}) - (T_1 - T_{inf})}{\ln\left(\frac{T_6 - T_{inf}}{T_1 - T_{inf}}\right)}$$

$$UA_a = Q_a / LMTD_a$$

$$Q_a = m_{10} \cdot h_{10} + m_6 \cdot h_6 - m_1 \cdot h_1$$

call *LiBrCalcTfromPX* (*Pl*; x_1

T_1)

Pump

$$m_2 = m_1$$

$$x_1 = x_{LiBrH_2O}(T_1; Pl)$$

$$rho1 = \rho_{LiBrH_2O}(T_1; x_1)$$

$$h_1 = h_{LiBrH_2O}(T_1; x_1)$$

$$Pump1 = \frac{m_1}{rho1} \cdot (Pm - Pl) \cdot 1000$$

$$h_2 = h_1 + \frac{Pump1}{m_1}$$

$$h_2 = h_{LiBrH_2O}(T_2; x_2)$$

Solution HEX1

$$m_3 = m_2$$

$$m_5 = m_4$$

$$h_3 = h_{LiBrH_2O}(T_3; x_3)$$

$$h_4 = h_{LiBrH_2O}(T_4; x_4)$$

$$T_4 = T_{LiBrH_2O}(Pm; x_4)$$

$$h_5 = h_{LiBrH_2O}(T_5; x_5)$$

$$eps1 = 0,64$$

$$eps1 = \frac{T_4 - T_5}{T_4 - T_2}$$

$$LMTD_{SHX1} = \frac{(T_4 - T_3) - (T_5 - T_2)}{\ln\left(\frac{T_4 - T_3}{T_5 - T_2}\right)}$$

$$UA_{SHX1} = Q_{SHX1}/LMTD_{SHX1}$$

$$Q_{SHX1} = m_1 \cdot (h_3 - h_2)$$

$$Q_{SHX1} = m_5 \cdot (h_4 - h_5)$$

Solution HEX2

$$m_{13} = m_3$$

$$m_{15} = m_{14}$$

$$eps2 = 0,64$$

$$eps2 = \frac{T_{14} - T_{15}}{T_{14} - T_3}$$

$$LMTD_{SHX2} = \frac{(T_{14} - T_{13}) - (T_{15} - T_3)}{\ln\left(\frac{T_{14} - T_{13}}{T_{15} - T_3}\right)}$$

$$UA_{SHX2} = Q_{SHX2}/LMTD_{SHX2}$$

$$Q_{SHX2} = m_3 \cdot (h_{13} - h_3)$$

$$Q_{SHX2} = m_{14} \cdot (h_{14} - h_{15})$$

Upper Generator

$$m_{13} = m_{14} + m_{17}$$

$$m_{17} = m_{13} \cdot (1 - x_{13}) - m_{14} \cdot (1 - x_{14})$$

$$x_{14} = x_{LiBrH_2O}(T_{14}; Ph)$$

$$T_{17} = T_{LiBrH_2O}(Ph; x_{13})$$

$$h_{17} = h(Water; T = T_{17}; P = Ph)$$

$$h_{14} = h_{LiBrH_2O}(T_{14}; x_{14})$$

$$h_{13} = h_{LiBrH_2O}(T_{13}; x_{13})$$

$$LMTD_G = \frac{(T_{21} - T_{14}) - (T_{22} - T_{17})}{\ln\left(\frac{T_{21} - T_{14}}{T_{22} - T_{17}}\right)}$$

$$UA_D = Q_g / LMTD_G$$

$$Q_g = m_{21} \cdot cp \cdot (T_{21} - T_{22})$$

$$Q_g = m_{17} \cdot h_{17} + m_{14} \cdot h_{14} - m_{13} \cdot h_{13}$$

Solution Valves

$$m_6 = m_5$$

$$h_6 = h_5$$

$$\text{call } Q_{LiBrH_2O}(h_6; Pl; x_6)$$

$$q_6; T_6; xx1)$$

$$m_{16} = m_{15}$$

$$h_{16} = h_{15}$$

$$h_{15} = h_{LiBrH_2O}(T_{15}; x_{15})$$

$$\text{call } Q_{LiBrH_2O}(h_{16}; Pm; x_{16})$$

$$q_{16}; T_{16}; xx2)$$

Low Generator/High Condenser

$$m_{16} = m_7 + m_4$$

$$m_{18} = m_{17}$$

$$m_{16} \cdot (x_{16}) = m_4 \cdot (x_4)$$

$$T_7 = T_{LiBrH_2O}(Pm; x_{16})$$

$$h_{18} = h(Water; T = T_{18}; X = 0)$$

$$T_{18} = T(Water; P = Ph; X = 0)$$

$$LMTD_{CG} = \frac{(T_{18} - T_4) - (T_{18} - T_{16})}{\ln\left(\frac{T_{18} - T_4}{T_{18} - T_{16}}\right)}$$

$$Q_{CG} = UA_{CG} \cdot LMTD_{CG}$$

$$Q_{CG} = m_{17} \cdot h_{17} - m_{18} \cdot h_{18}$$

$$m_{17} \cdot h_{17} + m_{16} \cdot h_{16} = m_7 \cdot h_7 + m_4 \cdot h_4 + m_{18} \cdot h_{18}$$

$$x_4 = x_{LiBrH_2O}(T_4; Pm)$$

Condenser

$$m_8 = m_{19} + m_7$$

$$h_7 = h(\text{Water}; T = T_7; P = Pm)$$

$$h_8 = h(\text{Water}; T = T_8; X = 0)$$

$$T_8 = T(\text{Water}; P = Pm; X = 0)$$

$$LMTD_C = \frac{(T_7 - T_{inf}) - (T_8 - T_{inf})}{\ln\left(\frac{T_7 - T_{inf}}{T_8 - T_{inf}}\right)}$$

$$Q_C = UA_c \cdot LMTD_C$$

$$Q_C = m_7 \cdot h_7 + m_{19} \cdot h_{19} - m_8 \cdot h_8$$

Refrigerant Valves

$$m_{19} = m_{18}$$

$$h_{19} = h_{18}$$

$$T_{19} = T(\text{Water}; h = h_{19}; P = Pm)$$

$$m_9 = m_8$$

$$h_9 = h_8$$

Evaporator

$$m_{10} = m_9$$

$$T_9 = T(\text{Water}; h = h_9; P = Pl)$$

$$h_{10} = h(\text{Water}; T = T_{10}; X = 1)$$

$$T_{10} = T(\text{water}; p = Pl; x = 1)$$

$$LMTD_e = \frac{(T_l - T_{10}) - (T_l - T_9)}{\ln\left(\frac{T_l - T_{10}}{T_l - T_9}\right)}$$

$$Q_e = UA_e \cdot LMTD_e$$

$$Q_e = m_9 \cdot (h_{10} - h_9)$$

Calculating COP

$$COP = \frac{Q_e}{Q_g + Pump1}$$

Filling out results table

Concentrations

$$x_2 = x_1$$

$$x_3 = x_2$$

$$x_5 = x_4$$

$$x_6 = x_5$$

$$x_{13} = x_3$$

$$x_{15} = x_{14}$$

$$x_{16} = x_{15}$$

$$x_7 = 0$$

$$x_8 = 0$$

$$x_9 = 0$$

$$x_{10} = 0$$

$$x_{17} = 0$$

$$x_{18} = 0$$

$$x_{19} = 0$$

Pressures

$$P_1 = Pl$$

$$P_2 = Ph$$

$$P_3 = Ph$$

$$P_4 = Pm$$

$$P_5 = Pm$$

$$P_6 = Pl$$

$$P_7 = Pm$$

$$P_8 = Pm$$

$$P_9 = Pl$$

$$P_{10} = Pl$$

$$P_{13} = Ph$$

$$P_{14} = Ph$$

$$P_{15} = Ph$$

$$P_{16} = Pm$$

$$P_{17} = Ph$$

$$P_{18} = Ph$$

$$P_{19} = Pm$$

Cost Function

$$Index = 630,2/385,5$$

$$Cost_e = C_e \cdot UA_e \cdot 1000 \cdot Index$$

$$Cost_c = C_c \cdot UA_c \cdot 1000 \cdot Index$$

$$Cost_a = C_a \cdot UA_a \cdot 1000 \cdot Index$$

$$Cost_g = C_g \cdot UA_d \cdot 1000 \cdot Index$$

$$Cost_{cg} = C_{cg} \cdot UA_{CG} \cdot 1000 \cdot Index$$

$$C_e = 1,667$$

$$C_c = 1,636$$

$$C_a = 1,636$$

$$C_g = 0,960$$

$$C_{cg} = 0,454$$

$$Cost = (Cost_e + Cost_c + Cost_a + Cost_g) \cdot 1,17$$

Absorber Model

Equations

Model of a falling film absorber. The absorber is air cooled with forced convection over a vertical staggered tube bundle.

Discretization

$$N = 10$$

Number of control volumes in the absorber

Absorber geometry

$$m = 41$$

Number of pipes

$$H = 1,285 \text{ [m]}$$

Height of the horizontal pipe

$$D_o = 15,875 \cdot \left| 0,001000000 \frac{\text{m}}{\text{mm}} \right|$$

Outer diameter of the pipe

$$x_t = 1,651 \cdot \left| 0,001000000 \frac{\text{m}}{\text{mm}} \right|$$

Wall thickness of pipe

$$S_T = 2 \cdot r_{fin} \cdot \text{Cos}(45)$$

Transverse length between pipes

$$S_L = 2 \cdot r_{fin} \cdot \text{Cos}(45)$$

Longitudinal distance between pipes

$$n_{fin} = 500$$

Number of fins per meter

$$L_{fin} = D_o$$

Length of fins

$$th_{fin} = 0,12 \cdot \left| 0,001000000 \frac{\text{m}}{\text{mm}} \right|$$

Thickness of fins

Operating condition

$$\dot{m}_{in} = 0,01027$$

Mass flow of weak solution into the absorber

$$w_{in} = 0,64$$

Concentration of the solution into the absorber

$$T_{in} = 62,39 + 273,15$$

Temperature of the solution into the absorber

$$T_{inf} = 35 + 273,15$$

Temperature of the surrounding air

$$V_{inf} = 2,5$$

Fan speed

Constants

$$g = 9,81$$

Gravity

$$F = 0,89$$

Correction factor for two-row staggered grid

$$w_v = 0$$

The concentration of lithium bromide in the vapor is 0

Precalculations

$$r_o = D_o/2$$

Radius of tube

$$r_{fin} = r_o + L_{fin}$$

Radius of fin, measured from tube center

$$r = r_o - x_t$$

Outer radius of the pipe

$$L = 2 \cdot r_{fin} + 3 \cdot S_L$$

Length of absorber

$$W = m/4 \cdot (D_o + L_{fin} \cdot 2)$$

Width of absorber

$$V = W \cdot L \cdot H$$

Physical volume of absorber

$$A_{unfin} = r_o \cdot 2 \cdot \pi \cdot (H/N)$$

Unfinned area/element

$$A_{mfin} = ((\pi \cdot r_{fin}^2) - (\pi \cdot r_o^2)) \cdot (H/N) \cdot n_{fin}$$

Finned area/element

Setting boundary conditions

$$T_1 = T_{in}$$

Inlet solution temperature

$$\dot{m}_1 = \dot{m}_{in}/m$$

Inlet solution mass flow rate

$$\dot{m}_{v;N+1} = 0$$

Zero vapor velocity BC

$$w_1 = w_{in}$$

Inlet solution concentration

$$w_{N+1} = w_{out}$$

Outlet solution concentration

Calculating properties

$$P = P_{LiBrH_2O}(T_1; w_1)$$

Pressure in the solution is found based on temperature

$$MW_{LB} = MW(LiBr)$$

Molar weight of lithium bromide is found

$$c_{p_{inf}} = c_p(Air_{ha}; T = T_{inf}; P = P_{inf})$$

Heat capacity of surroundings

$$P_{inf} = 1 \cdot \left| 101,325000 \frac{\text{kPa}}{\text{Atm}} \right|$$

Pressure of the surrounding air

$$\rho_{inf} = \rho(Air_{ha}; T = T_{inf}; P = P_{inf})$$

Density of the surrounding air

$$\mu_{inf} = \mu(Air_{ha}; T = T_{inf}; P = P_{inf})$$

Viscosity of the

$$k_{inf} = k(Air_{ha}; T = T_{inf}; P = P_{inf})$$

Conductivity of the surrounding air

$$T_v = T(Water; P = P; X = 1)$$

$$\rho_v = \rho(Water; P = P; X = 1)$$

Density of the vapor

$$\mu_v = \mu(water; P = P; X = 1)$$

Vapor heat content

$$i_v = h(Water; P = P; x = 1)$$

Enthalpy of the vapor is found, the vapor considered

$$c_{p_1} = C_{p_{LiBrH_2O}}(T_1; w_1)$$

The heat capacity of the solution into the absorber

$$i_1 = h_{LiBrH_2O}(T_1; w_1)$$

Mixture enthalpy of the solution into the absorber

Calculating dimensionless numbers

$$Re_{inf} = \frac{\rho_{inf} \cdot V_{inf} \cdot (r_o \cdot 2)}{\mu_{inf}}$$

Reynolds number of the surrounding air around the pipe

$$Pr_{inf} = P_r(Air_{ha}; T = T_{inf}; P = P_{inf})$$

Prandtl number of the surrounding air

BEGIN DUPLICATE

duplicate $i = 2; N + 1$

Surface Properties

$$\rho_{sur;i} = \rho(Air_{ha}; T = T_{sur;i}; P = P_{inf})$$

Density of surroundings

$$\mu_{sur;i} = \mu(Air_{ha}; T = T_{sur;i}; P = P_{inf})$$

Viscosity of surroundings

$$cp_{sur;i} = c_p(Air_{ha}; T = T_{sur;i}; P = P_{inf})$$

Heat capacity of surroundings

$$Pr_{sur;i} = P_r(Air_{ha}; T = T_{sur;i}; P = P_{inf})$$

Prandtl number of surroundings

Solution properties

$$w_{if;i} = x_{LiBrH2O}(T_{if;i}; P)$$

Saturation mass fraction based on pressure and temperature at interface

$$i_i = h_{LiBrH2O}(T_i; w_i)$$

Enthalpy of solution based on temperature and concentration

$$\rho_i = \rho_{LiBrH2O}(T_i; w_i)$$

Density of the solution is found based on temperature and concentration

$$\mu_i = \nu_{LiBrH2O}(T_i; w_i)$$

Viscosity of the solution is found based on temperature and concentration

$$cp_i = C_{pLiBrH2O}(T_i; w_i)$$

Heat capacity of the solution is found based on temperature and concentration

$$K_i = Cond_{LiBrH2O}(T_i; w_i)$$

Conductivity of the solution is found based on temperature and concentration

$$\nu_i = \frac{\mu_i}{\rho_i}$$

$$Pr_i = cp_i \cdot \frac{\mu_i}{K_i}$$

$$w_{m;i} = w_i \cdot \left(\frac{\rho_i}{MW_{LB}} \right) \cdot \left| 1,000000000 \frac{\text{mol/L}}{\text{kmol/m}^3} \right|$$

The molar concentration is needed for the mass diffusivity correlation

$$D_{ab;i} = (3,11 \cdot 10^{-5} \cdot w_{m;i}^6 - 0,001407 \cdot w_{m;i}^5 + 0,02385 \cdot w_{m;i}^4 - 0,1836 \cdot w_{m;i}^3 + 0,5984 \cdot w_{m;i}^2 - 0,6082 \cdot w_{m;i} + 1,523) \cdot 10^{-9}$$

The mass diffusivity coefficient is found using the correlation

Heat transfer Areas

$$A_{i f ; i} = (r - \delta_i) \cdot \pi \cdot 2 \cdot (H/N)$$

The area of the interface between film and vapor

$$\eta_{fin;i} = \eta_{fin;annular;rect}(th_{fin}; r_o; r_{fin}; h_{inf;i}; k_{fin;i})$$

Using EES to find fin efficiency

$$A_{eq;i} = A_{unfin} + \eta_{fin;i} \cdot A_{mfin}$$

The equivalent area of the finned area

Precalculation

$$\Delta i_i = i_v - i_i$$

Enthalpy difference between the vapor and the control volume

Heat transfer coefficients

$$Nus_{sur;i} = 0,35 \cdot (S_T/S_L)^{0,2} \cdot Re_{inf}^{0,6} \cdot Pr_{inf}^{0,36} \cdot \left(\frac{Pr_{inf}}{Pr_{sur;i}} \right)^{0,25}$$

Correlation for the nusselt number of flow across a bank of tubes

$$Nus_{inf;i} = Nus_{sur;i} \cdot F$$

Nusselt number definition

$$k_{fin;i} = k(\text{'Aluminum'}; T_i)$$

Thermal conductivity of copper

$$h_{inf;i} = k_{inf} \cdot \frac{Nus_{inf;i}}{(r_o \cdot 2)}$$

Free stream heat transfer coefficient

$$k_{w;i} = k(\text{'Stainless_AISI304'}; T_i)$$

The pipe is considered steel and the thermal conductive coefficient is found

$$h_i = \left(0,029 \cdot (4 \cdot Re_i)^{0,53} \cdot Pr_i^{0,344} \right) \cdot \frac{K_i}{\delta_i}$$

Correlation used to find the convective heat transfer coefficient for the solution film

$$UA_i = \left(\left(\frac{1}{h_{inf;i} \cdot A_{eq;i}} \right) + \left(\frac{r_o}{k_{w;i} \cdot A_{unfin}} \right) \cdot \ln(r_o/r) + \left(\frac{1}{h_i \cdot A_{unfin}} \right) \right)^{-1}$$

Heat transfer coefficient from solution to ambient

$$UA_{sur;i} = \left(\left(\frac{1}{h_{inf;i} \cdot A_{eq;i}} \right) + \left(\frac{r_o}{k_{w;i} \cdot A_{unfin}} \right) \cdot \ln(r_o/r) \right)^{-1}$$

Heat transfer coefficient from inner wall to ambient

Boundary conditions

$$\Delta i_i \cdot \Delta m_i = \frac{K_i \cdot A_{if;i}}{\delta_i} \cdot (T_{if;i} - T_i)$$

Energy balance

Mass conservation

$$\dot{m}_{v;i} - \dot{m}_{v;i+1} = \Delta m_i$$

Mass balance for vapor

$$(1 - w_i) \cdot \dot{m}_i = (1 - w_{i-1}) \cdot \dot{m}_{i-1} + (1 - w_v) \cdot \Delta m_i$$

Mass balance for water in solution

$$\dot{m}_{i-1} + \Delta m_i = \dot{m}_i$$

Mass balance for solution

$$\Delta m_i = K_{m;i} \cdot A_{if;i} \cdot \rho_i \cdot (w_i - w_{if;i})$$

Change in mass flow/absorbed mass flow is calculated

$$K_{m;i} = \left(Sh_i \cdot \frac{D_{ab;i}}{\delta_i} \right)$$

Mass transfer coefficient

$$Sh_i = 1,099 \cdot 10^{-2} \cdot (4 \cdot Re_i)^{0,3955} \cdot Sc_{s;i}^{1/2}$$

Sherwood number for the solution is found using correlation

$$Sc_{s;i} = \frac{\mu_i}{(\rho_i \cdot D_{ab;i})}$$

Schmidt number is found

Energy Balance

$$\dot{m}_{i-1} \cdot i_{i-1} + \Delta m_i \cdot \Delta i_i = \dot{m}_i \cdot i_i + Q_{a;i}$$

Energy balance for solution

$$Q_{a;i} = U A_i \cdot (T_i - T_{inf})$$

Heat from solution to surroundings

$$Q_{a;i} = U A_{sur;i} \cdot (T_{sur;i} - T_{inf})$$

Heat from surface to surroundings

Momentum

$$u_i = \frac{\dot{m}_i}{(\rho_i \cdot \delta_i \cdot 2 \cdot \pi \cdot r)}$$

Mean velocity of the solution film

$$\delta_i = \left(3 \cdot \left(\frac{\mu_i}{\rho_i^2} \right) \cdot \frac{\Gamma_i}{g} \right)^{1/3}$$

Film thickness is calculated

$$\Gamma_i = \frac{\dot{m}_i}{(\pi \cdot 2 \cdot r)}$$

Mass flow per wetted perimeter is calculated

$$Re_i = u_i \cdot \delta_i \cdot \frac{\rho_i}{(\mu_i)}$$

Reynolds number for the solution/film is found

Control Equations

$$A_{v;i} = (r - \delta_i)^2 \cdot \pi$$

Cross sectional area of vapor flow

$$v_{v;i} = \frac{\dot{m}_{v;i}}{(\rho_v \cdot A_{v;i})}$$

Velocity of vapor

$$Q_{v;i} = \Delta m_i \cdot \delta i_i$$

Vapor heat content

$$Re_{v;i} = v_{v;i} \cdot (r - \delta_i) \cdot 2 \cdot \rho_v / \mu_v$$

$$test_i = \dot{m}_{i-1} \cdot i_{i-1} + \Delta m_i \cdot \Delta i_i - \dot{m}_i \cdot i_i - Q_{a;i}$$

end

END DUPLICATE

Energy and Mass balance verification

$$\Delta M = (\dot{m}_N - \dot{m}_1) \cdot m$$

Change in total solution mass flow

$$M_{out} = \dot{m}_{in} + \Delta M$$

Total outlet mass flow

$$Q_a = \text{Sum}(Q_{a;i}; i = 2; N + 1) \cdot m$$

Total heat supply from hot water

$$Q_v = \text{Sum}(Q_{v;i}; i = 2; N + 1) \cdot m$$

Total heat of condensation

$$Q_{vv} = \Delta M \cdot i_v$$

Total heat of condensation, no enthalpy reference

$$Q_{in} = \dot{m}_{in} \cdot i_1$$

Inlet solution heat, no enthalpy reference

$$Q_{out} = M_{out} \cdot (i_{N+1})$$

Outlet solution heat, no enthalpy reference

$$E_{bal} = Q_v - M_{out} \cdot (i_{N+1}) - Q_a + \dot{m}_{in} \cdot i_1$$

Residual for energy conservation

$$E_{balP} = E_{bal}/Q_a$$

Percentage error in energy conservation

Cost Function

$$L_{tu} = H \cdot m$$

Total length of tubes is found

$$C_{tu} = 8 \cdot 10^{-5} \cdot D_o^3 - 0,0058 \cdot D_o^2 + 0,442 \cdot D_o + 1,2957$$

Cost function for tube in euro per meter as a function of the diameter

$$A_{fin} = H \cdot n_{fin} \cdot W \cdot L$$

Total area of fins

$$C_{fin} = 2$$

Cost of aluminium sheets used for fin, in euro per square meter

$$Cost = C_{tu} \cdot L_{tu} + C_{fin} \cdot A_{fin}$$

Total cost of the absorber is found

Generator Model

Equations

Generator Model

Inputs

$$n = 12$$

Number of passes for each tube/pipe

$$m = 11$$

Number of pipes/tubes in parallel

$$N_h = n$$

Variable used in the discretization numbering

$$N_s = n + 1$$

Variable used in the discretization numbering

$$P_h = 17, 69$$

The pressure in the generator

$$T_{in} = 99, 72 + 273, 15$$

Temperature of the strong solution inlet

$$w_{in} = 0, 5744$$

Concentration of the strong solution inlet

$$w_{N_s} = 0, 64$$

Concentration of the weak solution outlet

$$T_{h;in} = 150 + 273, 15$$

Temperature of the heat source inlet

$$T_{N_s+1} = 140 + 273, 15$$

Temperature of the heat source outlet

$$Q_{in} = 3487$$

Heating input (is used to determine the mass flow of the heat source liquid)

Properties of the heat source liquid

$$\rho_{hf} = 1016$$

Density of the heat source liquid

$$\mu_{hf} = 0, 00139$$

Viscosity of the heat source liquid

$$k_{hf} = 0, 198$$

Conductivity of the heat source liquid

$$cp_{h,f} = 2721$$

Heating value of the heat source liquid

$$Pr_{h,f} = cp_{h,f} \cdot \mu_{h,f} / k_{h,f}$$

Prandtl number of the heat source liquid is found

$$g = 9,81$$

Gravity defined

Physical dimensions

$$D_t = 12,7 \cdot \left| 0,001000000 \frac{\text{m}}{\text{mm}} \right|$$

Diameter of each tube

$$x_t = 1,651 \cdot \left| 0,001000000 \frac{\text{m}}{\text{mm}} \right|$$

Thickness of the tube wall

Calculating Initial Conditions

$$m_1 = m_{in} / m$$

Inlet mass flow of strong solution is divided by the number of tubes

$$T_1 = T_{in}$$

The inlet temperature of strong solution is defined

$$w_1 = w_{in}$$

The inlet concentration of strong solution is defined

$$i_{s;1} = h_{LiBrH2O}(T_{in}; w_{in})$$

The enthalpy of the strong solution inlet is found

$$cp_1 = Cp_{LiBrH2O}(T_1; w_1)$$

The heat capacity of the strong solution inlet is found

$$\rho_1 = \rho_{LiBrH2O}(T_1; w_1)$$

The density of the strong solution inlet is found

$$m_{N_s+N_h+1} = m_{h;in} / m$$

The inlet mass of heat source liquid is divided by the number of tubes

$$T_{N_s+N_h+1} = T_{h;in}$$

The inlet temperature of the heat source liquid is defined

$$dT = T_{N_s+N_h} - T_{N_s+1}$$

The temperature difference in the heat source liquid is calculated

$$Q_{in} = m_{h;in} \cdot cp_{h,f} \cdot (T_{h;in} - T_{N_s+1})$$

The mass flow of the heat source liquid is found

Design Parameters for Generator

$$S_L = 2 \cdot D_t$$

The distance between the center of two pipes in the flow direction (downwards)

$$H_j = S_L - D_t$$

The distance between pipes in the flow direction (horizontal)

$$S_T = 2 \cdot D_t$$

The distance between pipes normal to the flow direction (horizontal)

$$A_g = W_g \cdot L_g$$

Cross sectional area of the generator

$$H_g = (n + 1) \cdot H_j + (n + 1/2) \cdot D_t$$

Height of the generator is calculated

$$L_g = L_t$$

The length of the generator is calculated

$$W_g = m \cdot S_T$$

The width of the generator

$$V_g = W_g \cdot L_g \cdot H_g$$

Volume of the generator

$$r_o = D_t/2$$

Outer diameter of each tube

$$r_i = D_t/2 - x_t$$

Inner diameter of each tube

$$A = D_t \cdot \pi \cdot L_t$$

Surface area of each pass of the tubes

Solution

duplicate $i = 2; N_s$

Properties of the solution is found for each control volume of

$$\rho_i = \rho_{LiBrH2O}(T_i; w_i)$$

Density for each control volume

$$\mu_i = \mu_{LiBrH2O}(T_i; w_i)$$

Viscosity for each control volume

$$k_{s,i} = Cond_{LiBrH2O}(T_i; w_i)$$

Conductivity for each control volume

$$w_i = x_{LiBrH2O}(T_i; P_h)$$

Concentration for each control volume

$$c_{p,i} = C_{pLiBrH2O}(T_i; w_i)$$

Heating value for each control volume

$$i_{s;i} = h_{LiBrH2O}(T_i; w_i)$$

Enthalpy for each control volume

$$\nu_i = \frac{\mu_i}{\rho_i}$$

The Nusselt number for each control volume

$$Pr_i = c_{p,i} \cdot \frac{\mu_i}{k_{s;i}}$$

The Prandtl number for each control volume

$$k_{w;i} = k(\text{'Stainless_AISI304'}; T_i)$$

The thermal conductivity of the wall is found

Properties of the vapor for each control volume

$$c_{p,v;i} = c_p(\text{water}; T = T_i; P = P_h)$$

$$k_{v;i} = k(\text{water}; P = P_h; T = T_i)$$

$$\rho_{v;i} = \rho(\text{water}; P = P_h; T = T_i)$$

$$\mu_{v;i} = \mu(\text{water}; P = P_h; T = T_i)$$

Mass balance for the solution

$$m_i = m_{i-1} - m_{e;i}$$

m_e being the amount of evaporated solution in each control volume

$$w_i \cdot m_i = w_{i-1} \cdot m_{i-1}$$

The change in concentration is determined based on change in mass flow

Energy balance for the solution

$$0 = m_{i-1} \cdot (i_{s;i-1} - i_{s;i}) - m_{e;i} \cdot \delta i_i + Q_{d;i}$$

Energy balance for the generator

$$\delta i_i = i_{v;i} - i_{s;i}$$

Latent enthalpy

$$\Gamma_i = \frac{m_i}{(2 \cdot L_t)}$$

The mass flow per unit length is found

$$Re_i = 4 \cdot \frac{\Gamma_i}{\mu_i}$$

The Reynolds number of the solution is found

The convective heat transfer coefficient for the film boiling is found using Bromleys correlation

$$h_{s;i} = 1,10 \cdot Re_i^{-1/3} \cdot \frac{k_{s;i}}{\left(\frac{\nu_i^2}{g}\right)^{1/3}}$$

Calculation of the convective heat transfer coefficient inside the tubes

$$v_{hf;i} = \frac{m_{i+n}}{\left(\rho_{hf} \cdot \pi \cdot (D_t/2)^2\right)}$$

The velocity of the heat source liquid is found

$$Re_{hf;i} = \rho_{hf} \cdot D_t \cdot \frac{v_{hf;i}}{\mu_{hf}}$$

The Reynolds number of the heat source liquid is found

$$Nus_i = 4,36$$

The Nusselt number is found (for laminar flow)

The Nusselt number is found (for turbulent flow)

$$Nus_i = h_{hf;i} \cdot D_t / k_{hf}$$

The convective heat transfer coefficient is found

Calculating total heat transfer coefficient

$$U_i = \left(\left(\frac{1}{h_{s;i}} \right) + \left(\frac{1}{h_{hf;i}} \right) + \left(\left(\frac{1}{k_{w;i}} \right) \cdot \ln(r_o/r_i) \cdot r_o \right) \right)^{-1}$$

Total heat transfer coefficient is found

$$Q_{d;i} = U_i \cdot A \cdot (T_{i+n} - T_i)$$

The energy transfer from the heat source liquid to the solution and vapor is calculated

$$Q_{d;i} = h_{hf;i} \cdot A \cdot (T_{i+n} - T_{sur;i})$$

The temperature on the surface of the tube wall is determined

Mass balance for the vapor

$$m_{v;i} = m_{v;i+1} + m_{e;i}$$

$$m_{vt;i} = m_{v;i} \cdot m$$

The mass flow of the vapor in each control volume is multiplied by the number of tubes

$$u_{v;i} = \frac{m_{vt;i}}{(\rho_{v;i} \cdot A_g)}$$

The velocity of the vapor flow

$$Di_{v;i} = h(\text{water}; P = P_h; T = T_i) - h_{LiBrH2O}(T_i; w_i)$$

The change in enthalpy for each control volume is calculated

$$Q_{v;i} = m_{e;i} \cdot Di_{v;i}$$

The energy transfer from the film to the vapor in each control volume

$$i_{v;i} = h(\text{water}; P = P_h; T = T_i)$$

The enthalpy in each control volume is calculated

$$Q_{avg;i} = m_{e;i} \cdot i_{v;i}$$

The energy transfer from solution to vapor in each control volume

$$test_i = m_{i-1} \cdot (i_{s;i-1} - i_{s;i}) - m_{e;i} \cdot \delta i_i + Q_{d;i}$$

end

A loop for the heat source liquid is used to make an energy and mass balance

duplicate $j = N_s + 1; N_s + N_h$

$$m_j = m_{j+1}$$

Mass balance for the heat source liquid

$$m_j \cdot cp_{hf} \cdot (T_{j+1} - T_j) = Q_{d;j-n}$$

Energy balance for the heat source flow

end

$$E_{bal} = Q_{in} - Q_v - m_{N_s+N_h+2} \cdot (i_{s;N;s} - i_{s;1})$$

An energy balance is used to control the conservation of energy

$$Q_v = \text{Sum}(Q_{v;i}; i = 2; N_s) \cdot m$$

The total energy transfer from solution to liquid is calculated

$$i_{vt} = \frac{\text{Sum}(Q_{avg;i}; i = 2; N_s)}{(m_e/m)}$$

An average enthalpy of the vapor is calculated

$$T_v = T(\text{Water}; P = P_h; H = (i_{vt}))$$

The temperature of the vapor leaving the generator is found based on the average enthalpy

$$i_v = h(\text{water}; P = P_h; T = T_v)$$

The outlet enthalpy of the vapor is found

$$m_{v;N;s} = m_{e;N;s}$$

The vapor mass flow in the first control volume is defined as the amount of mass evaporated in the adjacent solution cell (boundary condition)

$$m_e = (\text{Sum}(m_{e;i}; i = 2; N_s)) \cdot m$$

The outlet mass flow vapor out of the generator is found

$$m_{N_s+N_h+2} = m_{N_s} \cdot m$$

The outlet mass flow of the weak solution is found

Cost function

$$L_{tu} = L_t \cdot m \cdot n$$

Total length of the tubes

$$C_{tu} = 8,42$$

Cost of the tube in euro per meter

$$C_{ss} = 30 \cdot 2 \cdot (H_g \cdot W_g + H_g \cdot L_g + L_g \cdot W_g)$$

Cost of the chassis surrounding the tubes

$$C_t = C_{tu} \cdot L_{tu} + C_{ss}$$

Total cost of the generator

Condenser Model

Equations

Condenser Model

Inputs

$$H = 0,4$$

Height of the horizontal tube

$$m = 10$$

Number of tubes

$$\dot{m} = 0,001313$$

Inlet mass flow of the refrigerant

$$D_o = 15,875 \cdot \left| 0,001000000 \frac{\text{m}}{\text{mm}} \right|$$

Outer diameter of the tube

$$x_t = 1,651 \cdot \left| 0,001000000 \frac{\text{m}}{\text{mm}} \right|$$

Wall thickness of tube

$$T_{inf} = 35 + 273,15$$

Ambient temperature

$$T_{in} = 99,72 + 273,15$$

Temperature of refrigerant at inlet

$$P = 17,69$$

Pressure in the condenser

$$n_{fin} = 500$$

Number of fins per meter

$$th_{fin} = 0,12 \cdot \left| 0,001000000 \frac{\text{m}}{\text{mm}} \right|$$

Fin thickness

$$L_{fin} = 15,875 \cdot \left| 0,001000000 \frac{\text{m}}{\text{mm}} \right|$$

Fin length

$$P_{inf} = 1 \cdot \left| 101,325000 \frac{\text{kPa}}{\text{Atm}} \right|$$

Ambient Pressure

$$V_{inf} = 2,5$$

Fan speed

$$g = 9,81$$

Gravity

$$F = 0,64$$

Correction factor for one-row staggered grid

Precalculations

$$h_{in} = h(\text{water}; P = P; T = T_{in})$$

Inlet enthalpy

$$T_{sat} = T(\text{water}; P = P; X = 1)$$

Saturation temperature at the condenser pressure

$$T_{out} = T(\text{water}; P = P; X = 0)$$

Outlet temperature

Determining the geometry of the condenser

$$r_o = D_o/2$$

Radius of tube

$$r_{fin} = r_o + L_{fin}$$

Radius of fin, measured from tube center

$$r = r_o - x_t$$

Inner radius of the tube

$$D = r \cdot 2$$

$$S_T = 2 \cdot r_{fin} \cdot \cos(45)$$

Transverse length between tubes

$$S_L = 2 \cdot r_{fin} \cdot \cos(45)$$

Longitudinal distance between tubes

$$L = D_o + 2 \cdot r_{fin}$$

Length of condenser

$$W = m \cdot (D_o + L_{fin} \cdot 2)$$

Width of condenser

$$V = W \cdot L \cdot H$$

Physical volume of condenser

$$A_{unfin} = r_o \cdot 2 \cdot \pi \cdot H \cdot m$$

Unfinned area/element

$$A_{mfin} = ((\pi \cdot r_{fin}^2) - (\pi \cdot r_o^2)) \cdot H \cdot n_{fin} \cdot m$$

Finned area/element

$$A_{eq} = A_{unfin} + \eta_{fin} \cdot A_{mfin}$$

The equivalent area of the finned area

$$\eta_{fin} = \eta_{fin;annular;rect}(th_{fin}; r_o; r_{fin}; h_{inf}; k_{fin})$$

Using EES to find fin efficiency

Ambient properties

$$cp_{inf} = c_p(Air_{ha}; T = T_{inf}; P = P_{inf})$$

Heat capacity of surroundings

$$\rho_{inf} = \rho(Air_{ha}; T = T_{inf}; P = P_{inf})$$

Density of the surrounding air

$$\mu_{inf} = \mu(Air_{ha}; T = T_{inf}; P = P_{inf})$$

Viscosity of the air

$$k_{inf} = k(Air_{ha}; T = T_{inf}; P = P_{inf})$$

Conductivity of the surrounding air

$$Pr_{inf} = P_r(Air_{ha}; T = T_{inf}; P = P_{inf})$$

Prandtl number of the surrounding air

$$Re_{inf} = \frac{\rho_{inf} \cdot V_{inf} \cdot (r_o \cdot 2)}{\mu_{inf}}$$

Reynolds number of the surrounding air around the tubes

Surface properties

$$T_{sur} = \frac{T_{inf} + \frac{T_{in} + T_{sat}}{2}}{2}$$

$$\rho_{sur} = \rho(Air_{ha}; T = T_{sur}; P = P_{inf})$$

Density of surroundings

$$\mu_{sur} = \mu(Air_{ha}; T = T_{sur}; P = P_{inf})$$

Viscosity of surroundings

$$cp_{sur} = c_p(Air_{ha}; T = T_{sur}; P = P_{inf})$$

Heat capacity of surroundings

$$Pr_{sur} = P_r(Air_{ha}; T = T_{sur}; P = P_{inf})$$

Prandtl number of surroundings

$$k_{fin} = k('Aluminum'; T_{in})$$

Thermal conduction in the fins

Outer heat transfer

$$Nus_{sur} = 0,35 \cdot (S_T/S_L)^{0,2} \cdot Re_{inf}^{0,6} \cdot Pr_{inf}^{0,36} \cdot (Pr_{inf}/Pr_{sur})^{0,25}$$

Nusselt number of flow across a bank of tubes

$$Nus_{inf} = Nus_{sur} \cdot F$$

Nusselt number definition

$$h_{inf} = k_{inf} \cdot \frac{Nus_{inf}}{(r_o \cdot 2)}$$

Free stream heat transfer coefficient

$$k_w = k('Stainless_AISI304'; T_{in})$$

Conductivity of the tube wall, made of stainless steel

Vapor Properties for condensation

$$Pr_v = Pr('water'; P = P; X = 1)$$

$$\rho_v = \rho('Water'; P = P; x = 1)$$

$$\mu_v = \mu('Water'; P = P; x = 1)$$

$$k_v = k('Water'; P = P; x = 1)$$

Liquid Properties for condensation

$$Pr_l = Pr('water'; P = P; x = 0)$$

$$\rho_l = \rho('Water'; P = P; x = 0)$$

$$\mu_l = \mu('Water'; P = P; x = 0)$$

$$k_l = k('Water'; P = P; x = 0)$$

$$h_{fg} = h('water'; P = P; X = 1) - h('water'; P = P; X = 0)$$

Latent energy of condensation

$$\nu_R = 1,13 \cdot \left(\frac{(\rho_l \cdot (\rho_l - \rho_v) \cdot g \cdot h_{fg}) \cdot H^3}{\mu_l \cdot k_l \cdot (T_{sat} - T_{inf})} \right)^{1/4}$$

Nusselt number of the refrigerant

$$\nu_R = h_R \cdot H / k_l$$

The heat transfer coefficient for the condensation inside the tubes is found

$$UA_R = \left(\left(\frac{1}{h_{inf} \cdot A_{eq}} \right) + \left(\frac{r_o}{k_w \cdot A_{unfin}} \right) \cdot \ln(r_o/r) + \left(\frac{1}{h_R \cdot A_{unfin}} \right) \right)^{-1}$$

UA value for the condenser is calculated

Cost Function

$$L_{tu} = H \cdot m$$

Total length of the tubes is found

$$C_{tu} = 8 \cdot 10^{-5} \cdot D_o^3 - 0,0058 \cdot D_o^2 + 0,442 \cdot D_o + 1,2957$$

Cost function for the tubes in euro per meter as a function of the diameter

$$A_{fin} = H \cdot n_{fin} \cdot W \cdot L$$

Total area of the fins

$$C_{fin} = 3$$

Cost of aluminium sheets used for the fins in euro per square meter

$$Cost = C_{tu} \cdot L_{tu} + C_{fin} \cdot A_{fin}$$

Total cost of the condenser

Evaporator model

Equations

Evaporator geometry

$$H = 0,60$$

Height of the horizontal tube

$$m = 23$$

Number of tubes

$$D_o = 15,875 \cdot \left| 0,001000000 \frac{\text{m}}{\text{mm}} \right|$$

Outer diameter of the tube

$$x_t = 1,6 \cdot \left| 0,001000000 \frac{\text{m}}{\text{mm}} \right|$$

Wall thickness of tube

$$n_{fin} = 500$$

Number of fins per meter

$$th_{fin} = 0,12 \cdot \left| 0,001000000 \frac{\text{m}}{\text{mm}} \right|$$

Fin thickness

$$L_{fin} = 15,875 \cdot \left| 0,001000000 \frac{\text{m}}{\text{mm}} \right|$$

Fin length

$$T_{in} = 13,18 + 273,15$$

Inlet temperature

$$T_{inf} = 27 + 273,15$$

Ambient temperature

$$P = 1,516$$

Pressure in the evaporator

$$P_{inf} = 1 \cdot \left| 101,325000 \frac{\text{kPa}}{\text{Atm}} \right|$$

Ambient pressure

$$V_{inf} = 2,5$$

Fan speed

$$x_{in} = 0,075$$

Inlet quality of the refrigerant

$$x_{out} = 0,999$$

Outlet quality of the refrigerant

$$\dot{m} = 0,001313$$

Inlet mass flow of the refrigerant

$$g = 9,81$$

Gravity

$$F = 0,76$$

Correction factor for two-row staggered grid

Operating condition

$$T_{out} = T_{in}$$

Determining the geometry of the evaporator

$$r_o = D_o/2$$

Radius of tube

$$r_{fin} = r_o + L_{fin}$$

Radius of fin, measured from tube center

$$r = r_o - x_t$$

Inner radius of the tube

$$D = r \cdot 2$$

Inner diameter of tube

$$L = 2 \cdot r_{fin} + S_L$$

Length of evaporator

$$W = m/2 \cdot (D_o + L_{fin} \cdot 2)$$

Width of evaporator

$$V = W \cdot L \cdot H$$

Physical volume of evaporator

$$A_{unfin} = r_o \cdot 2 \cdot \pi \cdot H \cdot m$$

Unfinned area/element

$$A_{mfin} = ((\pi \cdot r_{fin}^2) - (\pi \cdot r_o^2)) \cdot H \cdot n_{fin} \cdot m$$

Finned area/element

$$\eta_{fin} = \eta_{fin;annular;rect}(th_{fin}; r_o; r_{fin}; h_{inf}; k_{fin})$$

Using EES to find fin efficiency

$$A_{eq} = A_{unfin} + \eta_{fin} \cdot A_{mfin}$$

The equivalent area of the finned area

$$S_T = 2 \cdot r_{fin} \cdot \text{Cos}(45)$$

Transverse length between tubes

$$S_L = 2 \cdot r_{fin} \cdot \text{Cos}(45)$$

Longitudinal distance between tubes

Ambient properties

$$c_{p_{inf}} = c_p(Air_{ha}; T = T_{inf}; P = P_{inf})$$

Heat capacity of surroundings

$$\rho_{inf} = \rho(Air_{ha}; T = T_{inf}; P = P_{inf})$$

Density of the surrounding air

$$\mu_{inf} = \mu(Air_{ha}; T = T_{inf}; P = P_{inf})$$

Viscosity of the air

$$k_{inf} = k(Air_{ha}; T = T_{inf}; P = P_{inf})$$

Conductivity of the surrounding air

$$Pr_{inf} = P_r(Air_{ha}; T = T_{inf}; P = P_{inf})$$

Prandtl number of the surrounding air

$$Re_{inf} = \frac{\rho_{inf} \cdot V_{inf} \cdot (r_o \cdot 2)}{\mu_{inf}}$$

Reynolds number of the surrounding air around the tubes

Surface properties

$$T_{sur} = \frac{T_{inf} + T_{in}}{2}$$

$$\rho_{sur} = \rho(Air_{ha}; T = T_{sur}; P = P_{inf})$$

Density of surroundings

$$\mu_{sur} = \mu(Air_{ha}; T = T_{sur}; P = P_{inf})$$

Viscosity of surroundings

$$c_{p_{sur}} = c_p(Air_{ha}; T = T_{sur}; P = P_{inf})$$

Heat capacity of surroundings

$$Pr_{sur} = P_r(Air_{ha}; T = T_{sur}; P = P_{inf})$$

Prandtl number of surroundings

$$k_{fin} = k(\text{'aluminum'}; T_{in})$$

Thermal conductivity of copper

Outer heat transfer

$$Nus_{sur} = 0,35 \cdot (S_T/S_L)^{0,2} \cdot Re_{inf}^{0,6} \cdot Pr_{inf}^{0,36} \cdot (Pr_{inf}/Pr_{sur})^{0,25}$$

Nusselt number of flow across a bank of tubes

$$Nus_{inf} = Nus_{sur} \cdot F$$

Nusselt number definition

$$h_{inf} = k_{inf} \cdot \frac{Nus_{inf}}{(r_o \cdot 2)}$$

Free stream heat transfer coefficient

$$k_w = k('Stainless_AISI304'; T_{in})$$

Free stream heat transfer coefficient

Inner convection

Liquid and vapor properties

$$Pr_l = Pr(water; P = P; x = 0)$$

$$Pr_v = Pr(water; P = P; x = 1)$$

$$\rho_l = \rho(Water; P = P; x = 0)$$

$$\rho_v = \rho(Water; P = P; x = 1)$$

$$\mu_l = \mu(Water; P = P; x = 0)$$

$$\mu_v = \mu(Water; P = P; x = 1)$$

$$k_l = k(Water; P = P; x = 0)$$

$$k_v = k(Water; P = P; x = 1)$$

$$iter = 99$$

Number of iterations (qualities teste)

duplicate $i = 1; Iter + 1$

$$x_i = x_{in} + \frac{x_{out} - x_{in}}{iter} \cdot (i - 1)$$

The quality for each iteration is determined

$$V_{l;i} = \frac{\dot{m}/m \cdot (1 - x_i)}{(r^2 \cdot \pi \cdot \rho_l)}$$

The liquid velocity is found

$$V_{v;i} = \frac{\dot{m}/m \cdot x_i}{(r^2 \cdot \pi \cdot \rho_v)}$$

The vapor velocity is found

$$Re_{l;i} = \rho_l \cdot V_{l;i} \cdot D / \mu_l$$

The liquid Reynolds number is found

$$Re_{v;i} = \rho_v \cdot V_{v;i} \cdot D / \mu_v$$

The vapor Reynolds number is found

$$\nu_i = (1,3 + 128 \cdot D) \cdot Pr_l^{0,9} \cdot Re_{l;i}^{0,23} \cdot Re_{v;i}^{0,34} \cdot (\rho_l / \rho_v)^{0,25} \cdot (\mu_v / \mu_l)$$

The falling film Nusselt number is found

$$h_{film;i} = \nu_i \cdot k_l / D$$

Heat transfer coefficient is found for each quality

end

$$h_{film} = \frac{\text{Sum}(h_{film,i}; i = 1; iter + 1)}{(iter + 1)}$$

The falling film heat transfer coefficient is found as an average

$$UA = \left(\left(\frac{1}{h_{inf} \cdot A_{eq}} \right) + \left(\frac{r_o}{k_w \cdot A_{unfin}} \right) \cdot \ln(r_o/r) + \left(\frac{1}{h_{film} \cdot A_{unfin}} \right) \right)^{-1}$$

Calculation for overall heat transfer coefficient

Cost Function

$$L_{tu} = H \cdot m$$

Total length of the tubes

$$C_{tu} = 8 \cdot 10^{-5} \cdot D_o^3 - 0,0058 \cdot D_o^2 + 0,442 \cdot D_o + 1,2957$$

Cost function for the tubes in euro per meter as a function of the diameter

$$A_{fin} = H \cdot n_{fin} \cdot W \cdot L$$

Total area of the fins

$$C_{fin} = 3$$

Cost of fins in euro per square meter

$$Cost = C_{tu} \cdot L_{tu} + C_{fin} \cdot A_{fin}$$

Total cost of the evaporator